

Controlled aggregation of peptide substituted perylene-bisimides

by

Joseph Keith Gallaher



A thesis

submitted to Victoria University of Wellington

in fulfilment of the

requirements for the degree of

Master of Science

in Chemistry

Victoria University of Wellington

2012

Abstract

In recent years there has been an intersection of supramolecular chemistry and materials science, with a particular focus on the controlled self-assembly of functional building blocks. The impetus for assembly of organised architectures is a requirement due to organic electronic device performance being sensitive to the geometric configuration of adjacent molecular semiconductors, interacting by means of overlapping π -orbitals to create electronic conduction.

Inspired by the formation of elegant supramolecular structures in nature, this work employs perylene bisimides coupled to synthetic peptides which are able to control the assembly of chromophores in solution. Through examining the perturbations of optical absorption and fluorescence spectroscopic signatures, the presence of aggregates, and also the geometric configurations of adjacent chromophores are determined. By exploring these features as a function of peptide design, pH, solvent composition, and ionic strength, it is demonstrated that aggregation is strongly induced by the peptide and the aromatic core, with significant dependence on the electrostatic repulsion between peptide segments. By manipulating solvent compositions, we demonstrate the ability to induce controlled reorganisation of aggregates through the introduction of charge onto the peptide sequence in high water concentration solution. Furthermore, application of the exciton model to absorption spectra establishes the tuneability of aggregates by specific ion binding between neighbouring peptides. Our results demonstrate the capability of peptide sequences to drive aggregation of molecular semiconductor building blocks; moreover, the peptides allow fine tuning of the electronic overlap between neighbouring building blocks. The proof of concept paves the way for further investigation into utilising this assembly control for device fabrication, in particular, we see this work being applicable to biosensor devices.

Publication

The following publication was based upon work carried out during this research project, with the key results discussed in chapters 4 and 5 of this thesis.

‘Controlled aggregation of peptide substituted perylene-bisimides’ Gallaher, J. K.; Aitken, E. J.; Keyzers, R. A.; Hodgkiss, J. M. *Chem. Commun.*, **2012**, 48, 7961–7963.

Acknowledgments

This thesis would not have come together if not for the help and support I have received from a number of people. When I thought of all the people I want to take the time to thank, I had assumed the words would fall onto the page. However, now that my time has come to actually write this it has dawned on me that thanking the people who have helped me get to where I am today is one monumental task.

First and foremost, I must thank my supervisor Dr. Justin Hodgkiss for his knowledge and support. Although my stay in the research group is far from over, I want to take the time to express my gratitude for your supervision. Through the course of this project you have always made me feel that I had what it took to do the research, showing unwavering belief in my ability; your patience and sharing of knowledge is very much appreciated. Additionally, the input/feedback I received from you, even whilst you were travelling the world was amazing and held in high regard. I look forward to starting the next phase of my research career with you... after a little rest and relaxation.

I also want to take time to thank Dr. Robert Keyzers, whose support and input in this work has certainly contributed greatly to the end results. Although having me knock on your office door with questions (at times on a daily basis) may have driven you near madness, you always appeared happy to offer advice. Although this project has reached a conclusion for myself, I hope our research collaboration continues into the future. Additionally, I wish to extend my thanks to the Curtis-Gordon Research Scholarship for funding through the duration of this project, the financial support you have provided me is much appreciated.

To the staff, fellow postgraduate students, and friends here in the School of Chemical and Physical Sciences at VUW, I extend my thanks to you all. The random chats in the corridors, and the condolences when science was beating my soul through multiple failed reactions or senseless results has been thoroughly enjoyed. In particular, Cole (Colin Ross) Lomas and Martin (Monty Scribble) Heeley are worthy of named

mentions for not only the proof reading of this thesis, but as the ‘first’ members of the Hodgkiss group here at VUW we have certainly shared some good times. Thanks also goes to the rest of the Hodgkiss group, it has been a pleasure to work alongside you in the lab, and I know our friendship will keep us in touch. Further notable mention goes out to members of the CMFC; our mutual appreciation of fine scotch whisky over the course of this project has kept me sane (and a little insane at times).

Special mention must go to my fiends outside of the university, and although you have all been severely neglected during the writing of this thesis, you were all there for moral support, and the promise to celebrate with me at the end. I appreciate the attempts some people made to hide the ‘glazing over of the eyes’ when the topic of conversation switched to my university work; my life is blessed to have you all apart of it.

Finally, I must show the immense appreciation I have for the support of my family. My parents get first mention: Mum, Dad, Andrea, and Graham, you have all shaped me who I am today. Even when you had no idea if a result I got was good or bad, you were always there to help me keep the greater picture in perspective and remember to sometimes just live a little. I also much express my appreciation for the support I have received from my grandparents, you have all played a major role in allowing me to get to the position I am today, no words can express how grateful I am. The sincere thanks also extends out to the rest of my family, my sisters and little brother, uncles, aunties, cousins. I love you all.

Sláinte.

Table of Contents

Abstract	ii
Publication	iii
Acknowledgments	iv
Table of Contents	vi
List of Figures	viii
List of Schemes	x
List of Tables	xi
List of abbreviations	xii
1 Background	1
1.1 Introduction	1
1.2 Perylene bisimides - a brief overview	2
1.2.1 Structure and optoelectronic properties	3
1.2.2 Basics of assembly in solution	5
1.3 Organic semiconductor self-assembly through nature mimics	7
1.3.1 Principles of self-assembling peptide amphiphiles	8
1.3.2 Peptide templated assembly of molecular semiconductors	12
1.4 Summary	15
1.5 Research aims	15
2 Synthesis and molecular design of peptide-PBI derivatives	16
2.1 Introduction	16
2.2 Molecular design of peptide-PBI library	17
2.3 Synthesis and structural characterisation	21
2.4 Summary	25
3 Spectroscopic probes of peptide-PBI aggregation	26
3.1 Introduction	26

3.2	Spectroscopic perturbations observed in PBI core interactions	27
3.2.1	Promoting monomers vs. semi-crystalline aggregates	27
3.2.2	Combination of PBI signatures through solvent tuning	29
3.2.3	Exciton model applied to aggregates in water	32
3.2.4	Tuning aggregates through pH changes	36
3.3	Effects of peptide sequence on aggregation	41
3.3.1	Incorporation of an H-bonding section	41
3.3.2	Reducing the number of ionisable groups	45
3.3.3	Incorporation of sterically demanding amino acids	46
3.4	Summary	49
4	Solvent composition dependent peptide-PBI aggregation	51
4.1	Introduction	51
4.2	From monomers to cofacial peptide-PBI aggregates	53
4.3	Reorganisation of peptide-PBI aggregates	55
4.4	Summary	60
5	Counterion effects on peptide-PBI aggregation	62
5.1	Introduction	62
5.2	Sensitivity of PBI aggregates to ionic strength	63
5.3	Cross-linking of PBI aggregates via specific ion binding	66
5.4	Summary	72
6	Conclusions	73
7	Future Work	74
8	Experimental	76
	Appendix	87
	References	98

List of Figures

1.1	Chemical structure of a simple PBI derivative	3
1.2	Electronic absorption spectrum of a typical isolated PBI chromophore	4
1.3	Frontier orbitals of a PBI derivative	5
1.4	Triple H-bond formation to direct PBI assembly	7
1.5	General molecular structure of a peptide amphiphile	9
1.6	Synthesis of different fluorophore-peptide conjugates	13
1.7	Structure of a naphthalene bisimide dipeptide conjugate	14
2.1	Library of PBI derivatives synthesised	17
2.2	Designing the peptide sequences	18
2.3	Peptide precursors sorted by design modifications	20
2.4	Example FTIR spectrum showing imide formation	23
2.5	HMBC and COSY correlations confirming peptide-PBI structure . . .	24
3.1	Peptide-PBI conjugate 6 absorption and emission spectra	28
3.2	Peptide-PBI conjugate 6 absorption in various alcohols	30
3.3	Absorption spectrum of peptide-PBI conjugate 6 in distilled water . .	33
3.4	Energy diagram for aggregated dimers	34
3.5	Energy diagram for aggregated dimer with rotational offset	35
3.6	Optical spectroscopy of peptide-PBI aggregates in acidic pH	37
3.7	Cryo-SEM images of peptide-PBI 6 in distilled water	39
3.8	Cryo-SEM images of peptide-PBI 6 in dilute HCl	40
3.9	Peptide-PBI conjugates with particular design features	41
3.10	Absorption spectra of peptide-PBI 8 in various solvents	42
3.11	Absorption spectra of peptide-PBI 9 in distilled water	46
3.12	Absorption spectra of peptide-PBI 10 in distilled water	47
4.1	Key compounds used for solvent composition studies	52
4.2	UV-vis absorption spectra of 8 in mixtures of DMSO and H ₂ O	54
4.3	Peak ratio variation in the DMSO/H ₂ O composition series	54
4.4	UV-vis absorption spectra of 8 in mixtures of MeCN and H ₂ O	56
4.5	Fraction of peptide-PBI 8 with vibronic peaks in MeCN/H ₂ O	57
4.6	Vibronic fraction of peptide-PBI 8 and 9 in MeCN and H ₂ O	59

5.1	Key compounds used for metal cation interaction studies	63
5.2	UV-vis absorption spectra of 8 with sodium perchlorate additions . .	65
5.3	Peak ratio changes with various concentrations of NaClO ₄	65
5.4	UV-vis absorption spectra of 8 with various salt additions	67
5.5	Vibronic peak ratios as a function of ionic strength of different salts .	68
5.6	Comparing two peptide-PBI conjugates with Zn(OAc) ₂ additions . .	70
8.1	Inversion of vial showing organogelation of peptide 3	78
8.2	Chemical structure of peptide 1	80
8.3	Chemical structure of peptide 2	80
8.4	Chemical structure of peptide 3	81
8.5	Chemical structure of peptide 4	81
8.6	Chemical structure of peptide 5	82
8.7	Chemical structure of peptide-PBI 6	83
8.8	Chemical structure of peptide-PBI 7	84
8.9	Chemical structure of peptide-PBI 8	84
8.10	Chemical structure of peptide-PBI 9	84
8.11	Chemical structure of peptide-PBI 10	85
8.12	Chemical structure of alkyl-PBI 11	85
8.13	¹ H NMR spectrum of peptide 3	88
8.14	¹³ C NMR spectrum of peptide 3	89
8.15	COSY NMR spectrum of peptide 3	90
8.16	HMBC NMR spectrum of peptide 3	91
8.17	HSQC NMR spectrum of peptide 3	92
8.18	¹ H NMR spectrum of peptide-PBI 8	93
8.19	¹³ C NMR spectrum of peptide-PBI 8	94
8.20	COSY NMR spectrum of peptide-PBI 8	95
8.21	HMBC NMR spectrum of peptide-PBI 8	96
8.22	HSQC NMR spectrum of peptide-PBI 8	97

List of Schemes

2.1	Amine condensation of PTCDA to form peptide-PBI conjugates . . .	22
4.1	Mechanism of aggregate reorganisation in MeCN/H ₂ O	61
5.1	Types of interactions of peptide-PBI with ions	71

List of Tables

1.1	Summary of N-methylated peptide amphiphiles	11
3.1	Vibronic peak ratios of 6 in water and DMSO	35
3.2	Vibronic peak ratios of 6 , 7 and 8 in H ₂ O	44
3.3	Vibronic peak ratios of changes upon reduced ionisable groups	46
3.4	Nature of aggregates in water and vibronic peak ratios	50

List of abbreviations

Ala	alanine
conc.	concentration
COSY	correlation spectroscopy
DIEA	<i>N,N</i> -diisopropylethylamine
DMSO	dimethylsulfoxide
EtOH	ethanol
Glu	glutamic acid
Gly	glycine
HMBC	heteronuclear multi bond correlation
HRMS	high resolution mass spectrometry
HSQC	heteronuclear single quantum coherence
IPA	isopropanol
IR	infrared
Leu	leucine
m	multiplet
MALDI	matrix assisted laser desorption ionisation
MeCN	acetonitrile
NMR	nuclear magnetic resonance
PBI	perylene-3,4,9,10-tetracarboxylic bisimide
PTCDA	perylene-3,4,9,10-tetracarboxylic dianhydride
q	quartet
SEM	scanning electron microscopy
SPPS	solid phase peptide synthesis
t	triplet
TEM	transmission electron microscopy
TFA	trifluoroacetic acid
UV-Vis	ultraviolet–visible spectroscopy

Chapter 1

Background

1.1 Introduction

Electronic devices have become abundant in our everyday lives, with a constant demand for increased device performance, and a decreased cost and size of each device. These demands, coupled with the advent of novel electronic applications, provide the impetus to continually enhance device performance. The incorporation of π -conjugated systems as the active components in semiconductor devices has lead to research in molecular semiconductors attracting a large amount of research attention in the scientific community.¹

One of the major challenges in the field of organic electronics based on organic molecules is the design of functional architectures which possess long range order. Long range supramolecular assembly is a requirement due to device performance relying on intermolecular electronic coupling of π -conjugated systems. Therefore, efficient organic semiconductor devices require a high degree of molecular organisation involving extended π -coupled networks which allow for strong π - π interactions.

The controlled formation of different kinds of supramolecular architectures in solution depends on a variety of factors, such as temperature, concentration, solvent composition, molecular structure, particular additives, and the relative ratio of hydrophilic/hydrophobic domains.²⁻⁴ The controlled self-assembly of functional materials is obtained only through the precise balance of each of these forces. In light of this challenge, inspiration can be gained from assembly methods utilised in nature by investigating the ‘toolbox’ employed in these systems. There are numerous complex functional supramolecular assemblies in nature, for example the double helix

of DNA, or chlorophyll assemblies for light harvesting.⁵ One approach employed to achieve supramolecular organisation of molecules on micrometer length scales is through the use of synthetic peptide derivatives.⁶ Recently, this methodology has gained considerable interest for the controlled assembly of π -conjugated materials, for the end goal of device application.

Although there are numerous molecular semiconductors that have been reported for various device applications,⁷ one interesting material that shows high promise is that of perylene-3,4,9,10-tetracarboxylic bisimide, commonly known as perylene bisimide (PBI).⁸ PBI derivatives are a promising component for organic electronic device applications due to their optical and electronic properties, stability, and ease of modification.

This chapter provides a brief overview of PBIs and highlights not only the optoelectronic properties, but also the molecular structure. A summary of the common strategies that are employed in assembling PBI chromophores in solution are highlighted, and demonstrate the need to further investigate the controlled assembly of PBIs for their use in optimised devices. One approach is to employ ‘nature’s toolbox’ of assembly, namely the use of synthetic peptide assembly. To this end, a review of the literature is presented highlighting the nanostructures commonly observed with this approach. Finally, the reports of tethering peptide sequences to other organic semiconductors is reviewed, which illustrates the need to further explore this relatively recent approach to molecular assembly.

1.2 Perylene bisimides - a brief overview

The initial applications for PBIs were predominately as industrial pigments, due to their inherent insolubility, thermal stability, light fastness, and chemical inertness.⁹ Recently, the applications of PBI derivatives are in the field of electronic materials, and are regarded as some of the best n-type semiconductors available, making them promising for electronic applications.¹ Studies of PBI have focussed on the electron-accepting properties and subsequently PBI derivatives have found use in organic light emitting diodes (OLEDs),¹⁰ photovoltaic devices,¹¹ and field effect transistors.¹² This section introduces the structure, electronic and optical properties of PBI, highlighting the key features for the attention they have attracted in the literature. Subsequently, a brief overview of the commonly employed methodologies for inducing extended π -stacks of PBI chromophores is discussed.

1.2.1 Structure and optoelectronic properties

The promising electronic properties of PBIs are a direct result of the structure of the chromophore. Figure 1.1 illustrates the chemical structure of a generic PBI derivative, highlighting two distinct sections that comprise the molecular structure. One region is the planar π -conjugated core, known as perylene, containing five fused aromatic rings. The bond lengths of this ring system, as determined from crystal structures, show that it can be regarded as two fused naphthalene rings.¹³ The second feature of the PBI molecule is the two electron withdrawing imide groups at the 3, 4 and 9, 10 positions (see Figure 1.1).

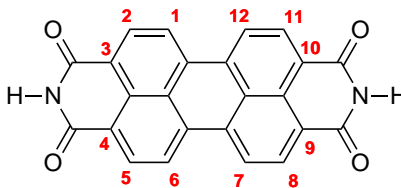


Figure 1.1 Chemical structure of *N,N'*-dihydro PBI, showing the numbering of the positions on the ring system.

The crystal packing of PBI dyes has been studied in the literature and have shown the propensity of PBIs to form cofacial π -stacks in a parallel orientation at a distance between 3.34 and 3.55 Å (compared to 3.55 Å for graphite).¹⁴ The propensity to form strong π - π interactions is attributed to the inherent insolubility of PBIs. Although this insolubility was initially exploited for use in pigments, favourable optical and electronic properties lead intensive research into synthesising soluble PBI derivatives, with the first being reported by Langhals *et al.* in the 1990s.¹⁵ This was achieved through the introduction of substituents on the PBI in order to inhibit aggregation between chromophores, and thus increase solubility. This was motivated by crystal packing investigations which showed that interaction of chromophores are sensitive to steric requirements of substituents.¹⁶

There are two common positions on the PBI chromophore that are used to attach various substituents; the ‘bay’ position, and the imide positions. The bay positions are the carbons labelled 1, 6, 7, and 12 (Figure 1.1), whereas the imide positions are the two nitrogen groups that comprise the imide moiety. Substitution at the imide position has no effect on disrupting the planar nature of the aromatic core. Whereas, substitution at the bay position has been shown to cause propeller-like twisting of the π -conjugated core.¹⁷ These reports demonstrate the ability to modulate the nature of chromophore assembly through the introduction of substituents on the PBI molecule.

One central factor for the research interest in PBI derivatives is the extraordinary

lightfastness and intense yellow-green photoluminescence observed in the absence of aggregation effects. The molar extinction coefficients of isolated PBI chromophores typically approach $10^5 \text{ M}^{-1} \text{ cm}^{-1}$, and have the fluorescence quantum yields near unity.¹³ These photophysical properties are attributed to the fused aromatic rings which form the π -conjugated core, which also has an optical band gap suitable for use in organic devices.

Figure 1.2 shows an example of the absorption and emission spectrum of an isolated PBI chromophore in solution. The lowest energy electronic transitions of PBIs are between the ground state (S_0) and first excited state (S_1), as shown in the Jablonski diagram. The vibronic progression observed in the spectra arises from the main vibrational mode coupled to an electronic excitation of perylene being the C=C stretch (approximately 1400 cm^{-1}). This is depicted by the energy diagram which correlates the peaks in the spectra to the corresponding electronic and vibrational states of perylene (*i.e.*, the 0-0, 0-1, and 0-2 transitions).

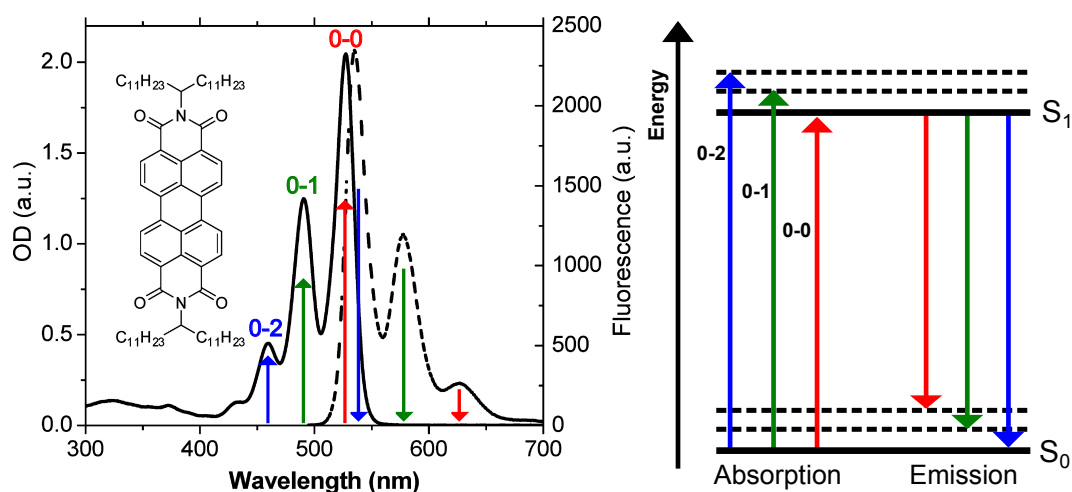


Figure 1.2 (Left) Electronic absorption (solid line) and emission (dashed line) spectrum of a typical isolated PBI chromophore. (Right) Jablonski diagram indicating the cause of the vibronic progression. Figure adapted from S. R. Marder *et al.*¹⁸

An important attribute of molecular semiconductors is that the optical spectroscopic signatures reflect the local environment of the chromophores, making optical spectroscopy an excellent probe of the nature of chromophores in solution.¹⁹ Aggregation is probed through analysing perturbations from the monomer spectrum that occur upon the formation of effective π -orbital electronic overlap between neighbouring chromophores. This concept is central to the work covered in this thesis, and is exploited to detect the presence of aggregates in solution as a result of substituents driving assembly. The details of this analysis is outside the scope of this brief literature review, but will be covered in detail in Chapter 3.

In order to exploit optical spectroscopy as a probe for the nature of chromophores in solution, the electronic properties of the PBI core needs to be largely unaffected by the substituents. This is because the perturbation of spectroscopic signatures needs to be a result of aggregation effects, and not from alterations to the π -conjugated system itself. Figure 1.3 shows the highest occupied molecular orbital (HOMO) and the lowest unoccupied molecular orbital (LUMO) for the electronic transition between the ground state (S_0) and first excited state (S_1) for PBI.²⁰ Because nitrogen atoms are located at nodes of the HOMO and LUMO, substituents at these positions impose little effect on the electronic transition of perylene. Additionally the symmetry of these orbitals means that the optical transition is polarised along the molecular axis of the PBI, in other words, along the N–N axis.

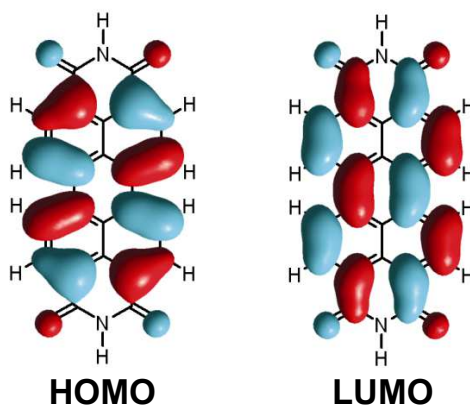


Figure 1.3 HOMO and LUMO frontier orbitals of *N,N'*-dihydro PBI.²⁰ Illustrating the nodes at the imide positions.

In contrast to the imide positions, the bay positions of PBI have significant orbital character; therefore substituents at these positions can impart changes to the absorption and emission properties of the PBI core. Based on the frontier orbitals, substituents at the imide positions are favourable to influence aggregation due to the negligible influence substituents at the imide positions have on the inherent optical properties of PBI monomers.²¹ Therefore, any change in the optical spectroscopic signatures of imide substituted chromophores are a direct result of the electronic environment of the chromophore, and not caused by substituents changing the electronic properties of the PBI core.

1.2.2 Basics of assembly in solution

The ability to affect the interaction of PBI chromophores in solution through the use of imide substituents is an important concept that is exploited in PBI research. Although some applications require the use of isolated chromophores, the discussion here is limited to the common techniques employed to form supramolecular architectures of PBI assemblies. Examples selected in this review that highlight common

approaches to PBI assembly. For a more detailed account, the reader is directed to a number of comprehensive reviews.^{18,22}

One of the simplest approaches of inducing aggregation of PBI in solution is through the incorporation of alkyl chains at the imide substituent to increase the solubility in nonpolar organic solvents. This generally results in isolated chromophores in solution. Aggregation can be induced by changing the polarity of the solvent so that assembly is induced in order for the system to reduce unfavourable solvent interactions.²³ Recently, this assembly approach has been shown to form PBI nanofibres which are able to form organogels,²⁴ or be used in field effect transistors.²⁵

An extension of this mode of self-assembly is to design PBI derivatives which are strongly amphiphilic by incorporating polar substituents at the imide positions. This increases the solvophobic/solvophilic forces that induce assembly upon solvent polarity changes by the embedding the aromatic PBI core inside an aggregate.²⁶ This mode of inducing aggregation has been shown to allow the formation of nanostructures including nanobelts,²⁷ nanotubes,²⁸ and micelles/vesicles.²⁹ However, one difficulty that remains with these methods of inducing assembly is the prediction as to the type of supramolecular architecture that will be formed. This task is challenging due to a main driving force of aggregation in such systems being π - π interactions of PBI cores, as this interaction lacks directionality. Furthermore, this task is particularly challenging with amphiphilic building blocks in water, as the hydrophobic force will have an extremely strong influence on aggregation.

One approach that has attracted considerable attention in the literature in recent years is the incorporation of substituents that are able to form additional interactions between molecules to complement π - π assembly.¹³ Interactions that have been exploited include metal-ligand coordination,³⁰ hydrogen bonding,^{31,32} and ionic assembly.³³ Covalent interactions (*i.e.*, metal-ligand coordination) add directionality towards aggregation, but lacks the ability for aggregates to be tuned due to the permanent nature of bond formation. In contrast, ionic assembly is a weak intermolecular interaction which allows for controlled tuning of aggregation, but is unable to promote directional assembly of molecules.

One example of noncovalent interactions controlling PBI assembly which has received considerable attention in the literature is that of triple H-bond formation of melamine and cyanurate/barbiturate derivatives.^{34,35} This triple H-bond formation has been shown to form strong networks, reminiscent of that observed in DNA base pairing in the field of supramolecular assembly, illustrating the directionality imposed on aggregation.³⁶ Figure 1.4 shows how this interaction is employed in the

PBI literature. Typically a melamine motif is incorporated as an imide substituent on a PBI derivative, and upon addition of a cyanurate moiety to solution, complexation can occur to induce assembly of chromophores.

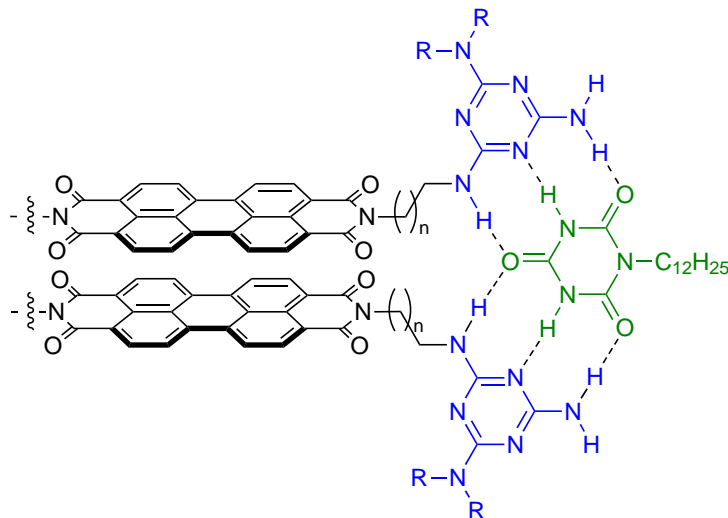


Figure 1.4 Generic PBI derivative which contains a melamine motif (blue) and the triple H-bond complexation with a cyanurate derivative (green) to induce assembly. Figure adapted from Würthner *et al.*³⁵

This approach therefore involves the addition of guest molecules in order to induce assembly, as opposed to self-assembly in solution. Recently, a study by Seki *et al.* reported the use of this approach to obtain organised lamellar architectures of PBI molecules.³⁷ In this study, the authors deposited these assemblies onto Si/SiO₂ substrate via spin coating for use in organic field effect transistors devices. However, the device exhibited poor performance, well below practical use. This highlights the need for further investigation on the controlled assembly of PBI chromophores in order for use in electronic applications. Current interest in the PBI literature is centred on obtaining precise control of π - π stacking to form organised supramolecular structures. The impetus for this is the drive to improve charge transport properties, which is of fundamental importance in applications of π -conjugated materials in optoelectronic devices.

1.3 Organic semiconductor self-assembly through nature mimics

Nature has perfected the controlled self-assembly of molecules via non-covalent interactions to achieve elegant structures such as the double helix of DNA and chlorophyll assemblies for light harvesting.⁵ The principles employed in nature to assemble complex structures has provided the incentive for scientists to attempt to mimic the

formation of complex assemblies.^{1,38} This is commonly investigated through manipulating noncovalent intermolecular interactions such as; hydrogen-bonding,³⁹ π - π interactions,⁴⁰ electrostatic interactions,⁴¹ or solvophobic effects.⁴²

Considerable attention in recent years has been devoted to the incorporation of organic semiconductors in DNA based assemblies.^{43,44} However, this approach is predominantly concerned with gaining a better understanding of the structure of biological materials through biolabelling.^{22,45} This assembly approach falls outside the scope of this work and is omitted from discussion, with the reader directed to a recent review article that explores the relevant concepts in detail.⁴⁶

Of interest here is the configurational specificity of proteins, motivating synthetic peptides to emerge as a promising class of compounds as templates for the assembly of molecules.^{47,48} Further promise is gained from the ability to synthesise peptides using well established, and conventional, methods, namely solid phase peptide synthesis.⁴⁹ This section provides a brief review of key results obtained through investigations on peptide-templated assembly of peptide amphiphile molecules reported in the literature. To this end, a review of recent work reported in the literature on the peptide-mediated assembly of functional materials are highlighted.

1.3.1 Principles of self-assembling peptide amphiphiles

Investigations into peptide driven assembly was inspired by Stupp *et al.* in 2001 who showed that peptide sequences with a hydrophobic tail assembled into nanofibres.⁴⁸ This class of compounds are known as peptide amphiphiles, due to their structural properties resembling those of amphiphilic surfactant molecules; namely a hydrophobic tail bound to a hydrophilic head group. These types of molecules have been shown to form a variety of supramolecular structures; including tubes,⁵⁰ ribbons,⁵¹ and micelles/vesicles.⁵² This is achieved through the combination of H-bonding, hydrophobic, and electrostatic interactions and varying the balance of these forces in solution.⁵³

Figure 1.5 shows the general structure that is incorporated into the supramolecular design of peptide amphiphiles, and highlights four key structural elements that are commonly employed.⁶ Region 1 consists of a hydrophobic domain, for example an alkyl tail of some length 'n'. Region 2 consists of a short peptide sequence that is capable of forming intermolecular H-bonds. Region 3 contains ionisable amino acids, which increases the solubility of the peptide molecule in aqueous environments. Region 4 is a domain that can add biological specificity, for example the inclusion

of a particular amino acid sequence that can interact with cells or proteins.⁵⁴

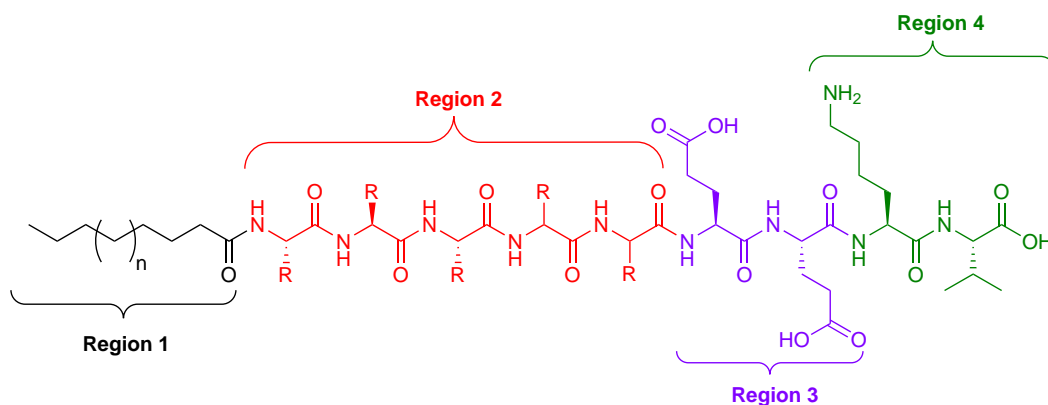


Figure 1.5 General molecular structure of a peptide amphiphile, indicating the common 4 regions that are commonly incorporated in the supramolecular design.

The amphiphilic nature of the molecule is an important characteristic, with studies demonstrating that long alkyl chains promote aggregation due to strong hydrophobic interactions when dispersed in water.⁵⁵ This is reminiscent of surfactant assembly, in which micelles and vesicles are commonly observed to embed the hydrophobic segment inside to reduce unfavourable interactions with the solvent.⁵⁶ The inclusion of ionisable amino acids in the peptide sequence results in nanostructures formed from peptide amphiphiles that are sensitive to pH and salt additions.⁶

This sensitivity is based on the fact that a change in pH (or ionic strength), modulates the extent of electrostatic repulsions that can occur between neighbouring peptide molecules, which hinders spontaneous assembly. Additionally, studies have been reported which exploit the ionisable amino acid residues through the coassembly of peptide amphiphiles which have oppositely charged groups. In these systems, aggregation is induced based on the electrostatic attraction between molecules in solution.^{57,58} Such studies demonstrate the influence that electrostatic interactions have on the self-assembly of peptide molecules in solution.

One of the central driving forces that drives peptide nanostructure assembly in solution is a result of the amino acids in Region 2, which are capable of forming intermolecular H-bonds, typically in the form of a β -sheet.⁶ An important study was conducted in 2006 by Paramonov *et al.* which investigated the role of H-bonding on the formation of peptide amphiphile nanostructures.⁵⁹ The authors probed this by sequentially inhibiting H-bond formation at various positions of a peptide amphiphile, through N-methylation of glycine (Gly) residues.

The findings from that study are summarised in Table 1.1, along with the general structure of the peptide amphiphile that was used by the authors. The influence of H-bonding was extracted through visualisation of nanostructures formed using

cryogenic transmission electron microscopy (cryo-TEM). Specifically, this was used to investigate what effects N-methylation had on disrupting nanofibre formation of the peptide amphiphile. In order to gain further insight into the relative strength of nanofibre interactions, the authors investigated the rheology of any solvent gelation that occurred. This gelation is a common observation in peptide amphiphile research, and is a result of a 3D-network of fibres forming which is able to trap solvent molecules.⁶⁰

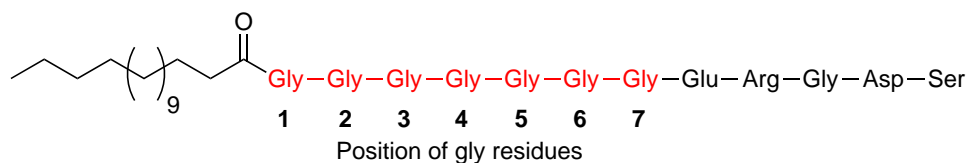
The first series of peptide amphiphiles investigated by Paramonov *et al.* (**A–H**) study the effect of sequentially increasing the number of N-methylated glycine residues, and therefore decreasing the ability of the molecules to form intermolecular H-bonds. The results showed that as H-bonding was inhibited close to the hydrophobic tail, the nanostructures changed from nanofibres to spherical micelles, as observed in cryo-TEM. This observation was supported by a weakening of the resulting gel, and eventually no stable gel being formed once spherical micelles were the dominant structures. The lack of gelation is rationalised based on the fact that micelles are unable to form long range order to trap solvent molecules, whereas such an interaction is possible through the entanglement of fibres in a nanofibre structure.⁶¹

The second series of peptide amphiphiles in the study (**H**, **I** and **O–S**) investigated the sequential N-methylation in the opposite direction to the previous series (starting at position 1). The cryo-TEM studies showed that the nanostructures formed for all peptide amphiphiles were spherical micelles, thereby illustrating that N-methylation close to the hydrophobic domain prevents fibre formation. This indicates the importance of H-bonding, and its specific location on the monomer, in directing the self-assembly into well defined fibres.

The study by Paramonov *et al.* interrogated the role of H-bonding further and explored the effects of having only one N-methylated glycine per peptide amphiphile (**I–N**). As observed by cryo-TEM, all peptide amphiphiles in this series assemble into fibres indicating that single methylation does not prevent nanofibre formation. However, when mechanical investigations were carried out, it became clear that although nanofibres were formed regardless of which glycine position was N-methylated, positions close to the core were unable to form stable gels, indicating a lack of interactions between fibrils in solution.

The findings from this study lead the authors to three conclusions as to the role of H-bonding in peptide amphiphile assembly; 1) Methylation in glycine positions 1–4 completely eliminates the ability for the fibres to network causing hydrogelation,

Table 1.1 Summary of N-methylated peptide amphiphiles prepared in the 2006 study of Paramonov *et al.*⁵⁹ Also included is the structure of the peptide amphiphile used in the study.



PA	Glycine Position ^a							nanostructure ^b	rheology ^c
	1	2	3	4	5	6	7		
A	G	G	G	G	G	G	G	F	Gel
B	G	G	G	G	G	G	NMeG	F	Gel
C	G	G	G	G	G	NMeG	NMeG	F	Gel
D	G	G	G	G	NMeG	NMeG	NMeG	F	wGel
E	G	G	G	NMeG	NMeG	NMeG	NMeG	—	—
F	G	G	NMeG	NMeG	NMeG	NMeG	NMeG	—	—
G	G	NMeG	NMeG	NMeG	NMeG	NMeG	NMeG	—	—
H	NMeG	NMeG	NMeG	NMeG	NMeG	NMeG	NMeG	—	—
I	NMeG	G	G	G	G	G	G	F	—
J	G	NMeG	G	G	G	G	G	F	—
K	G	G	NMeG	G	G	G	G	F	—
L	G	G	G	NMeG	G	G	G	F	—
M	G	G	G	G	NMeG	G	G	F	Gel
N	G	G	G	G	G	NMeG	G	F	Gel
O	NMeG	NMeG	G	G	G	G	G	—	—
P	NMeG	NMeG	NMeG	G	G	G	G	—	—
Q	NMeG	NMeG	NMeG	NMeG	G	G	G	—	—
R	NMeG	NMeG	NMeG	NMeG	NMeG	G	G	—	—
S	NMeG	NMeG	NMeG	NMeG	NMeG	NMeG	G	—	—

^aG indicates a standard glycine, NMeG indicates an N-methylated glycine residue was used.

^b'F' indicates the presence of nanofibres as the dominant structure (as observed from cryo-TEM), '—' indicates no fibres were observed, but rather spherical micelles.

^cBased on rheology data, either a Gel or wGel (weak gel) was observed, '—' indicates no gel was formed.

2) Two or more methylations of glycine positions 1–4 eliminates fibre formation entirely and instead spherical micelles are formed, and 3) Any methylations of glycine positions 5–7 will decrease the strength of a resulting gel, but will not explicitly eliminate the formation of nanofibres.⁵⁹

Therefore, it is apparent that H-bonding plays a significant role in the formation of peptide amphiphile nanostructures in solution. Without the ability to form such noncovalent intermolecular interactions, the assemblies observed appear to behave like traditional surfactant assemblies, thereby demonstrating that H-bonding is able to complement the hydrophobic driving force of assembly for amphiphilic molecules.

1.3.2 Peptide templated assembly of molecular semiconductors

The formation of well defined nanofibres using synthetic peptide molecules is a significant result that has promise for the organisation of molecules in functional materials. The motivation to select an organic semiconductor as the hydrophobic segment of a peptide amphiphile is driven by the promise H-bonding has to complement π - π assembly,⁶² enabling organised supramolecular structures which is fundamental for optimal performance in optoelectronic devices.

One class of organic semiconductors which has received considerable attention in research pertaining to device fabrication are oligo- and polythiophene derivatives. The interest in these compounds is motivated by the success such moieties have had in the field of organic electronics.¹ The first peptide-oligothiophene derivative was reported in 2004 by Klok *et al.*,⁶³ which incorporated a pentapeptide sequence of alternating glycine and alanine residues. These repeating amino acid residues have a high propensity to form intermolecular H-bonds, exploited in nature by the *Bombyx mori* (silk worm), of which the repeating glycine/alanine unit has been identified as the most important repeat sequence contributing to the strength of the fibre.⁶⁴

The results obtained by Klok *et al.* demonstrated that peptide sequences appeared to be able to control the nanostructure of the oligothiophene, thereby altering the electronic properties of the organic semiconductor. However, one drawback to novel oligothiophenes derivatives is the difficulty of synthetic procedures required for derivitisation.⁶⁵ Nevertheless, this is proof of concept that a peptide sequence can modulate the photophysics of a molecular semiconductor and has provided the impetus for the inclusion of various other π -conjugated materials in peptide systems.

A study by Ma *et al.* utilised three different π -conjugated materials, that were easily tethered to a peptide sequence.⁶⁶ This study investigated the effect a variety of pentapeptide sequences had on the assembly of π -conjugated materials, with a focus on exploring supramolecular hydrogelation. Figure 1.6 shows the synthetic protocol utilised in this study, highlighting the direct incorporation of fluorene (F), pyrene (P), and naphthalene (N) derivatives with solid phase peptide synthesis. This simple one step reaction to couple a peptide sequence to a molecular semiconductor is significant advantage for electronic device fabrication. Although, these π -conjugates molecules have found limited use in organic electronics, largely attributed to the wide band gap of these chromophores.^{67,68}

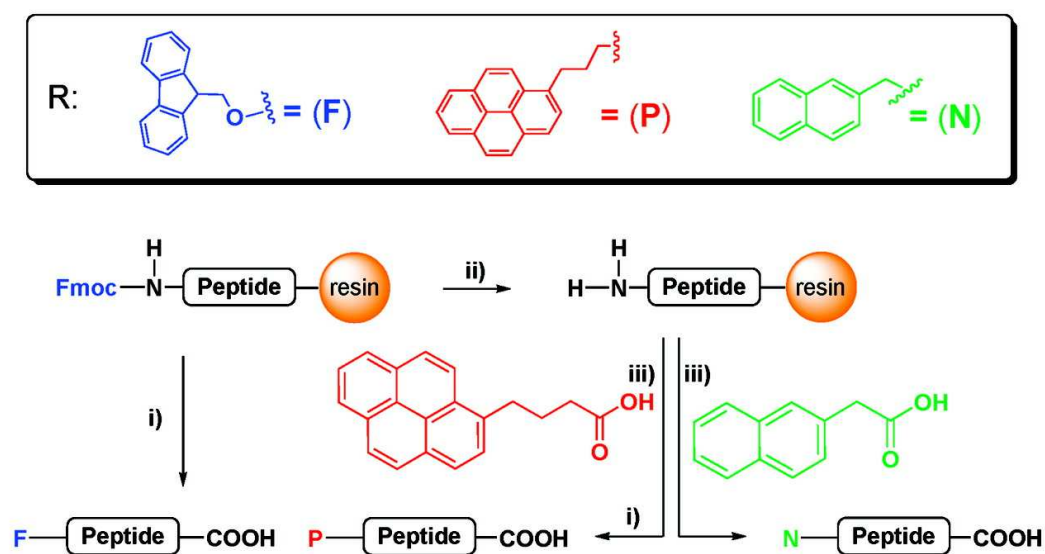


Figure 1.6 Synthesis of different fluorophore-peptide conjugates using fluorene (F), pyrene (P), and naphthalene (N) derivatives. i) 88% trifluoroacetic acid, 2% i -Pr₃SiH, 5% phenol, and 5% H₂O, ii) 20% piperidine in DMF, and iii) HBTU/HOBt, DIEA, DMF. Figure adapted from Ma *et al.*⁶⁶

The photophysics reported for each of the fluorophores-peptide conjugates illustrated that upon inducing aggregation in solution (through heating to 70 °C and then cooling), significant π -orbital electronic overlap occurs between chromophores, evident through photoluminescence quenching and excimer formation. Furthermore, TEM images showed the presence of self-assembled fibres in cryo-dried hydrogels. The results from Ma *et al.* found that through balancing the combination of hydrophobic demands of the chromophore, together with favourable π - π interactions in water, these forces were able to complement H-bonded directed assembly demonstrating the ability to drive aggregation of π -conjugated materials through balancing various forces acting on the system.

With the desire to use relatively straightforward synthetic techniques to exploit peptide assembly with molecular semiconductors for device applications, the utilisation

of chromophore derivatives has come to the fore. Recently, Parquette *et al.* reported the synthesis of three dipeptide naphthalene bisimide (NBI) derivatives, depicted in Figure 1.7.⁶⁹ In these derivatives, assembly is strongly promoted in aqueous media through increasing the hydrophobicity of the molecule. This study illustrates once more the importance of balancing the various forces that can drive self-assembly in solution.

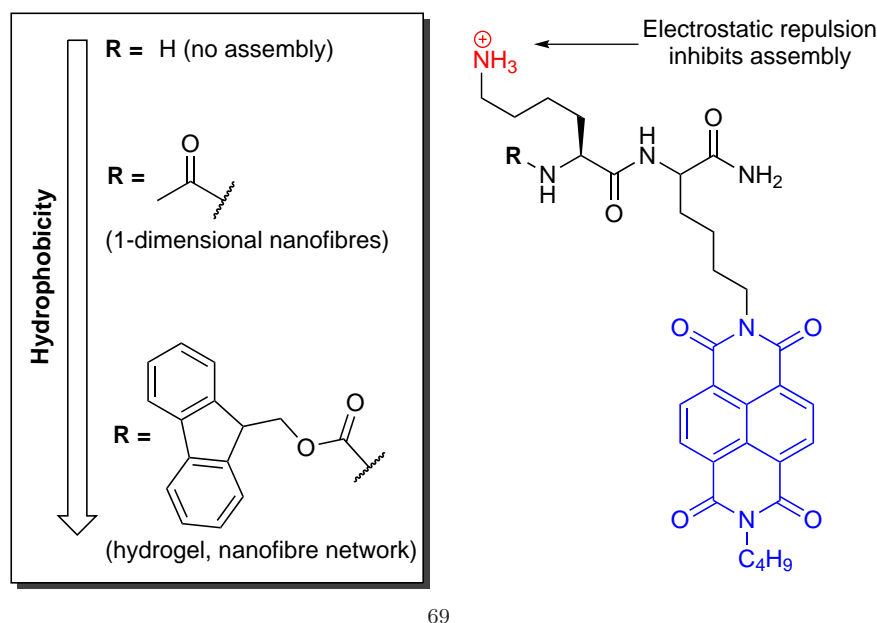


Figure 1.7 Design and structure of a naphthalene bisimide dipeptide conjugate. Figure adapted from Parquette *et al.*

The study by Parquette *et al.* presents TEM, and optical spectroscopy data that show the fluorenyl containing NBI-dipeptide conjugate exhibited solvent dependent aggregation. When a solvent was used that could satisfy the hydrophobic demands, such as 2,2,2-trifluoroethanol (TFE), isolated chromophores were present. However, when the NBI-dipeptide conjugate was dispersed in water, 1D nanofibres were observed. Furthermore, the spectroscopic perturbation from monomer signatures in the absorption spectrum of NBI chromophores, together with the strong photoluminescence quenching (15-fold) suggests the formation of co-facial NBI assemblies within the nanofibres.¹³ The peptide segment within the nanofibres possessed β -sheet H-bonding character, while assembly to the point of insolubility is prevented due to electrostatic repulsion between dipeptide segments.⁶⁹

1.4 Summary

This summary of the literature highlights the tethering of a peptide sequence to three organic semiconductors; namely pyrene, naphthalene, and fluorene moieties. These are the most commonly employed semiconductors that are investigated for the controlled assembly in solution through the use of peptide amphiphiles. These results illustrate the ability to modulate the assembly of π -conjugated molecules through the use of peptide assembly. However, the organic semiconductors used have had limited success in the field of organic electronics, largely attributed to their wide band gap. This highlights the need for further development in the field, with the extension to organic semiconductors which show a greater promise in device applications, due to more favourable optical and electronic properties. One such material is PBI, which has a relatively low optical band gap in comparison. Such peptide controlled assembly has not yet been explored for PBI.

1.5 Research aims

The overall goal of this research is to explore the controlled assembly of PBI chromophores in solution through the use of peptide directed assembly. Firstly, synthetic peptide sequences are to be tethered symmetrically to PBI at the imide position (Chapter 2). The use of imide substitution is motivated by the negligible influence substitution at this position has on the optical and electronic properties of the PBI core. As a result, optical spectroscopy is able to be used as a probe of the local electronic environment of PBI chromophores to determine the presence, and type, of aggregates in solution (Chapter 3).

The second goal of this research was to then investigate the tuneability of PBI aggregates in solution, through varying solvent mixtures (Chapter 4), and counterion additives (Chapter 5). The motivation for this research is the promise that controlled assembly of PBI chromophores could lead to applications in the field of organic biosensors, or the development of other novel devices.

Chapter 2

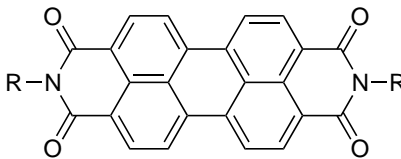
Synthesis and molecular design of peptide-PBI derivatives

2.1 Introduction

Nature has accomplished the assembly of building blocks into supramolecular architectures, such as chlorophyll assemblies for light harvesting.⁵ Such systems provide the motivation for the design of novel molecular building blocks which are capable of mimicking the intermolecular interactions that are employed in nature. This is commonly investigated through the incorporation of functional groups into building blocks which allow the manipulation of noncovalent intermolecular interactions such as; hydrogen-bonding (H-bonding),³⁹ π - π electronic overlap,⁴⁰ electrostatic interactions,⁴¹ solvophobic effects,⁴² or steric inhibition.⁷⁰

By designing molecular building blocks to contain motifs with the potential to form these noncovalent intermolecular interactions, it is possible to control the self assembly and form supramolecular structures. This work investigates the incorporation of a peptide sequence as imide substituents on a PBI core. Through modifying the design of the peptide sequence, a PBI conjugate library was obtained (Figure 2.1) in order to deduce the influence the peptide sequence has on the assembly in solution. This chapter also presents the synthetic protocols employed in order to obtain a peptide sequence symmetrically tethered to a PBI core, which was achieved in a two-step synthetic procedure, and highlights key structural characterisation data to confirm the identity of PBI derivatives. Firstly the peptide precursors (**1**, **2**, **3**, **4**, **5**) were synthesised, and subsequently tethered to a PBI core to form the various peptide-PBI conjugates (**6**, **7**, **8**, **9**, **10**). In a similar fashion, a reference compound was

synthesised (alkyl-PBI **11**) by coupling an alkyl chain to the PBI core to reference various optical spectroscopy measurements conducted in this work.



Peptide Precursors	Peptide-PBI Conjugates
1 : $\text{H}_2\text{N}-\text{Gly}-(\text{Glu})_3-\text{OH}$	6 : $\text{R} = \text{-}\overset{\text{O}}{\underset{\text{O}}{\parallel}}\text{-Gly}-(\text{Glu})_3-\text{OH}$
2 : $\text{H}_2\text{N}-\text{Gly}-(\text{Gly})_3-(\text{Glu})_3\text{OH}$	7 : $\text{R} = \text{-}\overset{\text{O}}{\underset{\text{O}}{\parallel}}\text{-Gly}-(\text{Gly})_3-(\text{Glu})_3\text{OH}$
3 : $\text{H}_2\text{N}-\text{Gly}-(\text{Ala})_3-(\text{Glu})_3\text{OH}$	8 : $\text{R} = \text{-}\overset{\text{O}}{\underset{\text{O}}{\parallel}}\text{-Gly}-(\text{Ala})_3-(\text{Glu})_3\text{OH}$
4 : $\text{H}_2\text{N}-\text{Gly}-(\text{Ala})_3-(\text{Glu})\text{OH}$	9 : $\text{R} = \text{-}\overset{\text{O}}{\underset{\text{O}}{\parallel}}\text{-Gly}-(\text{Ala})_3-(\text{Glu})\text{OH}$
5 : $\text{H}_2\text{N}-\text{Gly}-(\text{Leu})_3-(\text{Glu})_3\text{OH}$	10 : $\text{R} = \text{-}\overset{\text{O}}{\underset{\text{O}}{\parallel}}\text{-Gly}-(\text{Leu})_3-(\text{Glu})_3\text{OH}$
Reference Compound	
11 : $\text{R} = \text{-}\overset{\text{O}}{\underset{\text{O}}{\parallel}}\text{-C}_{12}\text{H}_{25}$	

Figure 2.1 Library of compounds synthesised, illustrating the peptide precursors (**1–5**), peptide-PBI conjugates (**6–10**), and the alkyl-PBI compound (**11**). Note, Gly, Ala, Leu, and Glu represent glycine, alanine, leucine, and glutamic acid (respectively).

2.2 Molecular design of peptide-PBI library

The stepwise assembly of the peptides (through solid phase peptide synthesis, discussed below), allowed for significant control over the type and sequence of amino acids used in the synthesis. Through modifying the amino acid residues that comprise the peptide sequence, three structural regions were made to influence the assembly of PBI cores. Since this process is discussed thoroughly in Chapter 3, the discussion here is reserved for the variations of peptide design, and the rationale to different design aspects of the peptide-PBI conjugates.

The library of compounds synthesised (illustrated in Figure 2.1), shows that the only PBI-derivative that does not possess a peptide sequence is the reference compound, alkyl-PBI **11**. Instead, this compound contains a straight chain alkyl substituent at each imide nitrogen, reducing its chemical functionality so as to prevent a driving of assembly through weak intermolecular interactions, for example hydrogen-bonding (H-bonding) of amide and carbonyl functional groups. Long alkyl chains symmetri-

cally tethered to the PBI core results in a structure comprised of non-polar functionality and is therefore readily soluble in organic solvents. This compound provides a reference for absorption and emission characteristics of isolated PBI chromophores (in chloroform (CHCl_3)). Such information will be utilised in this work when optical spectroscopy is used to probe the aggregation of peptide-PBI conjugates in solution, which is introduced in Chapter 3.

This means that the main design modifications of the library are concerned with the peptide-PBI conjugates. Arguably, the most important design feature of these compounds is the diverse solvation demands imposed by the large hydrophobic PBI core coupled to a hydrophilic peptide, generating amphiphilic character. An implication of this amphiphilic character is that solvophobic forces are expected to aid in driving the self-assembly in aqueous solution, in order to reduce unfavourable interactions. The second design element is concerned with the specific peptide precursor sequence tethered to the PBI core. Peptide segments in this work comprise three key structural features (illustrated in Figure 2.2) and are inspired from reports in the literature regarding self-assembled peptide amphiphiles.⁶ These key structural features are represented in three distinct regions of the peptide sequence. Through changing the amino acid residues in these key regions, the role of the peptide on self assembly can be deduced.

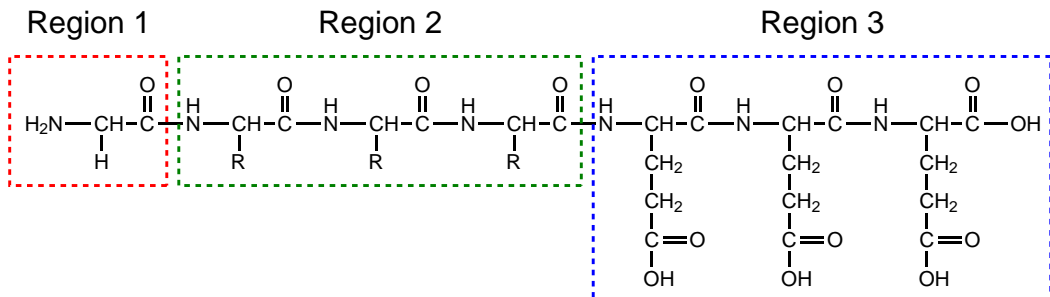


Figure 2.2 Molecular structure of a representative peptide segment showing three distinct chemical regions incorporated in the library of compounds.

One design feature that remains constant in all peptide sequences is the glycine in region 1. This amino acid residue with low steric demand is incorporated at this position in order to reduce possible steric inhibition of the amine condensation between the terminal NH_2 and PTCDA. A sterically bulky group in this position could hinder the rate of nucleophilic attack of the anhydride ring of PTCDA. The second design element is the short amino acid sequence in region 2, which consists of a short peptide sequence that contains amino acids with either a high propensity to form intermolecular hydrogen bonds, or have high steric demands of the side chain.

The third element incorporated into the design of peptide sequences is the addition

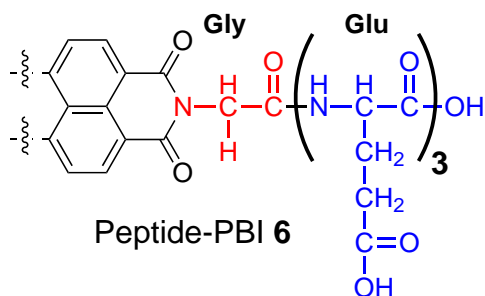
of amino acids with ionisable side chains, in region 3. These groups increase the solubility of peptide-PBI conjugates in aqueous solvents because the ionised form of these groups increases the hydrophilic nature of the compound. As a result, the solubility, and hence the potential driving force of assembly, becomes sensitive to the pH and presence of ions in aqueous solution. Noteworthy, only glutamic acid residues (weak acids, charged at basic pH) were used in region 3 of all peptide-PBI conjugates. The use of weak bases (charged at acidic pH), for example lysine residues, complicates the amine condensation (used in the synthetic procedure) due to each side chain having a terminal NH_2 group. Additional NH_2 groups on the peptide sequence can lead to side reactions due to nucleophilic attack on the anhydride of PTCDA from numerous NH_2 groups.

Figure 2.3 illustrates the modification of the peptide design incorporated into the PBI conjugate library. Peptide-PBI **6** is used as an initial peptide sequence to begin experimental proceedings. There are three types of modifications made to the peptide sequences, namely the incorporation of a region capable of H-bonding (peptide-PBI **7** and **8**), reduced number of ionisable amino acids (peptide-PBI **9**), and increased steric demand close to the PBI core (peptide-PBI **10**). Firstly, the peptide segment in peptide-PBI **6** has the principal exclusion of region two (discussed above) containing only one glycine (Gly) and three glutamic acid (Glu) residues, resulting in the charged amino acid residues being in close proximity to the PBI core. This peptide design aims to examine the influence of ionisable amino acid groups, and if the proximity to the PBI core has any large influence on the nature of aggregates formed.

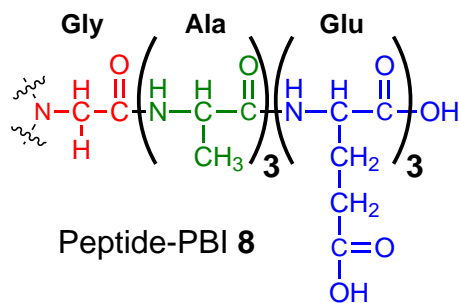
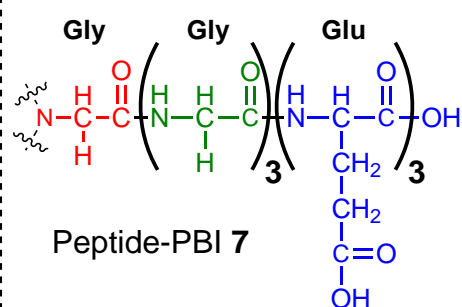
The incorporation of three glycine or alanine (Ala) amino acid residues increases the length of the peptide sequence and introduces a section capable of forming intermolecular H-bonds (*i.e.*, peptide-PBI **7** and **8**). These peptide sequences aim to elucidate the role intermolecular H-bonding has on the self assembly of peptide-PBI conjugates, and whether the addition of this interaction is able to ‘knit’ them together and enhance aggregate formation. Peptide-PBI **9** contains a similar peptide sequence to those with a H-bonding segment, however the notable difference is the reduction in the number of glutamic acid residues (from three to one). This peptide design, with a reduced number of ionisable carboxylic acid groups, aims to elucidate the influence electrostatic repulsion between ionised peptide sequences has on the self-assembly of peptide-PBI conjugates. This can be achieved through comparing the nature of aggregates formed by peptide-PBI **8**, which contains all three glutamic acid residues in the peptide sequence.

The final design modification conducted in this study was the inclusion of leucine

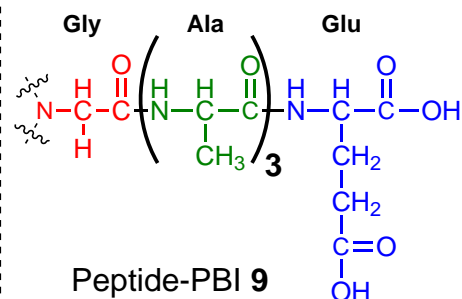
Initial peptide segment



H-bonding segment



Less ionisable groups



Added steric demand

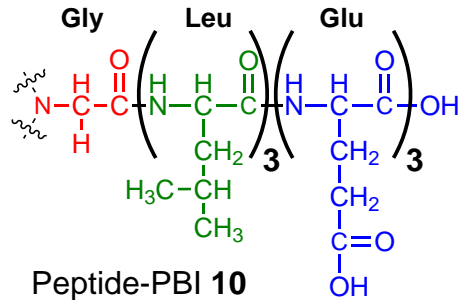


Figure 2.3 Different types of peptide modifications employed in the peptide segment of peptide-PBI conjugates in order to probe the influence the peptide has on PBI assembly.

(Leu) amino acids into region 2 of the peptide, to obtain peptide-PBI **10**. These amino acids contain an isopropyl- (ⁱPr) group, causing moderate steric demands near the PBI core compared to peptide-PBI **7** or **8**. This peptide design aims to deduce what effect increasing the steric bulk has on aggregation. For example, if the aggregation could be hindered or altered in order to accommodate the possible steric interactions. This can be deduced through the comparison of peptide-PBI **7** and **8** aggregates in solution, which lack the steric demands imposed on peptide-PBI **10**.

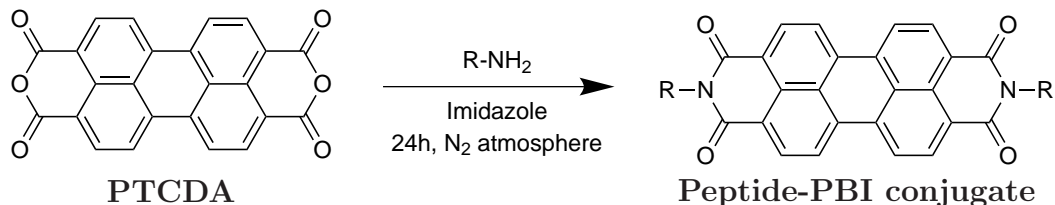
2.3 Synthesis and structural characterisation

The first stage in the synthesis of peptide-PBI conjugates was to synthesise the peptide to later be tethered to the PBI core. This was achieved using fluorenylmethyloxycarbonyl (Fmoc)-mediated solid phase peptide synthesis (SPPS), of which the protocol is well established in the literature.⁴⁹ The general procedure for SPPS involves the stepwise assembly of a peptide through consecutive coupling of amino acid residues, through the use of a solid resin support.

One of the most important advantages of SPPS compared to solution phase synthesis is that the coupling of amino acids to be carried out more rapidly and near completion. This is possible because the reagents used in the coupling reaction can be used in excess, and removed simply by washing after each reaction step. The ability to wash away reagents or cleaved protecting groups largely contributes to the high yields and good purity of peptides obtained via this method.^{71,72} The structural identity of the peptide precursors was confirmed through nuclear magnetic resonance (NMR) and mass spectrometry (MS) techniques, which indicated high purity therefore allowing the peptides to be used in subsequent reactions without further purification.

The next stage of the synthesis of peptide-PBI conjugates was to couple the peptide sequence to a perylene core. This was achieved through the condensation reaction of perylene-3,4,9,10-tetracarboxylic dianhydride (PTCDA) and the primary amine of each peptide precursor (illustrated in Scheme 2.1). This method, developed by Langhals *et al.* in the 1990s,¹⁵ is the most commonly employed approach to synthesise symmetrically *N,N'*-substituted PBI derivatives, and generally involves high reaction temperatures (≥ 140 °C) in solvents such as molten imidazole or quinoline under an inert atmosphere.¹⁸ There is high compatibility between the amine condensation reaction and the peptide (obtained from SPPS), due to the condensation

reaction in principle allowing any molecule possessing a single primary amine to attach to the PBI core. All PBI conjugates were obtained through this procedure, with the R group either being a peptide (for the synthesis of peptide-PBI conjugates) or a alkyl chain (for the synthesis of the reference compound **11**).



Scheme 2.1 Amine condensation of PTCDA with a primary amine, for the synthesis of peptide-PBI conjugates, R=peptide sequence.

The resulting peptide-PBI conjugates were subsequently purified using reverse phase column chromatography, and were obtained in good yields (70–85%, exact yields are presented in Chapter 8). The characterisation of the peptide-PBI conjugate library was made challenging due to the poor solubility of these compounds in many organic solvents, which significantly hindered nuclear magnetic resonance (NMR) and mass spectrometry (MS) experiments. Nevertheless, the structures were confirmed through the combination of 1-D and 2-D NMR, matrix assisted laser desorption ionisation MS (MALDI-MS), and Fourier transform infrared (FTIR) spectroscopy experiments. Key structural characteriation data will be highlighted here, using one peptide-PBI conjugate as an example, namely peptide-PBI **8**.

Firstly, the data obtained from FTIR spectroscopy provides key evidence for the success of the amine condensation with PTCDA. Figure 2.4 shows the FTIR spectrum of peptide-PBI **8** between 2000–400 cm^{-1} , with the key stretching frequencies labelled. This FTIR spectrum shows the disappearance of the characteristic anhydride carbonyl stretching band (1774 cm^{-1}), and the appearance of the *N*-imide carbonyl stretching band at 1661 cm^{-1} . Similarly, the C–O–C stretching band of the anhydride (1025 cm^{-1}) has disappeared and been replaced by the C–N stretching band of the imide at 1366 cm^{-1} . These spectral features indicate the conversion of the anhydride on PTCDA, to an imide on PBI. Additionally, the presence of the characteristic amide II band of secondary N-H bending (1544 cm^{-1}) provides evidence for the presence of the peptide sequence in the material.

This information indicates the success of the PTCDA/peptide condensation reaction. However, further characterisation information was required in order to confirm the structural identity. This was obtained through the use of MALDI-MS, which yielded the expected mass-to-charge ratio for each peptide-PBI conjugate (see Chapter 8). Further supporting evidence was obtained upon performing an MS-MS

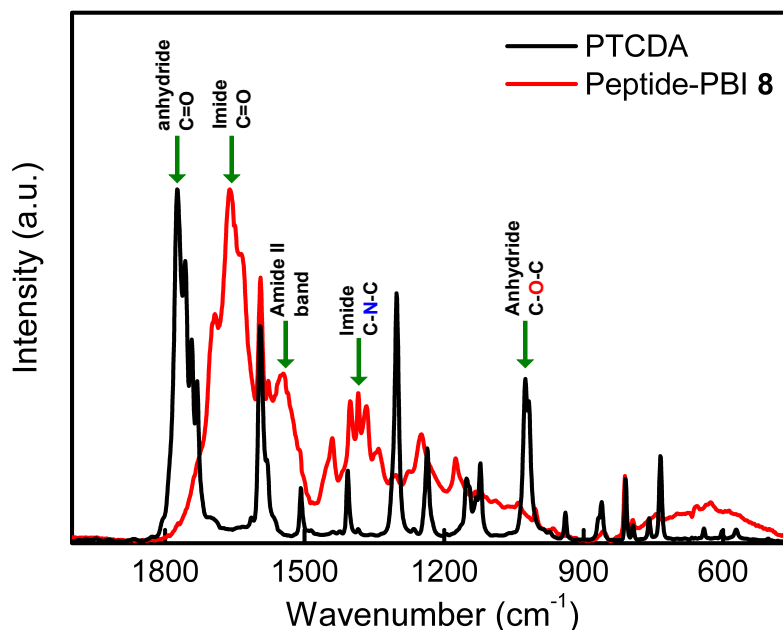


Figure 2.4 FTIR spectrum of peptide-PBI **8** showing the change in stretching frequencies to PTCDA. The disappearance of anhydride stretches and the appearance of imide stretches indicates imide formation.

spectrum and analysing the fragmentation of the peptide-PBI conjugate, which exhibited the expected fragmentation of the peptide sequence. Finally, the structural identity was conclusively confirmed through the use of NMR experiments, in particular through the use of HMBC (Heteronuclear Multiple Bond Correlation), HSQC (Heteronuclear Single Quantum Coherence), and COSY (homonuclear correlation spectroscopy) experiments.

Each of these NMR experiments are 2-dimensional and allow different structural information to be elucidated based on the observations of correlations between atoms in the molecule. A ^1H - ^1H COSY experiment exhibits correlation signals when protons are spin-spin coupled, *i.e.*, a signal is observed when there is a proton-to-proton interaction. In an HSQC experiment, correlations are observed between nuclei of two different types which are separated by one bond. The particular experiment used in this work investigated the correlations between the chemical shift of a proton with the chemical shift of a directly bound carbon. An HMBC experiment differs from an HSQC in that the heteronuclear couplings are detected over a longer range, typically 2–4 bonds. In this work, HMBC correlations between protons and carbons, which are two or three bonds away, were utilised in structure confirmation. Figure 2.5 shows a small section of peptide-PBI **8** (used as an example) highlighting the correlations that confirm the link between the peptide sequence and the PBI core. The connection of these two building blocks is confirmed upon the observation

of an HMBC correlation from the H₅ protons (*i.e.*, the protons attached to C₅) to C₃ (*i.e.*, the PBI carbonyl carbon). For this to be achieved, the first task was to determine the chemical shift of H₅ protons by assigning the chemical shifts along the peptide chain, through the combination of HSQC, HMBC, and COSY data.

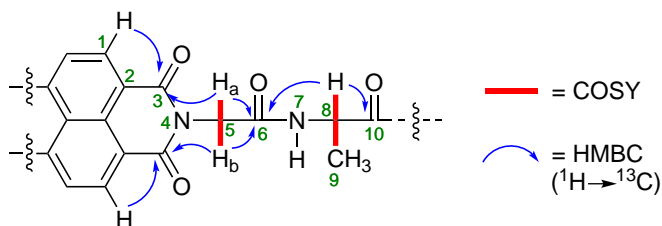


Figure 2.5 Structure of peptide-PBI **8** showing the HMBC and COSY correlations which confirming the coupling of a peptide sequence to the PBI core.

The HSQC correlation between H₈ and C₈ confirmed the direct bond between these two atoms. Furthermore, there was a COSY correlation between H₈ and H₉ protons (methyl group protons), and an HMBC correlation between H₉ and C₈. These correlations indicate that C₈ is part of an alanine residue. The elucidation of the exact alanine residue was achieved through noting an HMBC correlations from H₈ to both C₁₀ and to C₆, consistent with these atoms being two or three bonds apart. Although there were no HMBC correlations observed from H₇ to any neighbouring carbon atoms in peptide-PBI **8**, such correlations were observed in the peptide-precursor (peptide **3**). This leads one to believe that this N–H is still present in the sequence based on the expected mass obtained from MS, and the HMBC from H₈ to C₆, through N₇.

The observation of HMBC correlation from the protons on C₅ (*i.e.*, H_a and H_b) to C₆ show that this glycine residue is the next amino acid along the chain. These two protons show different chemical shifts from one another, which is consistent with the chiral centre at C₈ causing nearby protons to have slightly different chemical environments (causing them to be labelled H_a and H_b). These were both shown to be bonded to C₅ from a HSQC correlation, combined with the presence of a COSY correlation between the two protons. The final stage to confirm the coupling of the peptides to PTCDA was to elucidate a HMBC correlation between H₅ protons, and the C₃ carbon which comprises the carbonyl of the PBI. The chemical shift of C₃ was separated from the carbonyl groups in the peptide sequence through the observation of an HMBC correlation from H₁ (PBI aromatic proton) to C₃. Subsequently, the link of PBI between the peptide sequence was confirmed due to the presence of an HMBC correlation between protons H_a and H_b, and C₃. Although peptide-PBI **8** is used as an example here, the same analysis was carried out to confirm the structure of all other peptide-PBI conjugates in the library, with data presented in the experimental chapter.

2.4 Summary

In summary, this chapter presents the synthetic protocols employed to synthesise a variety of peptide-PBI conjugates via the combination of two well established literature methods. Firstly, the peptide sequences were synthesised using SPPS and obtained in good purity which allowed them to be used without purification. Subsequently, each peptide precursor was tethered to a PBI core via an amine condensation with the PTCDA starting material. By analysing FTIR spectroscopy, mass spectrometry, and 2-D NMR experiments, the structural identity of the peptide-PBI conjugates was confirmed. Additionally, this chapter presents the modification of peptide sequences by exploiting the stepwise assembly of SPPS, in order to allow investigations as to the influence the peptide segment has on the self-assembly of the PBI core. This elucidation is to be achieved by comparing the nature of aggregation upon; inclusion of a section capable of forming H-bonds, reducing the number of ionisable groups on the peptide, and increasing the steric hindrance close to the PBI core.

Chapter 3

Spectroscopic probes of peptide-PBI aggregation

3.1 Introduction

An interesting challenge of supramolecular and materials chemistry is to design organic semiconductors for use as building blocks that can self-assemble to form elaborate superstructures. Often these superstructures are desired because they provide optical and electronic properties not observed by individual units, for example efficient energy transfer along a π -stacked aggregate.⁷³ This is achieved via the electronic coupling between transition dipoles or via effective overlap of π -orbitals.⁷⁴ This work exploits the optical and electronic properties of PBIs in order to monitor the local electronic environment of PBI molecules. The optical properties of perylene are attributed to the large π -conjugated system (*i.e.*, five fused aromatic rings) present in these molecules. Through examining the perturbation of spectroscopic signatures, the application of weakly coupled H- (and J-) aggregate theory makes optical spectroscopy an excellent probe of the nature of perylene assembly.^{19,75,76} The result is that optical spectroscopic signatures can be used to identify the presence of aggregates and determine the geometric configuration of neighbouring chromophores in an aggregate.

This chapter is concerned with exploiting solvent and pH dependent aggregation of peptide-PBI conjugates in order to demonstrate the ability to elucidate the type and extent of aggregation using optical absorption and fluorescence spectroscopy. Spectroscopic signatures of peptide-PBI **6** are highlighted as clear examples. Subsequent work in this chapter investigates the influence the peptide tethered to a PBI

core has on the assembly process. This is achieved by carrying out various spectroscopic measurements as a function of peptide design through the incorporation of an H-bonding region (peptide-PBI **7** and **8**), reduction in the number of ionisable groups (peptide-PBI **9**), and inclusion of sterically bulky groups near the PBI core (peptide-PBI **10**). The results demonstrate that different modes of aggregation are induced by the peptide sequence, with significant influence from the electrostatic repulsions between glutamic acid residues.

3.2 Spectroscopic perturbations observed in PBI core interactions

Due to a hydrophilic peptide sequence being tethered symmetrically to a hydrophobic PBI core, there is diverse functionality present within each peptide-PBI conjugate. This yields a chromophore that has significant amphiphilic character due to the diverse solvation demands. It has been demonstrated in the literature that solvent selectivity can strongly effect self-assembly kinetics, as well as nanostructure assemblies, of amphiphilic PBI derivatives.^{26,32} This section demonstrates the solvent dependence of peptide-PBI conjugate aggregation, with a significant focus on elucidating the nature of aggregates using absorption spectroscopy through the application of the exciton model. Throughout this section, peptide-PBI **6** (((Glu)₃-Gly)₂-PBI) is employed as an example, due to its short peptide sequence being the simplest design.

3.2.1 Promoting monomers vs. semi-crystalline aggregates

To elucidate the influence solvent has on tuning the self-assembly of peptide-PBI conjugates, the spectral characteristics in different solvents were compared to known monomer and aggregate PBI signals. Figure 3.1 shows absorption and emission spectra of peptide-PBI **6** in dimethylsulfoxide (DMSO), acetonitrile (MeCN), and in the solid state. Also included is the absorption spectrum of dilute alkyl-PBI **11** in chloroform as reference of PBI monomers in solution, as reported in the literature.²³ These data illustrates the presence of isolated PBI chromophores of peptide-PBI **6** in DMSO due to a resolved monomer vibronic progression and strong photoluminescence. In contrast, the spectrum in MeCN exhibits pronounced spectral broadening comparable to the absorption in the solid state. This indicates efficient π - π electronic overlap between PBI cores in MeCN, and aggregation.

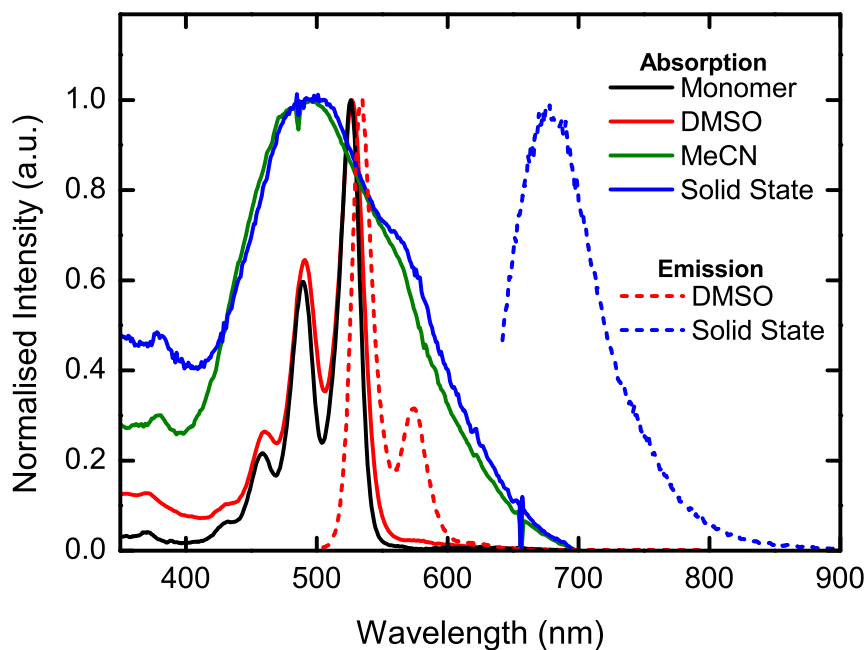


Figure 3.1 Normalised absorption spectra of peptide-PBI **6** (3.0×10^{-6} M) in DMSO, MeCN and in the solid state. Also included is the absorption spectrum of dilute alkyl-PBI **11** (2.0×10^{-6} M) as a PBI monomer reference. Additionally the emission spectra in DMSO and the solid state are presented.

Absorption features of isolated PBI chromophores are evident by pronounced vibronic peaks in the range of 450-525 nm, and a shoulder at 425 nm, as depicted by alkyl-PBI **11** in chloroform. These peaks correspond to the 0-0, 0-1, 0-2, and 0-3 electronic transitions, with the vibronic progression $A_{0-0} > A_{0-1} > A_{0-2}$. Separation of these peaks is approximately 1400 cm^{-1} , caused by the main vibrational mode coupled to an electronic excitation in perylene being the C=C stretch. Monomer emission depicts the same peak structure in a mirror image of the absorption and has high intensity, due to perylene having a near unity fluorescence quantum yield.⁷⁷ The similarity of the absorption and emission spectra of peptide-PBI **6** in the polar aprotic solvent DMSO to that of alkyl-PBI **11** illustrates the predominance of monomers in DMSO solution. These results show that DMSO is able to solvate both the peptide component and the π -face of the PBI core, producing isolated chromophores in solution. On this basis, DMSO is considered a ‘good’ solvent for peptide-PBI **6**.

When peptide-PBI **6** is dispersed in the polar aprotic solvent MeCN, a new absorption band emerges around 565 nm, and the electronic transitions to higher energy levels (0-1 and 0-2) are enhanced in comparison to the 0-0 transition. This pronounced spectral broadening is reminiscent of spectra found in liquid crystalline phases of PBI derivatives,⁷⁸⁻⁸⁰ and therefore indicates long range order with many

chromophores contributing to the formation of an exciton band. It is concluded that MeCN can be considered a poor solvent for peptide-PBI **6**, based on the strong perturbations from the monomer spectrum, indicating the formation of strongly coupled PBI cores and aggregation.

The broad spectrum observed being related to strong π - π electronic overlap is also supported by the same perturbation being observed for peptide-PBI **6** in the solid state, in which the lack of solvent forces significant aggregation. The efficient π - π interactions occurring in the solid state is evidenced from the dramatic photoluminescence quenching which is observed in the emission spectrum. Emission from this thin film provides a low intensity band (note spectra in Figure 3.1 are normalised) which lacks vibronic structure (*i.e.*, is not a mirror image of absorption) and is red-shifted from 535 nm (for monomer emission) to approximately 675 nm. This weakly emissive state is attributed to the emission from excimer states formed between neighbouring PBI cores upon photoexcitation. This assignment is supported by comparison to model cyclophane-PBI derivatives which form permanent aggregates due to two PBI cores being forced into close proximity by covalently bound imide substituents.⁸¹ This causes strong π - π electronic overlap of PBI cores, thereby allowing excimer emission to be characterised.

Based on the conclusion that peptide-PBI **6** forms semicrystalline aggregates in MeCN, it would be expected that emission from these aggregates (data not shown) would display excimer emission. Although there is substantial photoluminescence quenching from these aggregates, the emission spectrum obtained resembles that observed in DMSO in structure and wavelength position, indicating emission from a weakly coupled chromophore. This appears to provide a conflicting result for absorption and emission spectra. However, due to the weak emission intensity observed from an excimer, it is concluded that a small population of poorly coupled chromophores would significantly hinder the resolution of this emission. The use of a spectrofluorimeter with increased red sensitivity is expected to allow the excimer emission to be resolved. However, such an instrument was not available at the time of this study and this investigation was unable to be carried out.

3.2.2 Combination of PBI spectral signatures through solvent tuning

The results discussed in the previous section indicate that self-assembly of peptide-PBI **6** is solvent dependent, as two polar aprotic solvents (DMSO and MeCN) are able to induce different molecular interactions. To further explore this, a solvent

series was chosen in which the solubility of the peptide sequence was reduced by varying the H-bonding ability of the solvent. Figure 3.2 displays the spectra of peptide-PBI **6** in methanol (MeOH), ethanol (EtOH) and isopropanol (IPA). Upon increasing the size of the alkyl chain present on the alcohol, there is a reduction in vibronic structure and concurrently a broadening of the spectrum at longer wavelengths. These spectral features are a combination of monomer and aggregate signatures, illustrating that when the peptide segment is exposed to a poor solvent, aggregation is induced between molecules PBI, causing π - π interactions.

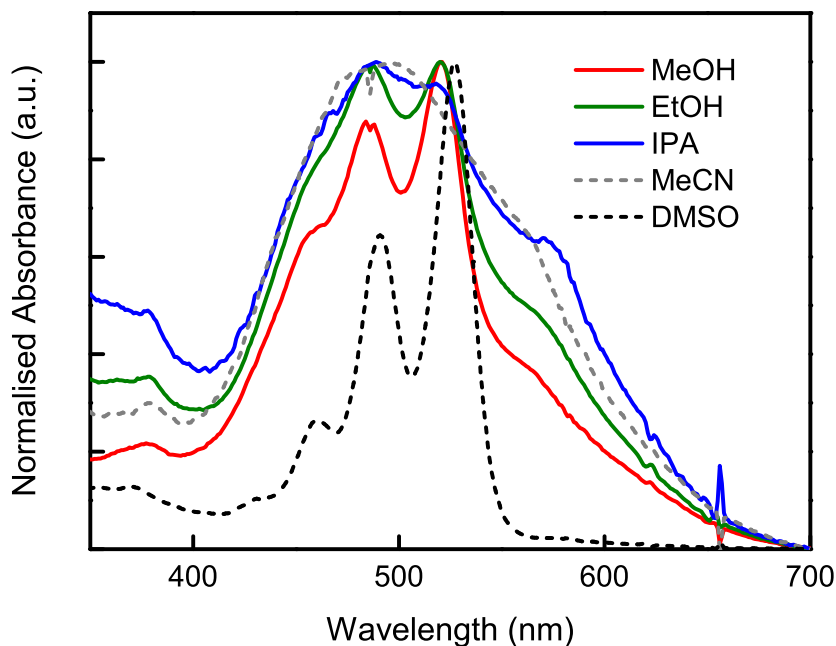


Figure 3.2 Absorption spectra of peptide-PBI **6** (3.0×10^{-6} M) in MeOH, EtOH, and IPA. Also included is the absorption spectrum in DMSO and MeCN for comparison. All spectra are normalised at λ_{\max} .

The series of alcohols were selected to probe the effects of peptide solubility, based on their decreasing ability to form H-bonds with increasing alkyl chain size.⁸² A reduction in H-bonding ability is expected to bring about less favourable interactions between the peptide sequence and the solvent, thus lowering peptide solubility (*i.e.*, peptide solubility is expected to follow MeOH > EtOH > IPA). The spectrum of peptide-PBI **6** in MeOH exhibits vibronic progression which reflects that of monomers, but with an increased absorption at longer wavelengths. Comparing this spectrum to that in EtOH shows an increased amount of spectral broadening, which is increased further in IPA. The appearance of monomeric vibronic progression and a concurrent broadening results from a linear combination of monomer and tightly bound aggregate signatures comprising the absorption spectrum, as evidenced upon comparison with the signatures in DMSO and MeCN.

In MeOH, the balance of solubility requirements are expected to result in favourable interactions with the peptide, and moderately favourable interactions with the PBI core. This is due to MeOH having good H-bonding ability, but also nonpolar character to solubilise the PBI core. The spectral features of MeOH show that there is a significant population of monomers in solution, and a fraction of tightly coupled aggregates contributing to the spectral broadening. From these observations it is concluded that aggregation of the peptide-PBI conjugate is driven by the combination of π - π , and solvophobic interactions, with a large number of chromophores being solvated.

On this basis, one would expect the spectrum in EtOH to exhibit more monomeric features than MeOH, based on the expectation that the longer alkyl chain is able to provide better solubility to the PBI core. However, the broad spectrum obtained does not support this conclusion, indicating that there is a greater drive for aggregation in EtOH. This can be rationalised through the reduced solubility of the peptide sequence on peptide-PBI **6** molecules having less favourable interactions with EtOH than MeOH. This conclusion is supported by the large spectral broadening observed in IPA. The largest alkyl group investigated results in the poorest solvent for the peptide segment, but has good hydrocarbon properties to aid in the solubility of PBI cores. The solvation of π -faces on PBI cores are overwhelmed by the weak H-bonding propensity for the peptides, causing the molecules to undergo aggregation. To this end, the spectrum of peptide-PBI **6** in IPA closely resembles that in MeCN and indicates a large presence of tightly bound aggregates in solution, with the contribution of monomer signatures being small.

The combination of these results show that a linear combination of monomer and semi-crystalline aggregate can be obtained by tuning the favourability of solvent interactions. When the peptide sequence tethered to the PBI core is exposed to a poor solvent, the aggregation is promoted in order to reduce unfavourable solvent-peptide interactions and a strong contribution of strongly coupled aggregates is observed in the absorption spectrum. If the solvent is able to accommodate the solvation demands of both the peptide and the PBI core, then aggregation is driven by π - π interactions, with the resulting spectrum having large monomer signature contributions. These results demonstrate the ability to tune peptide-PBI aggregation through solvent tuning. This principle is explored in greater detail in Chapter 4 through the variation of solvent compositions.

3.2.3 Exciton model applied to aggregates in water

The driving force of self-assembly of amphiphilic molecules in water typically involves the balance between various intermolecular interactions, for example; π - π , hydrophobic, H-bonding, and electrostatic interactions.⁸³ The first three forces generally promote aggregation, whilst interactions between ionised groups can either disrupt (electrostatic repulsion) or induce (electrostatic attraction) aggregation of molecular building blocks in solution. A corollary of tuning the favourability of interactions between solvent and peptide-PBI conjugates is to select a solvent that is good for the peptide, but poor for the PBI core, for example water.

Figure 3.3 shows the absorption spectrum of peptide-PBI **6** in distilled water, illustrating the formation of aggregates in solution due to absorption at longer wavelengths.¹³ Also observed is a redistribution of the vibronic progression (compared to the monomer progression) to yield a reversal in peak intensities, *i.e.*, $A_{0-1} > A_{0-0}$. The comparison of the spectrum of peptide-PBI **6** in water with MeCN and DMSO illustrates that there is some contributions of monomer and semicrystalline signatures. However, no linear combination of these two signatures can account for the redistribution of vibronic intensity, indicating that the nature of the aggregate is significantly different from the semicrystalline state observed in MeCN. The redistribution of oscillator strength can be explained by application of the molecular exciton model for dimer aggregates.^{84,85}

This model applies a point-dipole approximation and predicts that coupling of transition dipole moments creates two new exciton states due to effective π - π electronic coupling. This model treats the dye aggregates as a dimer and can be applied to explain the characteristic spectral features which occur for H- and J-aggregates. Both these aggregates are cofacial with parallel transition moments, but have different types of geometric distortions between the chromophores. Two chromophores in a J-aggregate configuration have a translation offset, whilst an H-aggregate configuration involve cofacially stacked chromophores with no slip.

An energy diagram for these two types of aggregates is shown in Figure 3.4 and illustrates the optical transitions of these cofacial aggregates. For an H-aggregate, the transition from the ground state to the upper exciton state is fully allowed, with the dimer possessing an overall dipole moment. In contrast, the transition from the ground state to the lower exciton state is forbidden due to the transition dipole of each chromophore being out of phase, causing no net dipole moment for the dimer. The exact opposite argument is used to explain the allowed/forbidden transitions in a J-aggregate.

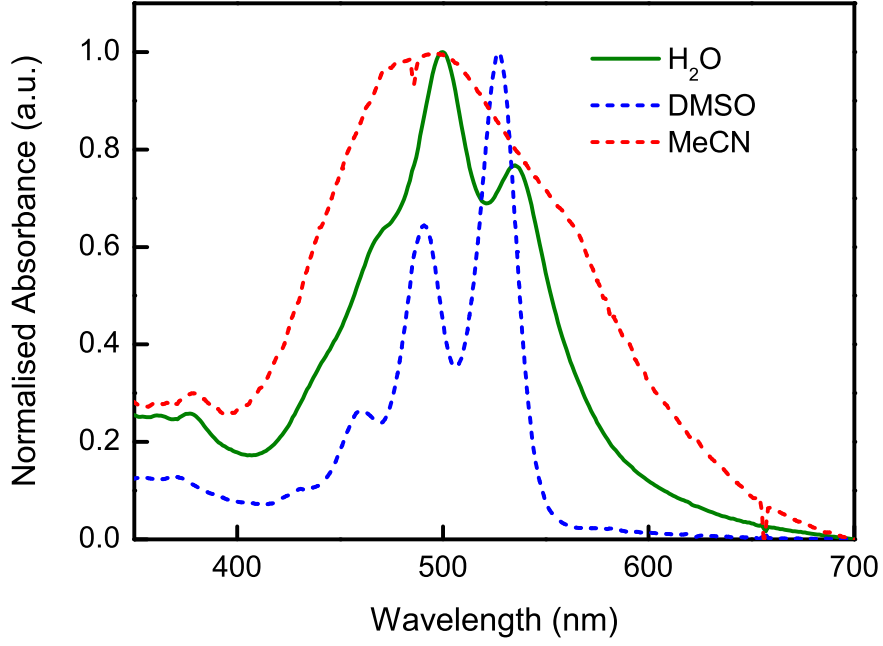


Figure 3.3 Absorption spectra of peptide-PBI **6** (3.0×10^{-6} M) in distilled water. Also included is the absorption spectrum in DMSO and MeCN for comparison. All spectra are normalised at λ_{\max} .

The arguments applied to the transitions from the ground state to a particular exciton state being allowed or forbidden in Figure 3.4 are based on strongly coupled H- and J- aggregates. In other words, for the H-aggregate reasoning, the transition dipoles of each chromophore are considered perfectly parallel to one another. Whilst in a J-aggregate, the transition dipoles are still parallel but are in phase with one another. These assumptions are useful for conveying the concepts of the exciton model, however these assumptions can break down when applied to weakly coupled aggregates (*i.e.*, not perfectly parallel, or not perfectly in phase). In such situations, a more rigorous application of the exciton model needs to be applied. The derivation and detailed description of the exciton model is omitted here, but the reader can find such details in the literature.^{84,86} One important prediction obtained from the exciton model is that the exciton splitting energy (2ϵ) that results from two interacting molecules is dependent on the relative orientation and distance between the chromophores. The exciton splitting energy, ϵ is given by equation 3.1:²⁰

$$\Delta\epsilon = 2\epsilon = \frac{2|\vec{\mu}|^2}{4\pi\epsilon_0 r^3}(\cos\varphi - 3\cos^2\theta) \quad (3.1)$$

where $\vec{\mu}$ is the transition dipole moment of the monomer, ϵ_0 the permittivity of a vacuum, r the distance between the centres of the two interacting molecules, and φ and

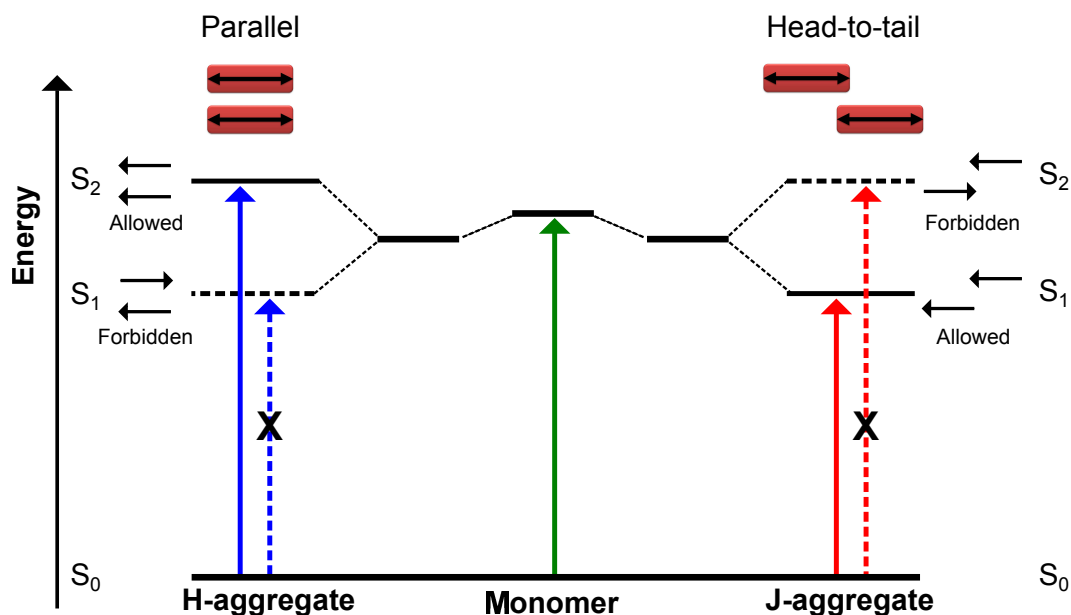


Figure 3.4 Energy diagram for aggregated dimers with coplanar transition dipoles, depicting the allowed and forbidden transitions to H- and J- aggregates based on the dipole phase relations.

θ are the rotational and slip offsets, respectively, between adjacent chromophores. This clearly shows the dependence the exciton splitting energy has on the relative orientation (and distance) of the interacting chromophores. An energy diagram of the exciton splitting for an H-aggregate is shown in Figure 3.5, illustrating the energetic splitting with constant slip angle ($\theta = 90^\circ$) as a function of rotational offset, φ . This shows that although the transition to the lower exciton state is usually forbidden in an H-aggregate, if there is a rotational displacement between cofacial chromophores (*i.e.*, a weakly coupled H-aggregate), the transition can gain oscillator strength by coupling to a vibrational mode (*i.e.*, the 0–1 becomes allowed). However, the zero vibration transition to the lower exciton state is forbidden, as it cannot gain oscillator strength by coupling to a vibration.¹⁹

Based on the predictions depicted in the energy diagram, the absorption spectrum of peptide-PBI **6** in water is indicative of weakly coupled H-aggregates being formed, due to the redistribution of oscillator strength to higher energy, and a relative weakening of the 0–0 vibronic peak. This type of aggregate is rationalised in distilled water based on the minimization of hydrophobic interactions in this cofacial arrangement, whilst electrostatic repulsions between ionised glutamic acid residues promote rotational displacement (pK_a glutamic acid side chain in water is approximately 4.2).⁸⁷ Although these repulsive forces favour the formation of monomers in solution, the large hydrophobic demands of the PBI core means these interaction forces are balanced in a twisted aggregate. Chapter 5 will further elucidate the effects electrostatic repulsion imparts on peptide-PBI aggregates.

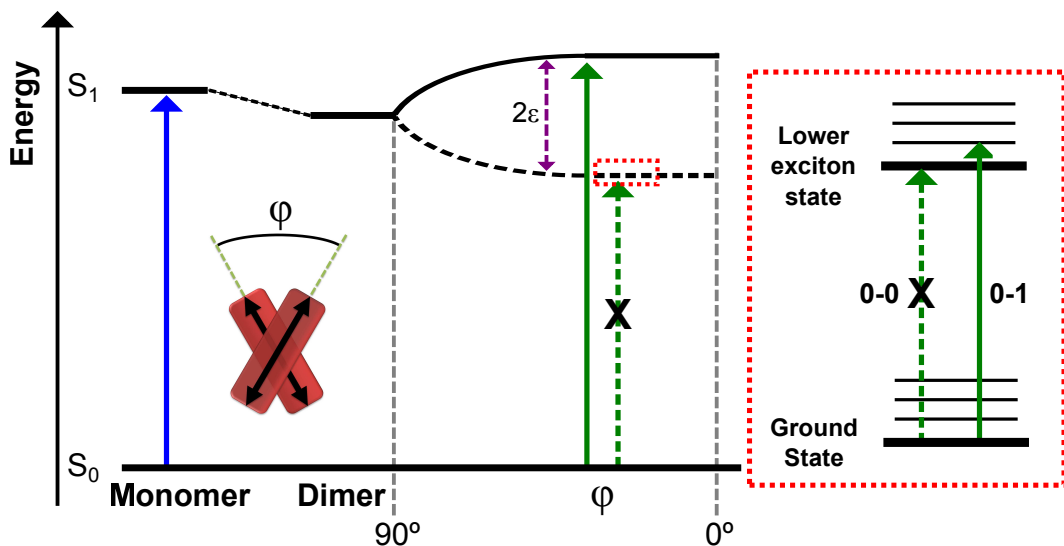


Figure 3.5 Energy diagram for aggregated dimers with transition dipoles with a rotational displacement (φ), illustrating the effects of twisting between adjacent chromophores on the transition energy and exciton splitting, ϵ . In this depiction, the translation component of equation 3.1 is constant, *i.e.*, $\theta = 90^\circ$. Box on the right depicts the transition to the lower exciton state gaining oscillator strength by coupling to a vibrational mode.

The exciton model has therefore allowed the elucidation of the extent of electronic coupling between PBI chromophores between peptide-PBI conjugates. The conclusion that there is a weakly coupled H-aggregate in solution is supported by similar spectroscopic signatures reported in the literature for model covalently bridged PBI dimers.^{24,88,89} These model PBI dimers follow the predictions made by the exciton model, showing that when adjacent chromophores have a limited twist there is a relative weakening of 0-0 peaks, with redistribution to the 0-1 band. Additionally, these studies show that by increasing the twisting between chromophores, through the incorporation of sterically bulky substituents, the effective coupling is decreased and the 0-0 transition recovers. Additionally, the exciton model indicates that the ratio of the 0-1 vibronic peak in relation to the 0-0 vibronic peak allows for insight into the extent of electronic coupling between adjacent PBI cores. To this end, the vibronic peak ratio of peptide-PBI **6** in distilled water was compared to the vibronic peak ratio observed in DMSO, summarised in Table 3.1.

Table 3.1 Vibronic peak ratios of peptide-PBI **6** in water and DMSO showing the change upon H-aggregate formation.

Solvent	Vibronic Peak Ratio ($\frac{A_{0-1}}{A_{0-0}}$)	Nature of molecules
Distilled water	1.38	Weakly coupled H-aggregate
DMSO	0.61	Isolated chromophores

Firstly, it is observed that the vibronic ratio of 0.6 for peptide-PBI **6** in DMSO reflects that of isolated chromophores in solution. Therefore, any ratio higher than

this can be considered to have some degree of cofacial pairing between chromophore transition dipoles. Peptide-PBI **6** in distilled water shows a significant increase in the vibronic peak ratio, consistent with cofacial interactions between chromophores. Upon aggregation in distilled water, the electrostatic repulsions between ionised glutamic acid residues on each peptide-PBI conjugate are in close proximity to their respective PBI cores, due to the short peptide sequence. In order for the aggregate to accommodate this, there is an increased twist between adjacent chromophores. However, this alone would cause a reduced excitonic coupling as the aggregates would become rotationally displaced and appear close to a monomer ratio. On the other hand, twisting of neighbouring molecules would expose PBI cores to water, which is a highly unfavourable interaction. Therefore, the twisting of an H-aggregate in peptide-PBI chromophores is a balance of these two forces acting on the system. This geometric information that we are able to infer from the optical signatures cannot easily be obtained by other experimental methods, such as nuclear magnetic resonance (NMR) spectroscopy or X-ray scattering techniques.

3.2.4 Tuning aggregates through pH changes

To investigate the extent of modulation from electrostatic repulsion, the pH of the solution is changed in order to observe the pH sensitivity of aggregates. Figure 3.6 shows the absorption and emission spectra of peptide-PBI **6** in distilled water (approximately pH = 7) and dilute HCl (approximately pH = 3) at acidic pH. At low pH values (*i.e.*, pH \lesssim 4) the carboxylic acid on the glutamic acid side chain is protonated, based on the pK_a in water (approximately 4.2). When the pH value is decreased (to acidic), there is a loss of vibronic peak resolution and spectral broadening in the absorption spectrum, while significant photoluminescence quenching is observed in the emission spectrum. These spectral changes indicate that when the glutamic acid residues are protonated, there is an increase in effective π - π electronic overlap of adjacent chromophores. Furthermore, at acidic pH the H-aggregate vibronic peaks are diminished, resulting in a signature reminiscent of semicrystalline aggregates in solution, similar to that observed in MeCN.

The lack of ionised glutamic acid residues reduces the electrostatic repulsions between peptide segments, hence the removal of the dominant driving force for cofacial twisting of the H-aggregate. A result of this is that the twisting between adjacent PBI chromophores is diminished, thus adjacent chromophores obtain efficient π -orbital overlap. This is apparent in the absorption spectrum of peptide-PBI **6** in acidic solution resembling similar spectroscopic features of peptide-PBI **6** in MeCN, indicating semicrystalline aggregates.

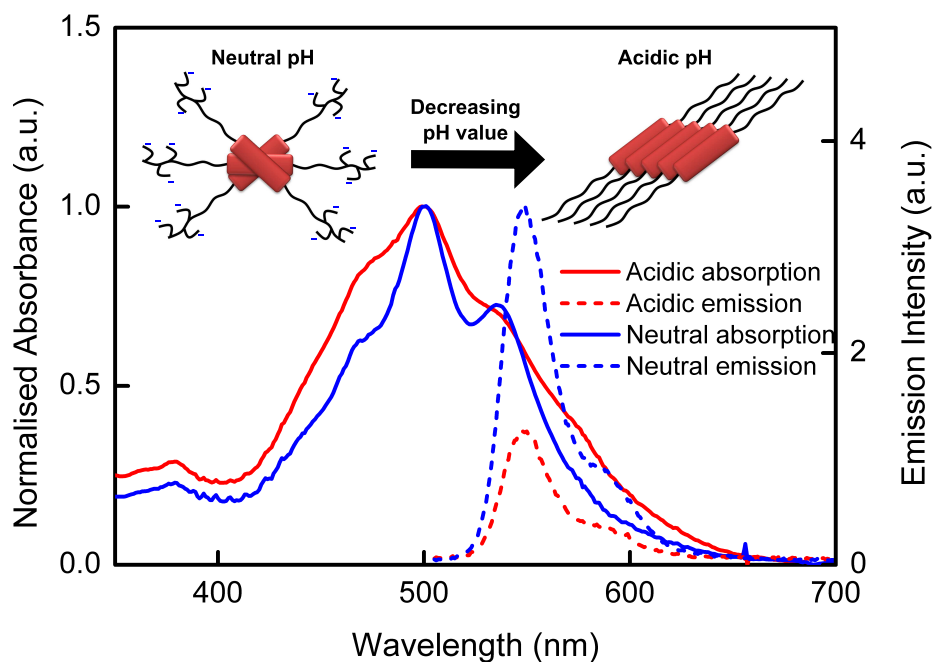


Figure 3.6 Absorption (solid line) and emission (dashed line) of peptide-PBI **6** (3.0×10^{-6} M) in neutral (distilled water) and acidic (1×10^{-3} M HCl) solution. Absorption spectra are normalised to λ_{max} , the excitation wavelength for emission was 500 nm. Also depicted is a schematic illustrating the formation of tightly coupled aggregates at acidic pH due to the lack of electrostatic repulsion between glutamic acid residues.

Supporting evidence for stronger interactions occurring in acidic solution, compared to neutral pH, is obtained from the emission spectra. The photoluminescence quenching which occurs in acidic solution is indicative of effective π - π electronic overlap of neighbouring PBI cores. Both neutral and acidic solution have emission spectral signatures of monomer emission. However, both these solutions see a dramatically reduced emission intensity compared to that of known monomer emission (*i.e.*, alkyl-PBI **11**, not shown). Such emission may be expected from a weakly coupled H-aggregate, *i.e.*, in distilled water, however tightly bound aggregates would be expected to produce excimer emission (see above). This monomer-like emission signature can be rationalised through the apparent solubility of peptide-PBI **6** in acidic solution. Upon dispersion of peptide-PBI **6** in acidic solution, the loss of ionised glutamic acid residues will reduce the solubility in water, increasing the impetus for aggregation. However, the presence of monomer emission indicates the presence of some monomers in solution, but likely not very many due to the hydrophobicity of the molecules. Nevertheless, emission from the monomers hinders resolution of excimer emission due to its weakly emissive nature.

To further investigate the effect changing the pH can impart on the self-assembly

in solution, cryogenic scanning electron microscopy (cryo-SEM) was performed in neutral and acidic solutions. Figure 3.7 presents cryo-SEM images of peptide-PBI **6** at neutral pH (distilled water). These images show the presence of well defined self-assembled nanofibres present in solution, on a micrometer length scale dimension. These fibres form an elaborate branched network with the thickest sections having a width of approximately 300 nm. Upon splitting into a branched fibre, the width is reduced to less than 100 nm. The absorption spectrum of peptide-PBI **6** in distilled water indicates the presence of weakly coupled H-aggregates. Combined with the cryo-SEM images, it can be concluded that these H-aggregates are self-assembled into a fibre network with long range order.

Figure 3.8 shows the cryo-SEM images for peptide-PBI **6** in acidic solution. The preparation of acidic solution cryo-SEM samples was identical (*e.g.* same volume, concentration, and etching procedure) to that used for the collected neutral solution images. This allows for direct comparison of the samples as only one variable has been changed, the pH value. The images obtained in acidic solution show the complete absence of fibre structures, and instead disordered, clump-like aggregates are present. There appears to be no long range order in this system, due to no obvious interaction occurring between aggregates in the cryo-SEM images.

The absence of electrostatic repulsion between glutamic acid residues, has been shown in the absorption spectrum to allow stronger electronic overlap between PBI cores due to spectral broadening. Furthermore, the inherent solubility of the molecule is also affected because removing the number of ionised groups will increase the dominance of the hydrophobic force. Clusters of strongly coupled aggregates present at acidic pH can be rationalised based on the combination of a reduced disruption of aggregation, and the minimisation of unfavourable hydrophobic interactions in the solvent.

The appearance of branched fibre motifs of PBI derivatives have recently been reported by Rybtchinski *et al.* .^{90,91} The fibres formed in such studies were formed through tuning the solvent environment to exploit the combination of hydrophobic interactions and intermolecular H-bonding. This resulted in PBI derivatives forming a three-dimensional network of bundled fibres, which were able to trap solvent molecules to form an organogel. The authors were able to investigate how the structures were ordered by performing cryogenic transmission electron microscopy (cryo-TEM). This elucidation is possible through cryo-TEM because dark-regions represent a tightly stacked conjugate system, possessing high electron density, whilst lighter-contrast areas represent a solvated hydrophilic environment.⁹²

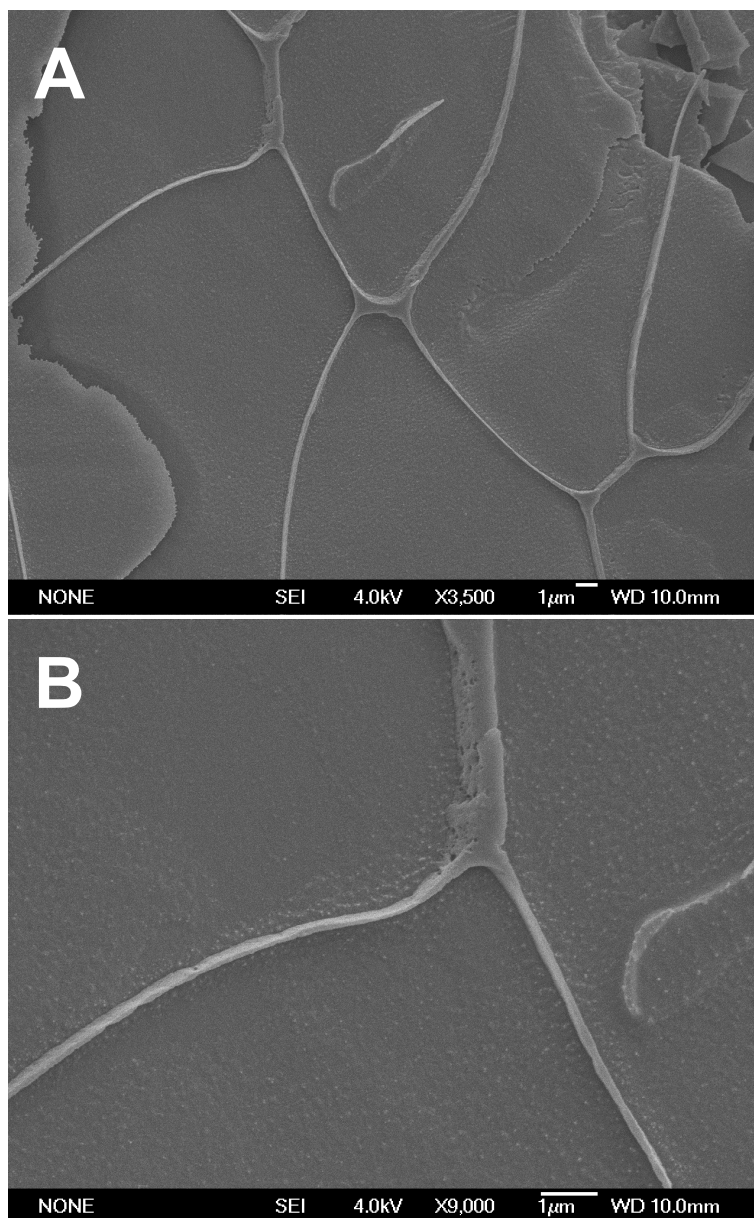


Figure 3.7 Cryo-SEM images of peptide-PBI **6** (0.26 wt%) in distilled water (pH \approx 7) showing the extended network of branched fibres formed through the self-assembly of weakly coupled H-aggregates in solution.

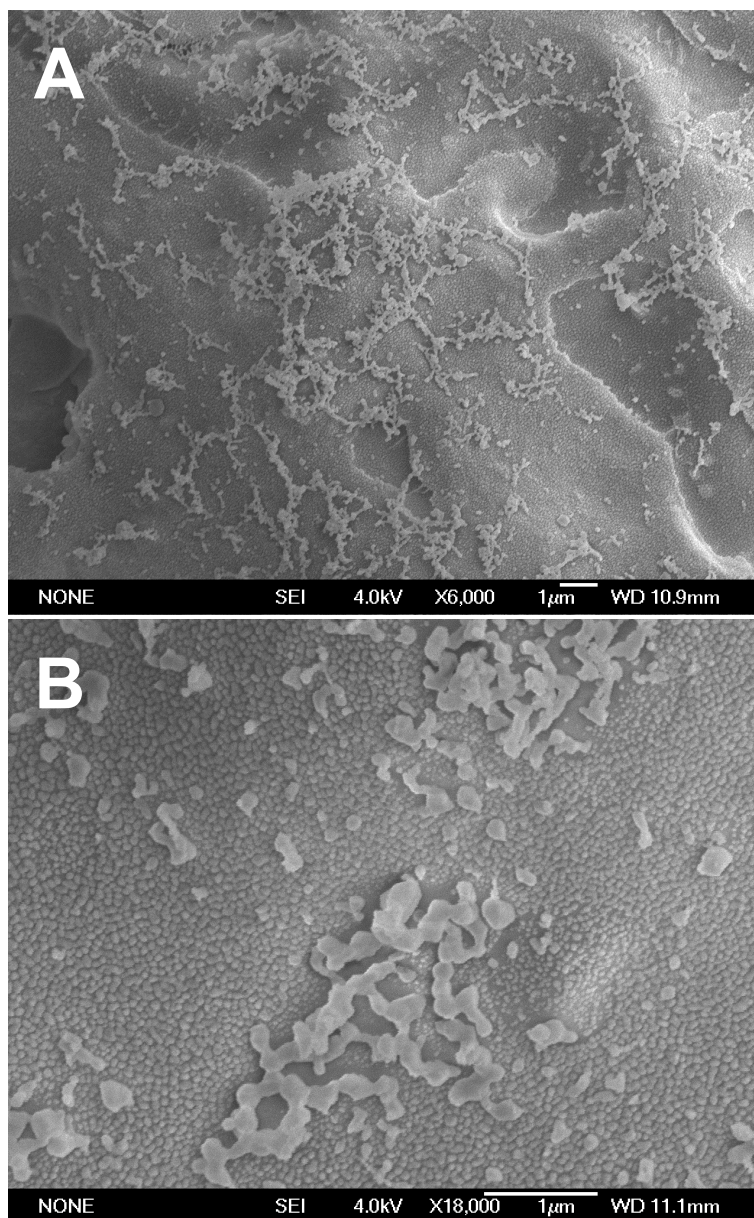


Figure 3.8 Cryo-SEM images of peptide-PBI **6** (0.26 wt%) in dilute HCl (1×10^{-3} M, pH ≈ 3) showing the lack of long range order present in the tightly bound, semicrystalline aggregates in solution.

Unfortunately, no cryo-TEM capabilities were available throughout this work so no further investigation of peptide-PBI **6** fibres could be obtained. However, cryo-TEM images of the peptide-PBI conjugate library are currently being investigated through collaboration with the Rybtchinski group, but will not be obtained in time to be included in this work. Cryo-TEM images should aid in determining the alignment of peptide-PBI conjugates (*e.g.* molecular alignment down the length, or across the width of the fibre). Furthermore, investigation as to what causes branching of the fibres could provide insight into the non-covalent intermolecular interactions that contribute to the directional assembly.

3.3 Effects of peptide sequence on aggregation

The previous section demonstrated the use of optical absorption and emission spectroscopy to elucidate the type and extent of aggregation in solution, via probing the π - π electronic coupling of PBI chromophores. In order to investigate what effect the peptide sequence imparts on the aggregation, spectroscopic measurements were carried out for a range of peptide-PBI conjugates depicted in Figure 3.9. This section explores the effects of incorporating certain design features into the peptide sequence, namely; the inclusion of an H-bonding region (peptide-PBI **7** and **8**), reducing the number of ionisable groups (peptide-PBI **9**), and introducing sterically bulky amino acid residues (peptide-PBI **10**).

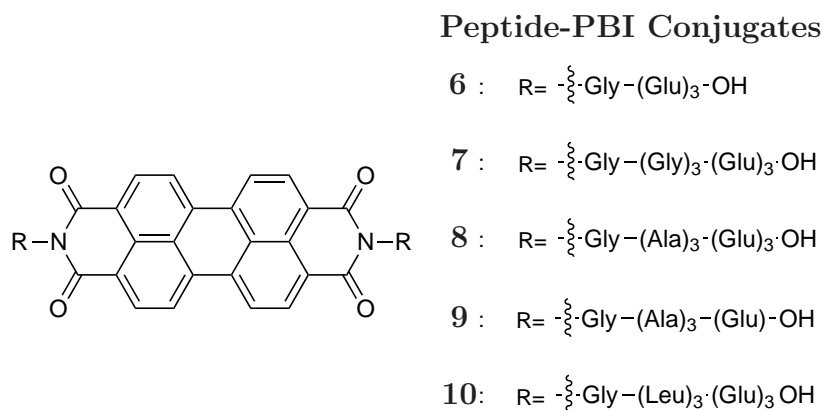


Figure 3.9 Key peptide-PBI conjugates illustrating the various design features employed to elucidate the influence the peptide segment has on the self-assembly.

3.3.1 Incorporation of an H-bonding section

In order to probe what effects H-bonding can have on the assembly of peptide-PBI conjugates, the peptide segment was extended to include three amino acid

residues capable of forming intermolecular H-bonds, namely glycine (peptide-PBI **7**) or alanine (peptide-PBI **8**). Figure 3.10 shows the absorption spectra of peptide-PBI **8** in DMSO, acidic and neutral water, and MeCN. These results show the appearance of a monomer vibronic progression in DMSO, a broad, featureless absorption in MeCN and acidic water, and a characteristic redistribution of oscillator strength to yield an inverted vibronic progression in neutral water. The inset displays the circular dichroism (CD) spectra in DMSO and neutral water, showing the absence of spectral features in DMSO and the appearance of a bisignate signature in neutral water. These results demonstrate that the solvent dependent aggregation remains in peptide-PBI conjugates upon the inclusion of a H-bonding section.

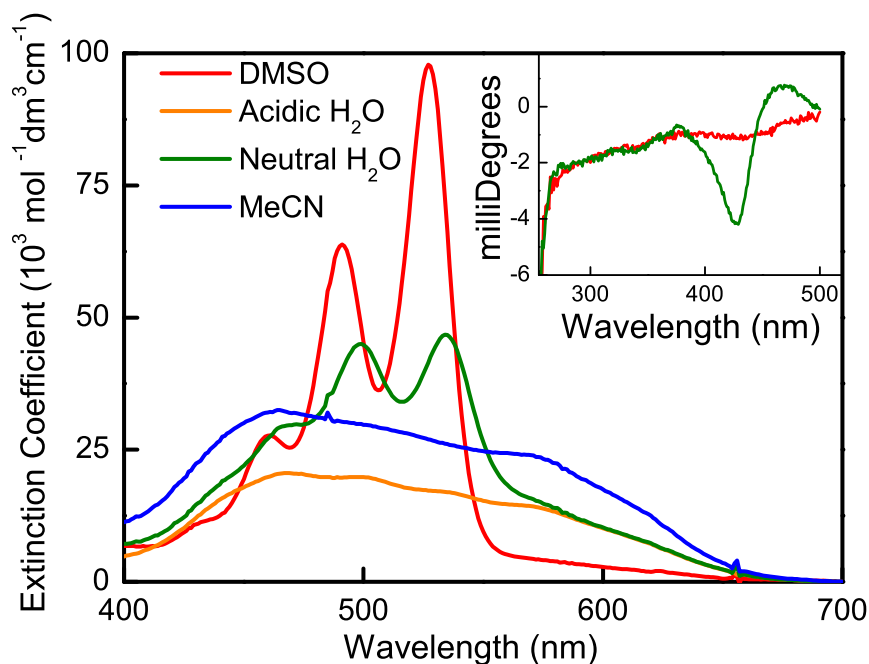


Figure 3.10 Absorption spectra of peptide-PBI **8** (3.0×10^{-6} M) in DMSO, acidic H₂O, neutral H₂O and MeCN. *Inset:* CD peptide-PBI **8** in DMSO and neutral H₂O, showing the formation of chiral aggregates in neutral H₂O induced through the chiral peptide tethered to the PBI core.

The spectral signatures of peptide-PBI **8** in DMSO reflect isolated chromophores in solution, due to the appearance of the characteristic vibronic progression, which was also observed in the absence of a region capable of H-bonding (*e.g.* peptide-PBI **6** in neutral water). Therefore, DMSO remains a good solvent for the peptide-PBI conjugate as it satisfies all solvation requirements of the molecule. The spectra of peptide-PBI **8** in MeCN and acidic water are very similar to those observed for peptide-PBI **6** in the same solvents which were comparable to the spectral signatures observed in the solid state. This indicates that the region potentially capable of H-bonding does not hinder the formation of semicrystalline aggregates in MeCN or acidic water. Note, the difference in extinction coefficient observed between acidic water and MeCN for peptide-PBI **8** is likely caused by the reduced solubility in

these solvents, which can result in a precipitation during the experiment producing changes in the concentration of solute in solution.

Interestingly, peptide precursor **3** (NH₂–Gly–Ala–Ala–Ala–Glu–Glu–Glu) which is the parent peptide of peptide-PBI **8**, formed a self-supporting gel in MeCN. This was evident through the ‘inversion-of-the-vial’ method which has been utilised in peptide amphiphile gelation studies.⁹³ The formation of a self-supporting gel is typically caused by the formation of a network of fibres, through extensive intermolecular interactions, which traps solvent molecules.^{60,61} This organogelation of peptide **3** in MeCN suggests that the tendency of the peptide to self-assemble into fibres through the formation of H-bonds, may drive the formation of the extended semicrystalline aggregates of peptide-PBI **8** in MeCN.

An interesting observation upon the inclusion of a H-bonding region is obtained in the CD spectrum of peptide-PBI **8**, shown in Figure 3.10. This shows the appearance of a bisignate signature which is indicative of a chiral aggregate in water. Furthermore, this feature appears in the region of PBI absorption which is indicative of chiral exciton coupling between PBI chromophores.⁹⁴ From this result, it is determined that the inclusion of chiral amino acid residues (*i.e.*, alanine) close to the PBI core are able to induce the formation of a chiral aggregates in distilled water. This is supported by the fact that no exciton couplet signature is observed from the isolated chromophores (in DMSO), or for peptide-PBI **7** (containing achiral glycine residues) in any solvent (data not shown). Additionally, the chromophores in water are arranged in a right-handed helix, based on the sign of the CD-couplet (negative to positive with increasing wavelength).³³

Chiral aggregates belong to an interesting class of PBI-aggregates, which are receiving considerable attention in the literature,^{33,34,95} due to their promise for application in novel optoelectronic applications.^{96,97} Although CD signatures presented in this work demonstrate the formation of these chiral structures, this avenue requires further investigation which falls outside the scope of this work. For example, only the naturally occurring L-alanine residue was employed in this investigation. In order to confirm that this residue imparts the chirality, D-alanine should be incorporated, which should yield the opposite handedness of the aggregate helix (*i.e.*, the inverted CD-couplet).

We now turn to the absorption spectrum of peptide-PBI **8** in water, which exhibits a redistribution of vibronic peak intensity to higher energy (*i.e.*, weakening of the 0-0 transition compared to the 0-1 transition). These data is consistent with the formation of a weakly coupled cofacial H-aggregate in solution, determined via the

application of the exciton model (see above). An important result of this H-aggregate configuration is that important information can be gained from comparing vibronic peak ratios of different compounds (*i.e.*, the relative rotational displacement between chromophores). To interrogate the effect the incorporation of an H-bonding segment has on self-assembly, the vibronic peak ratio ($\frac{A_{0-1}}{A_{0-0}}$) for peptide-PBI **7** and **8** were compared to peptide-PBI **6** in distilled water. The vibronic ratios of these conjugates are summarised in Table 3.2 and indicate there is a tuning of twisting between chromophores upon H-bonding amino acid incorporation.

Table 3.2 Vibronic peak ratios of peptide-PBI **6**, **7** and **8** in H₂O and alkyl-PBI **11** in chloroform as monomer reference.

PBI derivative	Vibronic Peak Ratio ($\frac{A_{0-1}}{A_{0-0}}$)
(Glu–Glu–Glu–Gly) ₂ – PBI (6)	1.38
(Glu–Glu–Glu–Gly–Gly–Gly–Gly) ₂ – PBI (7)	1.22
(Glu–Glu–Glu–Ala–Ala–Ala–Gly) ₂ – PBI (8)	0.86
(C ₁₂ H ₂₅) ₂ – PBI (11)	0.61

Recall that for peptide-PBI **6** the large vibronic peak ratio was rationalised through the balance of electrostatic repulsion of the short peptide, and unfavourable solvation of the hydrophobic PBI core. Comparison of the resulting vibronic peak ratio to the two peptide–PBI conjugates which contain H-bonding amino acids shows a decreased magnitude of the ratio. This indicates a decreased amount of π – π interactions of neighbouring PBI cores, implying a greater twisting of the H-aggregate. One immediate inference obtained from this comparison is that there is no evidence of H-bonding being able to ‘knit together’ the PBI chromophores. Formation of H-bonds between molecules would be expected to reduce the twisting of aggregates, due to the added driving force of assembly. Due to the inverse alteration being observed, the potential formation of H-bonds is likely overwhelmed by the electrostatic repulsion between ionised glutamic acid residues. The increased twist observed upon the inclusion of an H-bonding region can be rationalised by the extended length of the peptide which generates more hydrophilic character tethered to the PBI core. The presence of hydrophilic amino acid residues is therefore likely to aid in solvation close to the aromatic core, therefore the balance of forces causing the twist is dominated by electrostatic repulsion.

Although we do not find evidence that H-bonding drives twisted aggregation, we do observe a difference between the two types of H-bonding amino acids incorporated. This difference can be explained through considering the side chain present in these amino acid residues (*e.g.* either an H, or a CH₃ group). The difference in side chain can generate different effects in two ways. Firstly, due to glycine residues having a slightly higher propensity to form β -sheets than alanine residues,⁹⁸ the presence

of glycine amino acids in the H-bonding section could allow the formation of some H-bonds, which are formed stronger than the alanine derivative. This could cause a slight reduction in twisting between adjacent chromophores. Secondly, the greater degree of twisting observed with peptide-PBI **8** over peptide-PBI **7** could simply be explained by the additional steric demands of the CH₃ group in alanine residues. The exact reason is unable to be determined and is likely to be a combination of these factors.

3.3.2 Reducing the number of ionisable groups

The appearance of weakly coupled H-aggregates being formed in water for peptide-PBI conjugates, indicate that electrostatic repulsion between ionised glutamic acid residues influences the aggregation significantly in water. In order to investigate the role electrostatics have in imparting a twist between chromophores within aggregates, the effects observed upon reducing the number of ionisable groups on the peptide segment was studied. This was achieved by the synthesising peptide-precursor **4** (Glu-Ala-Ala-Ala-Gly-NH₂) containing only one glutamic acid residue, instead of three used previously in this work.

Figure 3.11 shows the absorption spectrum of peptide-PBI **9** ((Glu-Ala-Ala-Ala-Gly)₂-PBI) and peptide-PBI **8** in distilled water. These data illustrates that upon reducing the electrostatic repulsion between peptide sequences there is a substantial weakening of the 0-0 vibronic transition. These spectral features are consistent with H-aggregate formation, allowing important information to be obtained on the twisting between neighbouring chromophores from the vibronic peak ratio.

Recall that the twist present in H-aggregates of peptide-PBI conjugates is a result of a balance between hydrophobicity of the PBI core, and electrostatic repulsion between glutamic acid residues. In peptide-PBI **9** the electrostatic repulsion between peptide segments is reduced, based on the reduction in the number of ionisable groups from three to one (per peptide sequence). Therefore, any effect this has on the nature of the aggregate can be deduced through the analysis of the vibronic peak ratio.

Table 3.3 shows the vibronic peak ratio for these spectra and shows that there is a greater vibronic ratio of peptide-PBI **9** than peptide-PBI **8**. The increase in vibronic ratio observed is rationalised by the reduced electrostatic repulsion that drives rotational distortion. This effectively pushes the balance of forces in favour of the hydrophobic effect, in which a lower degree of twist in a cofacial configuration

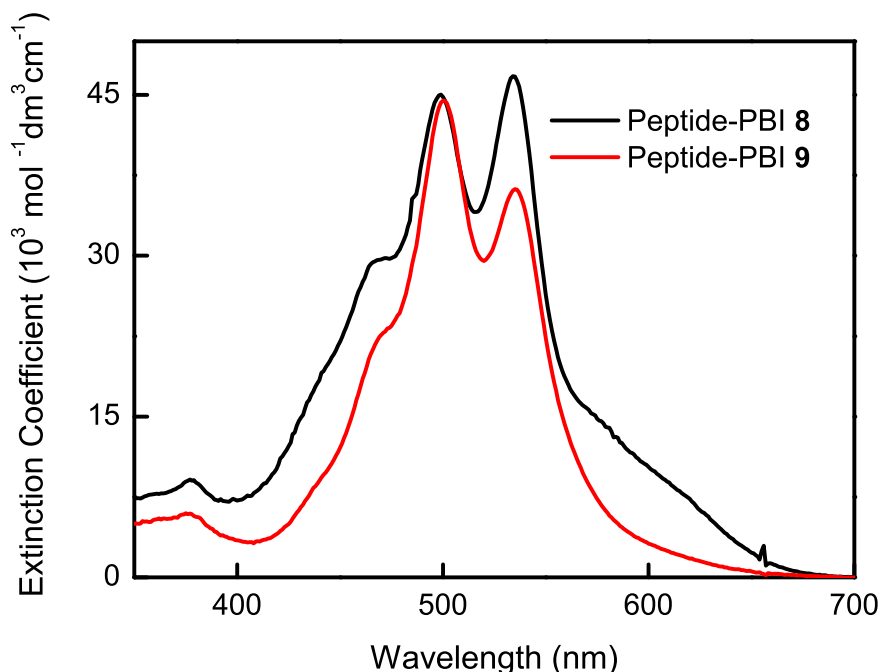


Figure 3.11 Absorption spectra of peptide-PBI **8** and **9** (3.0×10^{-6} M) in distilled water.

provides a minimisation of hydrophobic interactions in water. These results demonstrate the tuning of the aggregate structure through modulating the electrostatic repulsions between glutamic acid residues. This approach to controlling the nature of aggregates in aqueous solution is explored in detail in Chapter 5.

Table 3.3 Vibronic peak ratios of peptide-PBI **8** and **9** in H₂O, and **11** in chloroform as monomer reference.

PBI derivative	Vibronic Peak Ratio ($\frac{A_{0-1}}{A_{0-0}}$)
(Glu-Ala-Ala-Ala-Gly) ₂ - PBI (9)	1.23
(Glu-Glu-Glu-Ala-Ala-Ala-Gly) ₂ - PBI (8)	0.86
(C ₁₂ H ₂₅) ₂ - PBI (11)	0.61

3.3.3 Incorporation of sterically demanding amino acids

The incorporation of a H-bonding sequence into the peptide tethered to the PBI core indicated that an increased twist between coupled chromophores had some contribution from accommodating increased steric demand. To explore this concept, leucine amino acids were incorporated into the middle region of the peptide to obtain peptide-PBI **10** ((Glu-Glu-Glu-Leu-Leu-Leu-Gly)₂-PBI). This causes a relatively bulky group to be in close proximity to the PBI core. Figure 3.12 displays

the absorption spectrum of peptide-PBI **10** in distilled water, with peptide-PBI **8** included for comparison. The spectrum shows a vibronic progression reflecting that of monomers in solution, and concurrently a absorption band appears at longer wavelengths. The comparison with a known H-aggregate signature (*i.e.*, that of peptide-PBI **8**) shows a different perturbation from the monomer spectrum, indicating a different type of aggregate.

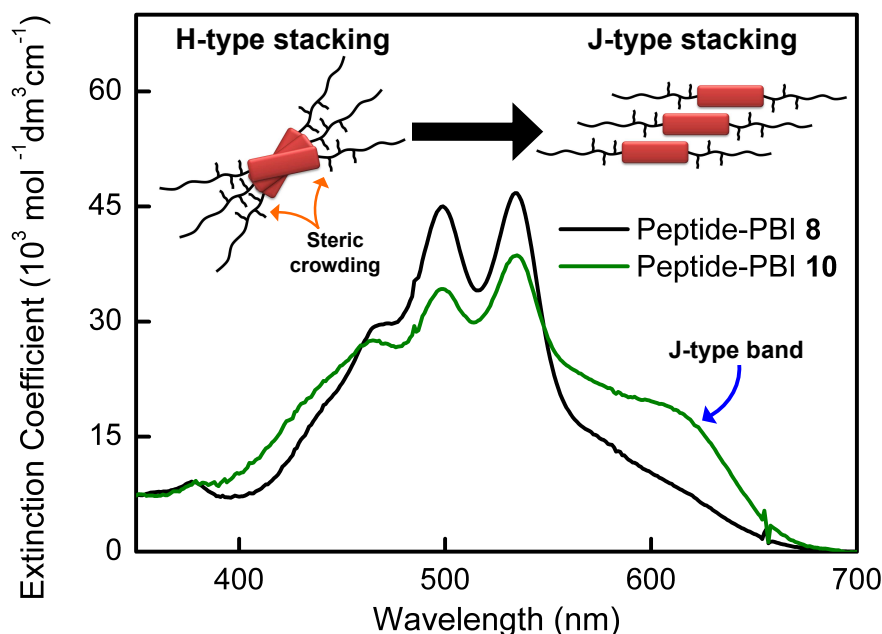


Figure 3.12 Absorption spectra of peptide-PBI **8** and **10** (3.0×10^{-6} M) in distilled water. Also shown is a schematic demonstrating the relieving of steric strain close to the PBI core with slipped geometry, *i.e.*, J-aggregate formation.

The spectral data for peptide-PBI **10** is consistent with the formation of a J-aggregate (*i.e.*, a cofacial aggregate having translational slipping as opposed to rotational displacements displayed for the other peptide-PBI conjugates). In the literature, J-aggregates of PBI derivatives are characterised by the concurrent appearance of a monomer vibronic progression and a broad absorption band appearing between 620–650 nm.^{99,100} This comparison with the literature supports the formation of J-aggregates in peptide-PBI **10**, with the J-type band appearing at approximately 615 nm, slightly higher energy than those reported in the literature. The formation of a J-aggregate configuration can be rationalised through the increase in steric bulk associated with the ¹Pr group compared to the CH₃ group of alanine (peptide-PBI **8**).

Increased steric bulk would cause unfavourable steric crowding close to the PBI core in an H-aggregate configuration, whereby the aggregate becomes thermodynamically unstable. In order to accommodate for the steric bulk, the molecular building blocks

adopt slipped J-aggregate geometry. The formation of J-aggregates through the minimisation of steric crowding has been reported in other PBI derivatives in the literature,²⁴ thereby supporting the formation of J-aggregates for peptide-PBI **10**. Similarly, the leucine amino acids possess a significant hydrophobic character, which could also influence the destabilisation of an H-aggregate geometry. On this basis, the formation of J-aggregates would be favoured in order to embed the ⁱPr group with the PBI core in order to minimise unfavourable hydrophobic interactions, similar to arguments put forward for H-bonding amino acids. The dominant driving force cannot be elucidated from these data, however these interactions may not be too different, thus a combination of the two is likely to occur.

Although the 615 nm peak appears consistent with J-aggregate formation, there remains ambiguity around its assignment. Uncertainty arises due to the position of the J-band being at relatively high energy compared to some derivatives in the literature. Furthermore, the slipped geometry in these types of aggregates generally results in relatively poor π - π electronic coupling between adjacent chromophores, which in turn yields high photoluminescence.¹⁰¹ The emission spectrum of peptide-PBI **10** in water (data not shown) exhibits strongly quenched photoluminescence, comparable with the H-aggregates formed with the other peptide-PBI conjugates. These contradictory observations highlight the need for further investigation to establish whether the signature observed is a true J-aggregate, or if it relates to a structural motif of a much larger aggregate related to the aggregates found in MeCN for all peptide-PBI conjugates.

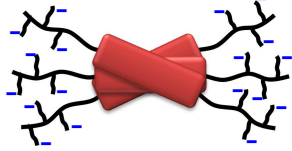
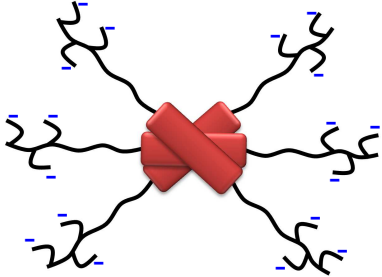



Unfortunately, such investigations were not carried out in this research due to time constraints. However, these investigations could be achieved by varying the steric bulk employed. For example, the comparison of alanine, leucine, and isoleucine could exhibit a direct trend caused from the increasing steric bulk. Furthermore, very bulky groups could be employed. For example, phenylalanine or tryptophan residues would be expected to have a high degree of steric crowding near the PBI core of a peptide-PBI conjugate. Issues that could arise with interpreting the use of side chains of a phenyl group derivative relate to the possibility of π - π interactions with the PBI core, therefore initial investigations are recommended to focus on alkyl bulk instead.

3.4 Summary

In summary, this chapter illustrates the solvent, and peptide sequence, dependent aggregation of peptide-PBI conjugates through the examination of optical absorption and fluorescence spectroscopic signatures. The perturbations of signatures from those observed from isolated chromophores demonstrate the ability to probe the geometric configuration between neighbouring chromophores. Through modulation of solvent environment it has been shown that monomers (in DMSO), semicrystalline aggregates (in MeCN) or a combination of these aggregates can be obtained in solution. Additionally, the application of the exciton model to peptide-PBI conjugates in water determined that weakly coupled H-aggregates were formed where the electrostatic repulsion between peptide segments strongly modulates the rotational displacements of adjacent chromophores. The influence of electrostatic repulsion results in aggregates that can be tuned through change in pH, observed through cryo-SEM images depicting a branched fibre network in neutral water, but semicrystalline type aggregates in acidic water. The tuning of peptide-PBI aggregates through solvent-dependence is investigated in detail in Chapter 4.

Subsequently this chapter investigated the influence the peptide is able to impart on the nature of aggregates formed in solution, in particular water. This was achieved through examining the change in the nature of aggregation as a function of peptide design. Due to the formation of H-aggregates for all but one peptide-PBI conjugate in water, important information is gained through analysing the vibronic peak ratios. Table 3.4 summarises these findings by linking the vibronic peak ratio to a schematic representation of the aggregate in solution. These results illustrate that the presence of a H-bonding sequence fails to knit together PBI chromophores, and instead increases the twisting within an H-aggregate. The addition of large steric bulk close to the PBI core appears to cause J-aggregate geometry to be favoured in order to reduce steric crowding. Additionally, by reducing the number of ionisable groups in the peptide sequence, the influence of electrostatic repulsion on the mode of aggregation was elucidated. This aggregation is strongly modulated by electrostatic repulsions between glutamic acid residues and is investigated in detail in Chapter 5.

Table 3.4 Summary of the nature of aggregates in water derived from the vibronic peak ratios observed.

Peptide-PBI derivative	Vibronic Peak Ratio ($\frac{A_{0-1}}{A_{0-0}}$)	Schematic of aggregate present
((Glu) ₃ -Gly))2 – PBI (6)	1.38	
((Glu) ₃ -(Gly) ₃ -Gly))2 – PBI (7)	1.22	
((Glu) ₃ -(Ala) ₃ -Gly))2 – PBI (8)	0.86	
(Glu-(Ala) ₃ -Gly))2 – PBI (9)	1.22	
((Glu) ₃ -(Leu) ₃ -Gly))2 – PBI (10)	...	

Chapter 4

Solvent composition dependent peptide-PBI aggregation

4.1 Introduction

Precise control of the self-assembly of molecular building blocks is an attractive approach to obtaining distinct supramolecular structures and is a major challenge in supramolecular and materials chemistry.¹⁰² Design of molecular building blocks often employ structural features which impart diverse solvation demands, creating amphiphilic molecules.¹⁰³ The self-assembly of amphiphilic molecules typically depends on the combination of molecular structure, intermolecular interactions, and solvent-molecule interactions.^{83,104–106} Supramolecular assemblies comprised of amphiphilic molecules have been shown to be sensitive to changes in solvent polarity. For example, it has been reported that *N*-stearoyl-L-glutamic acid forms nanofibres in chloroform, whilst in a 1:1 mixture of ethanol:water nanodisks are observed.¹⁰⁷ This illustrates that by varying solvent compositions, it is possible to tune the aggregation properties of molecular building blocks and change the nanostructure of aggregates.¹⁰⁸

Recently, there has been a growing interest regarding amphiphilic PBI derivatives in the literature, with numerous examples being reported from various research groups.^{26,29,109–111} Bay-unsubstituted PBIs (no substitution on the aromatic core) typically form columnar stacks due to their strong propensity to align via π - π interactions.¹¹² By varying the solvent compositions, studies have shown that assembly of PBI derivatives can be tuned to form various nanostructures; including spheres, wires, belts, and sheets.³² This tuning is achieved by varying the amount of good

solvent (*i.e.*, solvent promoting monomers) and bad solvent (*i.e.*, solvent promoting aggregation) that the molecules (or aggregates) are exposed to. Inducing organisation of functional materials could allow various types of supramolecular structures with desirable optical and electronic properties, for use in various applications. For example, the controlled reorganisation of functional materials is of interest as such systems could be applied to sensor applications.^{113–115} The principle employed in this application would be that molecules (or aggregates) undergo reorganisation in the presence of a particular target analyte, thus allowing optical changes (*i.e.*, increased photoluminescence) to be monitored indicating the presence (or absence) of the target analyte.¹¹⁶

This chapter investigates the solvent composition dependent aggregation of peptide-PBI conjugates **8** and **9** (see Figure 4.1) in various solvent compositions. These peptide-PBI conjugates form hydrophobically driven aggregates in water (due to the PBI core), whilst the hydrophilic peptide sequence contains two distinct regions, one capable of H-bonding, and another with ionisable glutamic acid residues. By varying the composition of DMSO-water mixtures we illustrate the ability to induce formation of H-aggregates from a solution containing isolated chromophores. Additionally it is demonstrated that by varying the composition of MeCN-water mixtures there is a reorganisation of strongly coupled aggregates. This reorganisation is determined to be driven by the electrostatic repulsion between glutamic acid side chains, when there is sufficient water to promote the ionisation of glutamic acid. A possible mechanism for this process was deduced using salt-doped solvent systems in order to screen the charge formation on ionisable side chains.

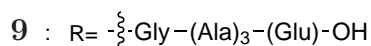
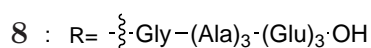
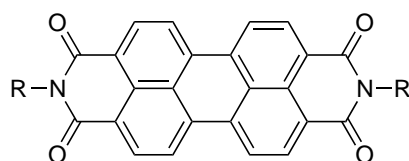


Figure 4.1 Key compounds utilised to investigate solvent composition dependent aggregation and reorganisation.

4.2 From monomers to cofacial peptide-PBI aggregates

It has been shown in the literature that solvent selectivity can strongly affect self-assembly kinetics as well as nanostructure assemblies of PBI derivatives.³² Recall that DMSO is considered a good solvent for peptide-PBI **8**, whilst water is considered a relatively bad solvent as there is a large amount of cofacial π - π aggregation. This section is concerned with the solvent induced assembly of peptide-PBI **8** using mixtures of good and bad solvents, and demonstrates the ability to induce aggregation of monomers to form extended cofacial aggregates.

In order to investigate the assembly of monomers of peptide-PBI **8** compositions of a DMSO-water solvent system were chosen. Figure 4.2 shows spectra of peptide-PBI **8** in solvent mixtures varying from neat DMSO to neat water. Upon addition of small percentages of water to the DMSO solution there is a decrease in vibronic peak intensity and concurrently a broadening of the spectrum at longer wavelengths. These spectral characteristics indicate the π - π aggregation of peptide-PBI **8** in water. Figure 4.3 shows how the vibronic peak ratio varies with solvent composition illustrating the progression from monomers at high DMSO concentration ($\geq 60\%$ DMSO), to cofacial H-aggregates with water additions.

At high DMSO concentration the vibronic peak ratio of 0.6 reflects that of a PBI core that is not coupled to other chromophores (determined from dilute solution of alkyl-PBI **11**). Small to moderate additions of water ($< 40\%$ v/v) appear to have no significant effect on the aggregation state of peptide-PBI **8**, indicating the resistance to moderate changes in solvent composition. Assembly of monomers is induced when the percentage of water is increased to approximately 50%. At this composition the PBI core is unable to be efficiently solvated due to its large hydrophobicity and the molecules assemble in order to reduce interactions between water and the PBI core. Cofacial aggregate formation allows the hydrophobic PBI core to be embedded in an aggregate, whilst the hydrophilic peptide is solvated. This driving force for cofacial aggregate formation grows as the water content increases further until the spectroscopic signatures begin to appear very similar to those of peptide-PBI **8** in neat water. This means that peptide-PBI **8** has a high propensity to self-assemble into H-aggregates in solvent compositions with a large percentage of water.

These results illustrate the control over aggregation of peptide-PBI **8** by varying solvent compositions from neat DMSO to neat water. It is demonstrated that although monomers appear to be resistant to small additions of a bad solvent, once

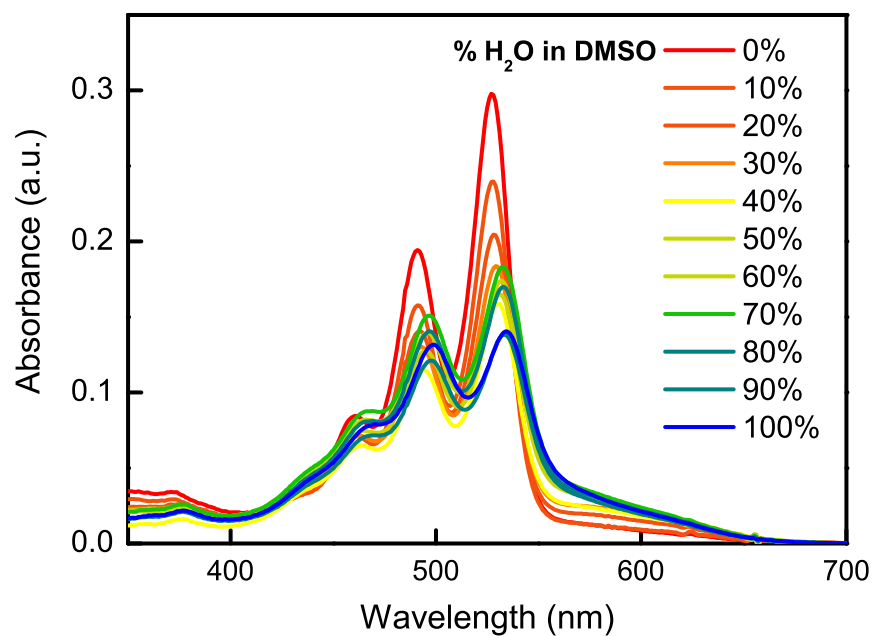


Figure 4.2 UV-Vis absorption spectra of peptide-PBI **8** (3.0×10^{-6} M) in various percentage compositions of DMSO and H₂O (*v/v*).

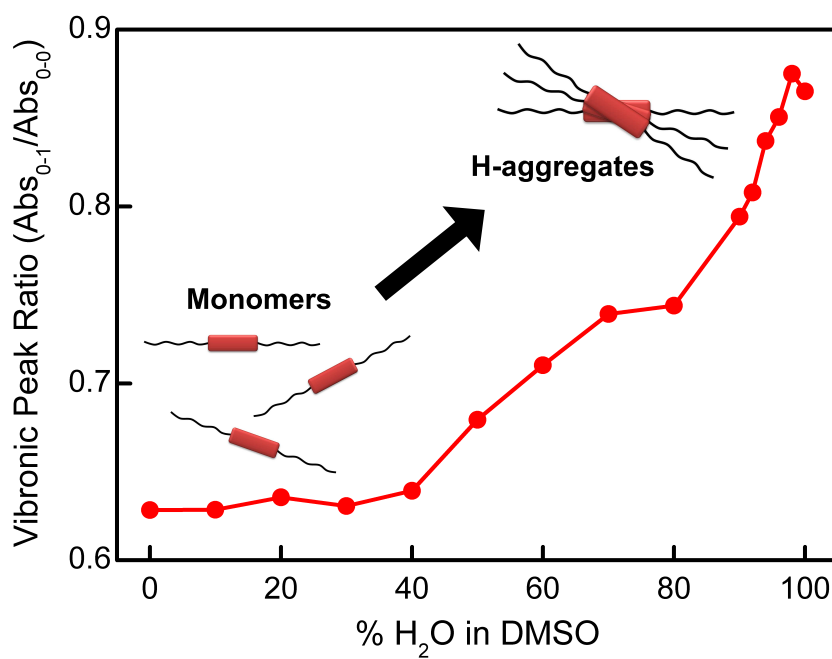


Figure 4.3 Vibronic peak ratios extracted from the spectral series in Figure 4.2 as a function of solvent composition. Also depicted is a schematic illustrating the nature of PBI molecules in solution.

a particular threshold is reached the hydrophobicity of the molecules overwhelms the solvation ability and aggregation occurs. Recently, a study reported the solvent induced aggregation of a chiral lactose-PBI derivative using the same binary solvent of DMSO and water.¹¹⁷ The results of this study agree with the observations made with peptide-PBI **8**, *i.e.*, increasing the concentration of water in DMSO leads to the appearance of aggregates in solution with the likely driving force being the hydrophobicity of PBI cores. The authors of that study also reported the appearance of circular dichroism spectroscopy (CD) bisignate signals as a function of increasing water percentage. These signals are a result of the chiral design of their lactose-PBI derivative and support the conclusions of solvent induced aggregation. Unfortunately CD spectra for peptide-PBI **8** for different solvent compositions were unable to be obtained due to time constraints. However, based on results reported in the literature and the spectral broadening seen with peptide-PBI **8**, it is almost certain that a CD signal would be observed at water percentages greater than 50%, approximately the point at which the population of aggregates reaches a considerable level.

4.3 Reorganisation of peptide-PBI aggregates

A corollary of varying solvent composition to tune aggregation can be applied with two solvents that are not entirely good or bad but induce different types of aggregates. Recall that in acetonitrile (MeCN) there are strong π - π interactions between neighbouring PBIs for peptide-PBI **8**. In order to investigate the sensitivity of these strongly coupled aggregates to solvent compositions, a solvent system of varying percentages of MeCN and water was prepared. This binary solvent system is interesting because peptide-precursor **3** (NH₂-Gly-Ala-Ala-Ala-Glu-Glu-Glu) formed an organogel when dissolved in MeCN (see Chapter 3); indicating it is a poor solvent for the peptide segment of peptide-PBI **8**. However, MeCN is a good solvent for perylene and thus it should be able to solvate the π -face of peptide-PBI **8**.

Figure 4.4 shows UV-Vis spectra of peptide-PBI **8** in solvent mixtures varying from neat MeCN to neat water. Upon addition of a small percentage of water to the MeCN solution, vibronic peaks begin to emerge. These peaks continually emerge with each increase in water addition, with A₀₋₀ being the most intense in the progression. The emergence of vibronic peaks implies water weakens the π - π coupling between neighbouring peptide-PBI **8**. At high water concentrations there is a redistribution of vibronic peak intensities and A₀₋₁ increases, indicating a reorganisation of aggregates caused by water addition.

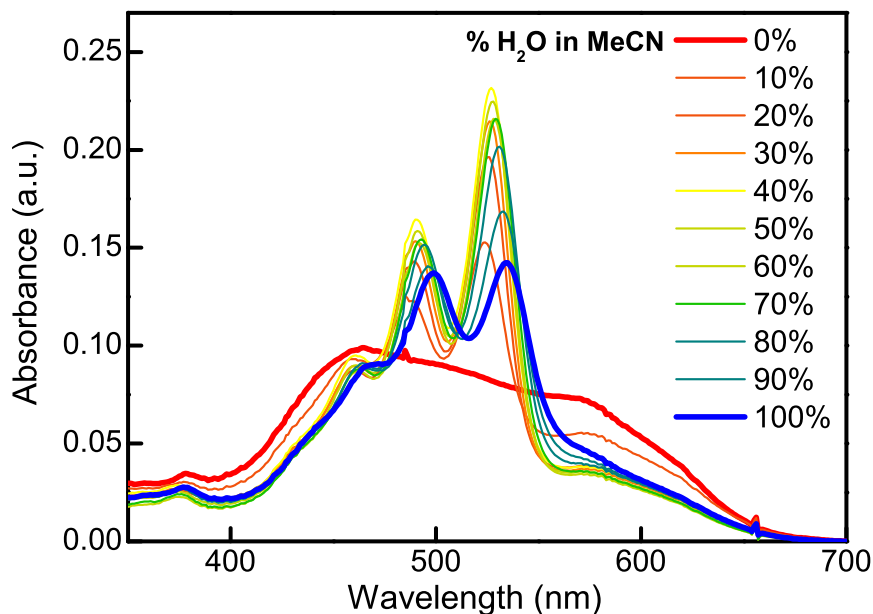


Figure 4.4 UV-Vis absorption spectra of peptide-PBI **8** (3.0×10^{-6} M) in various percentage compositions of MeCN and H₂O (v/v).

In order to gain further insight into this reorganisation process a more detailed analysis was conducted. Particularly useful information can be gained from changes in vibronic peak ratios and the fraction of vibronically structured components. In order to obtain this information some basic signal processing was performed on the MeCN/water spectral series, in particular the subtraction of the MeCN-like character from the other signals. This spectral processing was performed on the basis that oscillator strength is quantitatively redistributed from the broad signature (in MeCN) to a more structured vibronic progression,¹⁹ allowing for the each spectrum to be well fit to a linear combination of the MeCN and the structured vibronic spectrum.

Linear combinations were calculated by scaling the broad spectrum (MeCN) to the spectrum of interest (*e.g.* solution with some percentage of water) at 575 nm. This is approximately the centre of the shoulder at longer wavelengths observed in the MeCN spectrum. The scaled broad aggregate spectrum is then subtracted from the spectrum of interest and the vibronically structured component is elucidated. The vibronic ratio was calculated from this vibronic component (*i.e.*, after subtraction). The vibronic fraction was determined based on the vibronic component area and the initial spectrum area, as given on equation 4.1.

$$\text{Vibronic Fraction} = \frac{\text{Area}_{\text{Vibronic Component}}}{\text{Area}_{\text{Total}}} \quad (4.1)$$

Figure 4.5 illustrates how the fraction of the vibronically structured component varies with solvent composition. This analysis reveals three distinct regions: 1) A strongly coupled aggregate with a broad absorption at <5% water, 2) A rapidly increasing fraction of chromophores whose spectra resemble monomers with water addition, and 3) Formation of a different type of aggregate with vibronic structure at high (>80%) water content. Figure 4.5 also shows that the fluorescence intensity and vibronic peak ratios follow the population of monomers (*i.e.*, the vibronic fraction as a function of solvent composition).

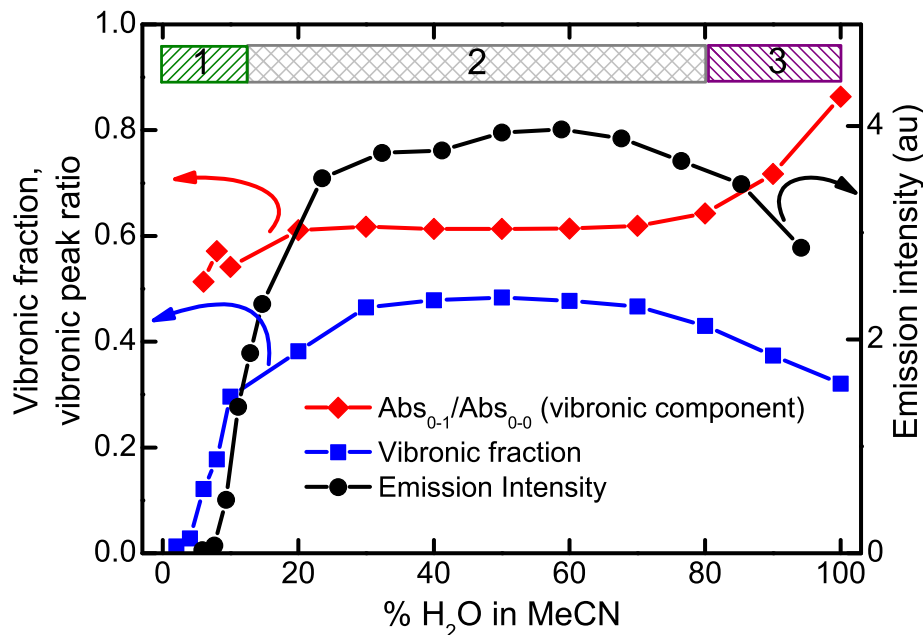


Figure 4.5 Fraction of peptide-PBI **8** chromophores with resolved vibronic peaks extracted from the spectral series in Figure 4.4, revealing three distinct regions. Also shown are the vibronic peak ratios (after the broad component is subtracted) and the fluorescence intensity, excitation wavelength for all spectra was at the 0-0 vibronic peak.

The emission spectra provide supporting evidence for these three distinct regions. In region 1 the system is weakly fluorescent, matching the excimer emission obtained for peptide-PBI **8** in MeCN (see chapter 3). This excimer emission is red-shifted to approximately 655 nm whereas the strong emission throughout region 2 is centred at approximately 544 nm. This strong emission matches that expected from isolated PBI chromophores, for example dilute alkyl-PBI **11** in chloroform. Observations that region 2 contains a significant fraction of monomers is supported by the vibronic peak ratio. Up to 80% water sees the constant ratio of approximately 0.6, this reflects a PBI core that is not coupled to other chromophores (comparable to that of alkyl-PBI **11**). However at high water percentages there is a redistribution of vibronic peak intensities in favour of A_{0-1} over A_{0-0} and they become almost equal, even after subtraction of the underlying broad component. This change in vibronic peak

ratio is a characteristic signature of H-aggregate formation (as discussed in chapter 3). The aggregate present at high water percentage is significantly different from the origin (*i.e.*, MeCN) and depicts the reorganisation ability in MeCN-water percentage compositions.

The next stage of the investigation of solvent composition dependent aggregation was to elucidate the driving force of the reorganisation of aggregates in MeCN and water compositions. Recall that pH dependent spectra (Chapter 3) indicated that electrostatic repulsion provided the impetus for twisted H-aggregate formation in neutral water. The significantly higher pK_a of carboxylic acids in MeCN (pK_a acetic acid in MeCN is approximately 24) ensures that the glutamic acid residues remain protonated initially.¹¹⁸ This suggests that the reorganisation from a tightly coupled aggregate into monomers could be driven by electrostatic repulsion between ionised glutamic acid residues (*i.e.*, going from region 1 to region 2, based on the introduction of water causing dissociation of carboxylic acid protons).

To confirm this, the solvent composition dependence of peptide-PBI **8** was repeated in the presence of an electrolyte to screen electrostatic repulsions. The salt additive used as an electrolyte was sodium perchlorate and was chosen on the basis that it is soluble in both water and MeCN. At the same time, the solvent composition dependence of peptide-PBI **9** was carried out. This peptide-PBI conjugate contains two less ionisable glutamic acid residues than that of peptide-PBI **8** and can therefore be used to elucidate the role of electrostatic repulsions through direct comparison.

Figure 4.6 shows the resulting vibronic fraction extracted from the spectral series of both peptide-PBI **8** and **9** with and without salt additions, the region indicators are the same as described in Figure 4.5. These quantities were obtained in the same manner as previously described, using the corresponding broad MeCN signature for each experiment. The change in vibronic fraction with and without salt indicates that the transition from region 1 to region 2 is suppressed in the presence of an electrolyte. Additionally the solvent composition dependence of peptide-PBI **9** shows that more water is needed in order to initiate the reorganisation of aggregates. This implies that the transition from strongly coupled aggregates to monomers is promoted by accommodating the charge formation on the peptide sequence when small percentages of water are added.

Electrostatic repulsion inducing the reorganisation is clearly observed in the comparison of the solvent composition dependence of peptide-PBI **8** with and without electrolyte additions. When electrolytes are present the transition from region 1 to region 2 occurs at approximately 20% water content instead of <5%. This

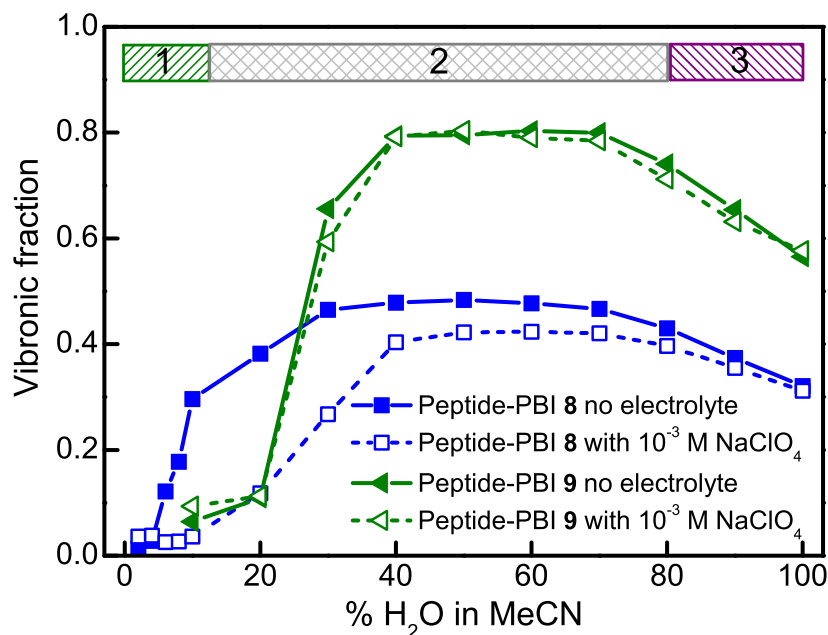


Figure 4.6 Fraction of peptide-PBI **8** and **9** chromophores with resolved vibronic peaks extracted from the corresponding spectral series in of Figure 4.4 with and without sodium perchlorate. The spectral series for peptide-PBI **9** is not shown but closely resembles that of peptide-PBI **8** in spectroscopic features.

means that more water is needed to impart enough ionised carboxylic acid groups to induce reorganisation and overcome the forces inducing aggregation in MeCN. A similar comparison can be made between the solvent composition experiments of peptide-PBIs **8** and **9**. The reorganisation of peptide-PBI **9** without electrolyte closely resembles that of peptide-PBI **8** with electrolyte additions confirming that electrostatic repulsion is the drive for aggregate reorganisation. Peptide-PBI **9** contains two fewer glutamic acid residues, thus reducing the number of ionisable groups on the molecule which has the same effect as screening the charge using electrolytes.

This is supported by the results of an experiment involving the addition of electrolyte to solvent compositions of peptide-PBI **9**. The charge screening effect of the electrolyte ions in solution has little effect on the amount of water required to induce reorganisation, as evidenced by the vibronic fractions being near identical with and without salt additions. Notably, the absolute value of the vibronic fractions between the two peptide-PBI conjugate experiments are significantly different. The order of two difference between the the two peptide-PBI conjugates implies that peptide-PBI **9** generates twice the population of vibronically structured chromophores than peptide-PBI **8** at 1:1 MeCN:H₂O composition. The reason this is considered to be an erroneous comparison is that **9** has less ionisable groups and therefore the repulsive forces are diminished compared to **8**. This leads to the conclusion that this

difference in absolute value is possibly an artefact from the method of derivation of the vibronic fraction, possibly caused from the H-aggregate signature of peptide-PBI **6** overlapping more with the ‘MeCN tail’ at longer wavelengths.

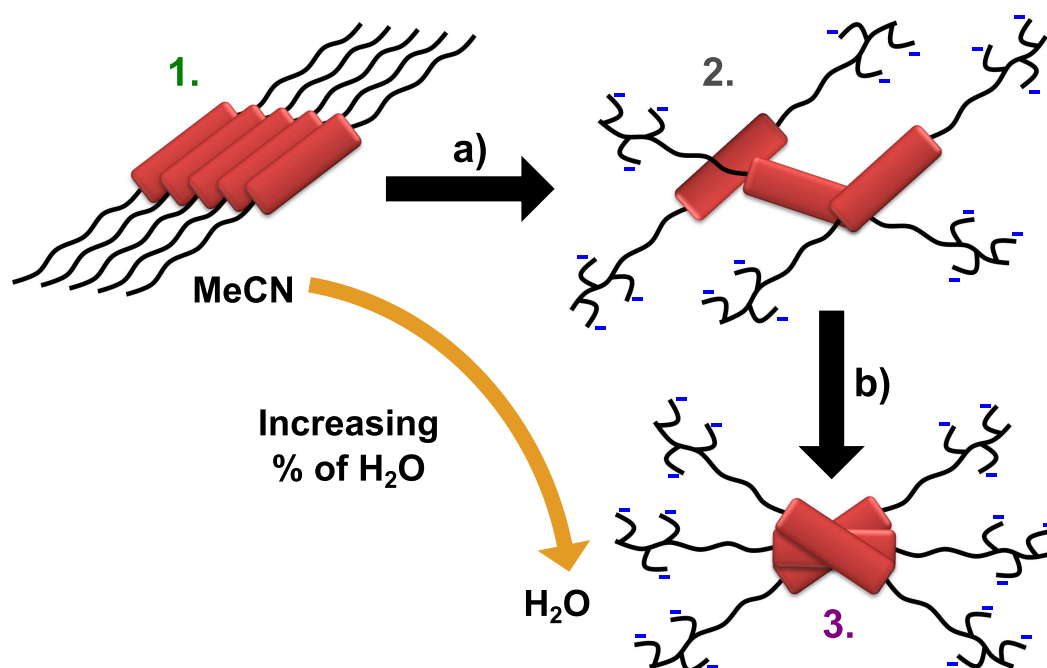
Recall that the vibronic fraction is derived based on a linear progression of a broad aggregate spectrum and a vibronically structured spectrum at one wavelength (575 nm). This is a simplification of the linear progression as it is expected there will be more than two components comprising the spectrum in water, for example monomers, H-aggregates and broad aggregate signals. Also the linear progression analysis conducted here was only performed at one wavelength, whereas the spectral features being considered span a considerable portion of the visible spectrum. In order to derive more accurate absolute values of the vibronic fraction more sophisticated analysis techniques could be utilised.

One approach could be using singular value decomposition (SVD) which has been applied to relatively complicated linear combinations in various spectroscopic experiment set-ups in the literature.^{119,120} Methods such as SVD are able to consider several components of a linear progressions over a range of wavelengths and therefore the simplification utilised in this work is not required. It is worthy to note however that the difference between values (*i.e.*, those calculated in this work and those by SVD) are predicted to only differ in the absolute value, meaning that the overall trend (and relative relationship between experiments) should remain the same.

4.4 Summary

In summary, this chapter demonstrates the ability to tune the nature of peptide-PBI conjugates in solution by taking advantage of the amphiphilic nature of the molecules. The diverse solvation demands incorporated in the design of peptide-PBI conjugates allow the solvent compositions percentages of a good solvent (DMSO) and a relatively bad solvent (water) to be varied in order to control aggregation. This type of experiment is able to induce aggregation of well solvated monomers into cofacial H-aggregates, as determined by monitoring the vibronic peak ratio as a function of solvent composition. Results from this experiment illustrate that although monomers are resistant to moderate additions of poor solvent (*i.e.*, monomers remain at < 40% water composition) it is the unfavourable interactions between the water and hydrophobic PBI core that provide the impetus for assembly.

Additionally this chapter demonstrates controlled reorganisation of peptide-PBI ag-



Scheme 4.1 Mechanism of the reorganisation of **8** upon; a) moving from neat MeCN to a MeCN/H₂O mixture, b) going to a high percentage composition of H₂O. The regions labelled 1, 2 and 3 correspond to those in Figure 4.5, and detailed in the text.

gregates by varying the solvent composition of two solvents that induce different aggregation types, namely MeCN and water. This binary solvent system induces a change from a strongly coupled aggregate (in MeCN) to a weakly coupled H-aggregate driven by electrostatic repulsion between ionisable groups on the peptide. A possible mechanism for this reorganisation was deduced by comparing the spectral analysis data for two peptide-PBI conjugate and by using electrolytes, a schematic of this is depicted in Scheme 4.1. This work demonstrates the ability of peptides to impart diverse solvation characteristics to PBI derivatives and provide a ‘control-handle’ for controlling the nature PBI aggregation in solution. The concept presented may find application in organic devices such as biosensors by monitoring the increased photoluminescence that occurs upon reorganisation.

Chapter 5

Counterion effects on peptide-PBI aggregation

5.1 Introduction

In nature, there are numerous complex functional systems which are composed of units organised hierarchically through multiple noncovalent interactions, typically over several length scales.^{121,122} One approach that is commonly employed to obtain supramolecular structures is through mixing different building blocks that are able to interact.¹²³ A classic example of this is the incorporation of cyanuric acid moieties into functional building blocks so that upon addition of melamine, complexation occurs between the molecules which aids in directing supramolecular assembly.¹²⁴ There are numerous examples reported in the literature demonstrating the ability of additives to direct (or change) the self-assembly of PBI derivatives in solution.^{31,34,35,125–127}

A corollary of varying additives to control the supramolecular structure involves the coupling of different molecular units by exploiting electrostatic interactions, commonly referred to as ionic self-assembly.¹²⁸ This technique provides a flexible method for the controlled assembly of molecular units, and has been utilised in the formation of various dye-surfactant supramolecular structures,^{129,130} including PBI derivatives.^{131,132} One particular adaptation of this approach is to use metal ions to induce assembly instead of surfactants. The desire to obtain functional materials sensitive to the presence of ions has received considerable attention, largely driven by the promise these materials have in recognition and sensor applications.^{133–135} The principle of organic semiconductor based sensor devices typically relies on monitoring

spectroscopic changes, either absorption or photoluminescence, in the presence (or absence) of target ions.¹³⁶ It is noteworthy that there are only a few reports of PBI derivatives being employed in fluorometric and colorimetric sensor devices for the detection of ions in the literature.^{137,138}

This chapter investigates the sensitivity of peptide-PBI aggregates (in particular peptide-PBI **8** and **9**, see Figure 5.1) to the presence of metal cations in aqueous solutions. By monitoring the spectroscopic signature of a weakly coupled H-aggregate as a function of ionic strength, we demonstrate the ability to reduce the twisting between PBI cores through non-specific ion interactions. Additionally it is demonstrated that metal cations with a propensity to form metal-carboxylate complexes can induce cross-linking of peptide-PBI conjugate molecules. These types of interactions were elucidated by varying the type of salt used and take advantage of the ionisable glutamic acid side chains being deprotonated at neutral pH.

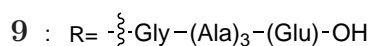
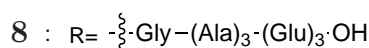
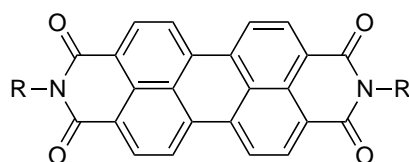


Figure 5.1 Key compounds utilised to investigate the types of interactions that can occur with different metal cations in solution.

5.2 Sensitivity of PBI aggregates to ionic strength

The design features incorporated into the peptide-PBI conjugates was based on commonly employed peptide amphiphile structures (see Chapter 3). Of particular interest in this section is that of the glutamic acid residues, which bear an ionisable carboxylic acid side chain. In distilled water, this ionisable side chain is present in the ionised state, (*i.e.*, negatively charged deprotonated carboxylate group). Illustrated previously in this work (Chapter 3) these ionisable glutamic acid residues impart pH sensitivity to peptide-PBI conjugates. A further implication of this is that the aggregates are also sensitive to ionic strength alterations in aqueous solutions (*i.e.*, the presence of ions in solution). This section is concerned with the ionic strength sensitivity of peptide-PBI **8** aggregates, and illustrates the ability to induce stronger PBI core overlap via addition of positively charged ions which screen the negative charges present on peptide segments, thus reducing electrostatic repulsion between peptide-PBI **8** molecules.

In order to investigate the sensitivity of peptide-PBI **8** aggregates to ionic strength, aqueous solutions of sodium perchlorate (NaClO_4) of various concentrations were prepared. Figure 5.2 shows spectra of peptide-PBI **8** in the presence of varying concentrations of NaClO_4 in water, normalised at the [0-1] peak. Upon the addition of ions to the solution there is a decrease in the intensity of the [0-0] vibronic peak, indicative of increasing H-aggregate character (*i.e.*, more effective cofacial π - π interactions of peptide-PBI **8** in solution). Figure 5.3 shows how the vibronic peak ratio, and emission intensity varies with the concentration of NaClO_4 and illustrates the progression of an H-aggregate with a large twist between units (from electrostatic repulsion), to an H-aggregate with less twisting, due to Na^+ ions screening the charge on glutamic acid residues.

These results show the sensitivity of peptide-PBI **8** to the presence of Na^+ ions in solution. The positively charged ions in solution enables charge screening of the glutamic acid residues, which causes an increase in π -orbital overlap, supported by the emission intensity which decreases as the concentration of Na^+ ions increases. This alteration in H-aggregate character is a subtle effect as the change in vibronic peak ratio occurs very gradually over a relatively large concentration range of Na^+ . Such a small change in aggregate signature is consistent with a non-specific ion screening effect as opposed to a direct ion interaction.

In comparison, a recent study reported the sensitivity of a PBI derivative (which featured two first generation *Newkome* type dendrimers) to Na^+ ion concentration.¹³⁹ The results of this study concur with the observations made with peptide-PBI **8**. That is, in the presence of Na^+ ions the aggregation (and subsequent π - π interactions) are enhanced, as evidenced by emission intensities and vibronic peak ratio changes. The authors of that study also investigate the effects of Li^+ and K^+ on the aggregation and find that the PBI aggregation is enhanced in the presence of all these ions.

Interestingly, the authors observe that these three alkali metal ions are able to enhance slightly different amounts of aggregation of the *Newkome*-PBI derivative. This was determined by treating the PBI-derivative as a surfactant molecule and the critical micelle concentration (cmc) was calculated. From these calculations it was reported that there was a slight difference of enhanced aggregation between Na^+ and K^+ ions (*i.e.*, cmc for Na^+ 0.94×10^{-5} M, and 1.18×10^{-5} M for K^+). From this result the authors conclude that Na^+ ions have a slightly higher affinity towards carboxylate groups. Regarding the investigations of the sensitivity of peptide-PBI **8** to ionic strength presented in this section, only Na^+ ions were utilised. However, based on the results reported in the literature it is expected that the other alkali

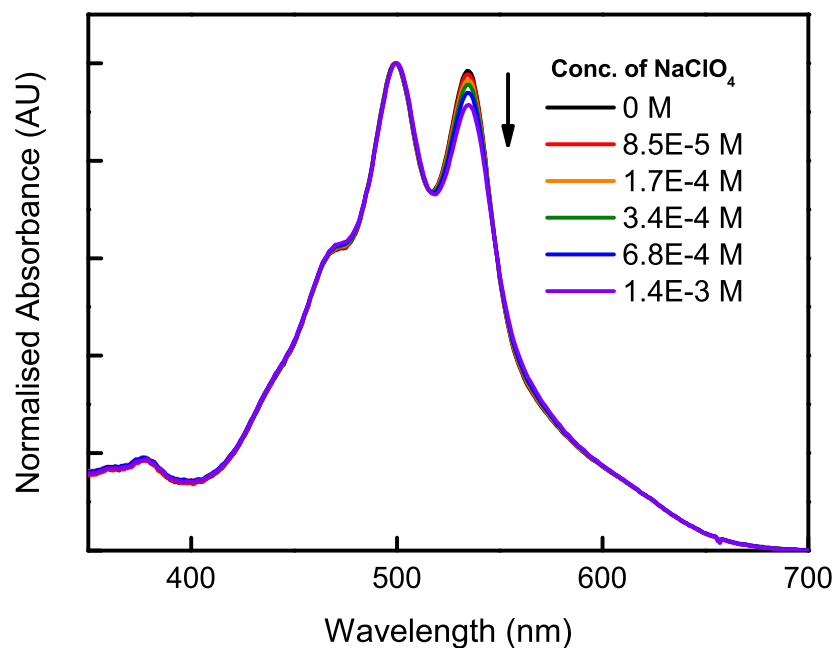


Figure 5.2 UV-Vis absorption spectra of peptide-PBI **8** (3.0×10^{-6} M) in the presence of various concentrations of NaClO_4 in water. The arrow indicates changes in A_{0-0} upon increasing the concentration of Na^+ ions in solution.

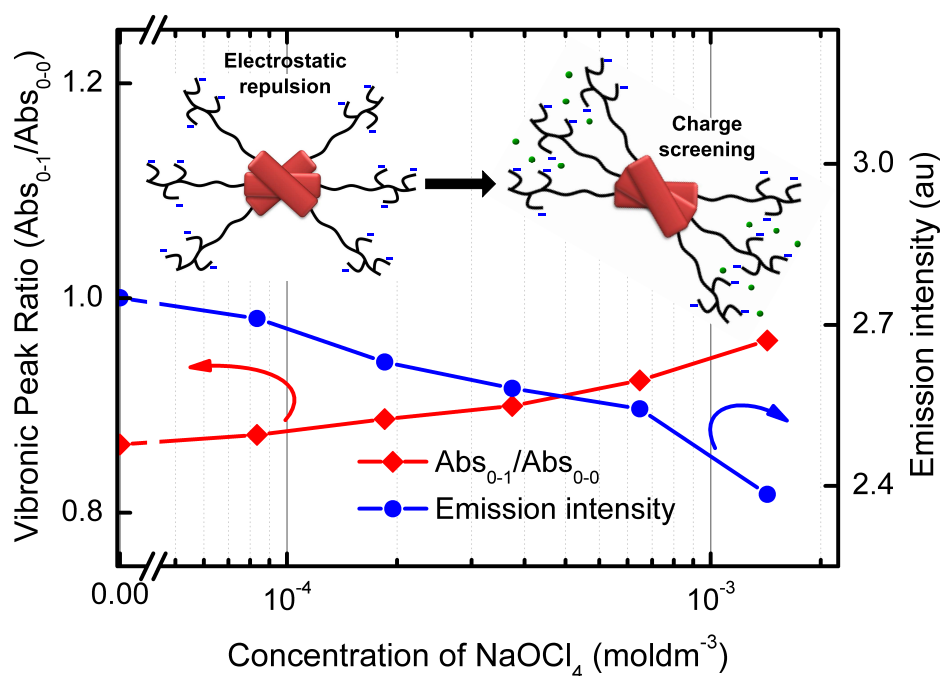


Figure 5.3 Vibronic peak ratios extracted from the spectral series shown in Figure 5.2, and emission intensity of peptide-PBI **8** as a function of NaClO_4 concentration. Also depicted is a schematic illustrating the nature of PBI aggregates upon increasing the concentration of NaClO_4 . The excitation wavelength for all emission spectra was at the [0-0] vibronic peak.

metal ions would enhance the H-aggregate of peptide-PBI **8** to a very similar extent to that of Na^+ ions.

5.3 Cross-linking of PBI aggregates via specific ion binding

The sensitivity of a *Newkome*-PBI derivative reported in the literature indicates that enhancing the aggregation of PBI molecules via the addition of ions to solution is likely not solely due to ionic strength variations (discussed in detail above).¹³⁹ This study reported the enhancement of PBI aggregates via the addition of monovalent counterions, and illustrated that Na^+ ions were able to enhance aggregation to a greater extent than K^+ ions. This section focusses on the investigation as to the influence various ions have on peptide-PBI aggregates, namely the differences observed between monovalent cations, coordinating divalent cations, and non-coordinating divalent cations. The results show that with ions with a high propensity to form metal-carboxylate complexes, specific ion binding can occur which is able to cross-link peptide-PBI aggregates.

Figure 5.4 shows the UV-Vis spectra of peptide-PBI **8** with various types of salts at a constant ionic strength of 6.8×10^{-4} M. These data clearly show that the enhancement of peptide-PBI **8** aggregation is dependent on the type of cation employed. All Na^+ containing salts show similar changes in the relative intensity of the [0-0] vibronic peak intensity compared to the [0-1] peak intensity. In contrast, the use of divalent cations (like Zn^{2+}) show a greater reduction in the [0-0] vibronic peak intensity than that observed for monovalent Na^+ ions. Interestingly, the divalent cation that is already ligated ($[\text{Cu}(\text{ethylenediamine})_2]^{2+}$) imparts changes that are similar to monovalent cation additions. The observations of enhanced H-aggregate formation of peptide-PBI **8** from the relative vibronic peak intensities is valid because all salt solutions were of the same ionic strength. This means that the effects observed are directly related to the type of cation used, not due to alterations in ion concentration.

In order to gain insight into the cause of different ion effects on peptide-PBI **8** aggregates a more detailed analysis was conducted. Useful information is gained from observing changes in vibronic peak ratios in relation to the various ions used. Figure 5.5 illustrates how the vibronic peak ratios change upon varying the ionic strength of the same salts shown in the spectral series in Figure 5.4. This analysis reveals two distinct types of ion interactions, 1) A large change in the vibronic

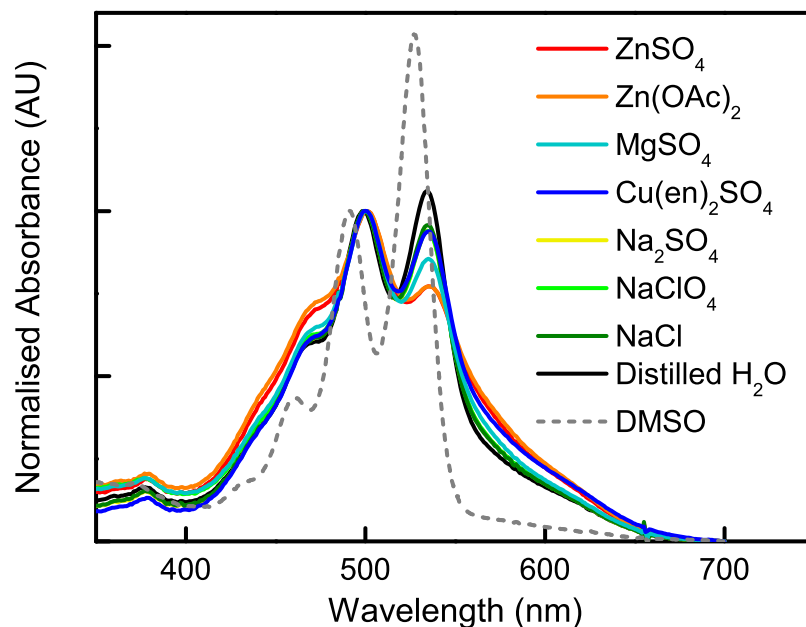


Figure 5.4 UV-Vis absorption spectra of peptide-PBI **8** (3.0×10^{-6} M) in the presence of various salts. All salt solutions have the ionic strength of 6.8×10^{-4} M. Also included is the spectra of peptide-PBI **8** (3.0×10^{-6} M) in distilled H₂O and DMSO for comparison.

peak ratio with divalent cations which are able to coordinate carboxylate groups (*e.g.* Zn²⁺ or Mg²⁺), and 2) A small change in the vibronic peak ratio with non-coordinating cations (*e.g.* Na⁺ or [Cu(en)₂]²⁺, where ‘en’ is ethylenediamine) in which modifications to aggregate nature is caused by variations in charge screening (*i.e.*, ionic strength).

To investigate the change imparted by each different ion, it was first important to determine if the anion has an effect on modifying the nature of peptide-PBI **8** H-aggregates. This was achieved by selecting salts with the same cation (*e.g.* Na⁺) and vary the type of anion of salts used. Comparing NaClO₄ with NaCl shows overlapping vibronic peak ratio changes, illustrating similar enhancement of peptide-PBI **8** aggregation. The only difference between the two salts is the type of anion, therefore this result indicates that monovalent anions have no influence on H-aggregate twist reductions. To interrogate this further, sodium sulfate (Na₂SO₄) was used and was shown to have the same vibronic peak ratio changes as the both NaCl and NaClO₄ as a function of ionic strength. Overlapping changes in the vibronic peak ratio for all Na⁺ salts indicate that divalent anions also have no effect. This lack of anion involvement in changing the nature of peptide-PBI **8** aggregates is further supported with ZnSO₄ and Zn(OAc)₂ comparisons, which show these two salts have overlapping vibronic peak ratio changes. These results combine to conclusively show

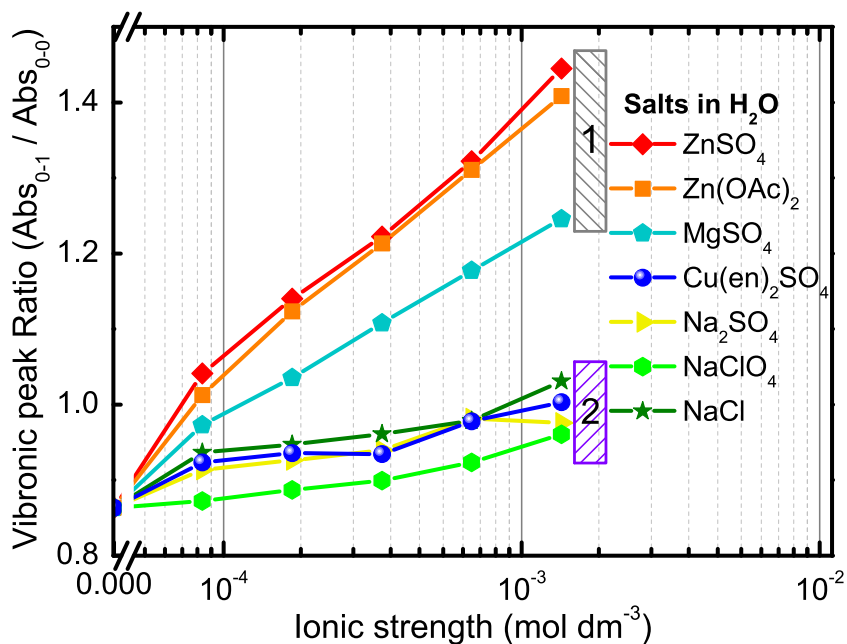


Figure 5.5 Changes in vibronic peak ratio of peptide-PBI **8** (3.0×10^{-6} M) as a function of ionic strength of various salts. Ratios were extracted from the spectral series presented in Figure 5.4, and depict two distinct ion effects. Region 1 involves specific ion binding, whilst Region 2 involves non-specific ion screening. Note ‘en’ in $\text{Cu(en)}_2\text{SO}_4$ represents the bidentate ligand ethylenediamine.

that the anion has no influence in increasing the degree of π - π interactions within H-aggregates of peptide-PBI **8**.

The next stage of analysis focussed on determining the cause of the large vibronic peak ratio changes for the divalent cations Zn^{2+} and Mg^{2+} . One significant difference between these divalent cations and Na^+ ions (apart from the increased charge) is that Zn^{2+} and Mg^{2+} are able to coordinate to oxygen atoms to form bidentate metal-carboxylate complexes.^{140–142} This implies that the large increase in vibronic peak ratio observed for the zinc and magnesium salts is caused by direct ion binding of carboxylate groups of the glutamic acid residues in peptide-PBI **8** (*i.e.*, chelation of two carboxylate groups to the divalent metal ion). This implies that there is a direct ion interaction with peptide-PBI **8** molecules, and not simply charge screening for these types of ions. Interestingly, the data presented in Figure 5.5 shows that this ion interaction also depends on the type of coordinating ion used, which implies that this divalent interaction is ion-specific. This is indicated by difference in total vibronic peak ratio changes for Zn^{2+} and Mg^{2+} ions.

This difference can be explained upon consideration of a study reported in 1970 by Bunting *et al.* which investigated the stability constants of various metal carboxy-

late complexes.¹⁴³ The authors report that there is a higher stability constant for metal-carboxylate complexes involving Zn^{2+} compared to Mg^{2+} for all carboxylate anions that were investigated. This greater stability constant for Zn^{2+} containing complexes implies that the propensity for complexation is greater for Zn^{2+} ions than for Mg^{2+} ions. Applying the findings from the literature to peptide-PBI **8** interactions with these two metal ions shows that the difference in reducing the twisting in H-aggregates, between the coordinating metal ions, is explained based on the relative propensity of the metal cation to form a carboxylate complex. Therefore this explains why a greater enhancement of H-aggregate spectroscopic signals is observed for Zn^{2+} ions than Mg^{2+} when at the same ionic strength.

To probe the hypothesis that metal-carboxylate complex formation is the mechanism involved in the enhancement of H-aggregate character (as opposed to only ionic strength), the comparisons to the non-coordinating copper salt ($\text{Cu(en)}_2\text{SO}_4$) becomes very significant. The cation in this metal salt involves a copper(II) centre with two ethylenediamine groups chelated. The cation, in this copper complex, is divalent but the copper lacks the ability to form a carboxylate complex with glutamic acid residues, therefore removing the ability for a direct ion interaction. The change in the vibronic peak ratio for this copper salt overlaps with the sodium salt ratios (see Figure 5.5). This provides conclusive evidence that ions unable to coordinate carboxylate groups cause a reduced twisting within peptide-PBI conjugate H-aggregates through non-specific charge screening. Whereas, ions with the ability to coordinate carboxylate groups have a greater effect on reducing the twisting between molecules within the H-aggregate.

With results showing that peptide-PBI **8** aggregate sensitivity to ions is ion specific and can be caused by direct ion interactions, investigations were conducted to determine how the formation of metal-carboxylate complexes causes such a large change in the vibronic peak ratio. In order to determine if the binding of glutamic acid groups involves an inter- or intra-molecular complexation to a metal ion, the ion-sensitivity of peptide-PBI **8** was compared to aggregates of peptide-PBI **9**. The comparison of spectroscopic changes for these two peptide-PBI conjugates aid in elucidating the mechanism because peptide-PBI **9** contains only one glutamic acid residue on each peptide segment, as opposed to the three contained in peptide-PBI **8**. Figure 5.6 illustrates the changes in vibronic peak ratios as a function of ionic strength for NaCl and Zn(OAc)_2 for those two peptide-PBI conjugates. The data indicates that the addition of Zn^{2+} ions has the same effect on both peptide-PBI conjugates. This provides evidence that the metal carboxylate complex that is formed is able to form even with the reduced number of glutamic acid residues of peptide-PBI **9** (compared to peptide-PBI **8**).

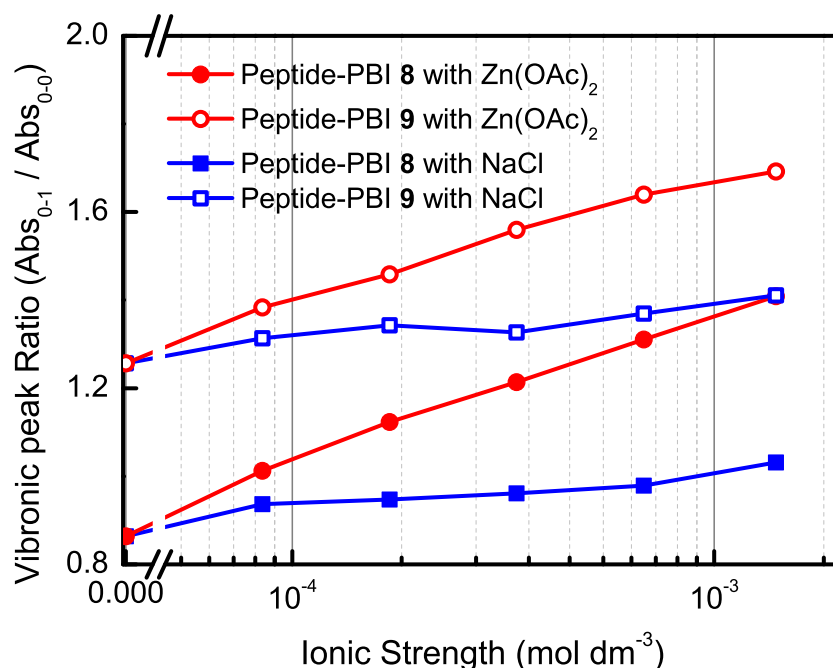
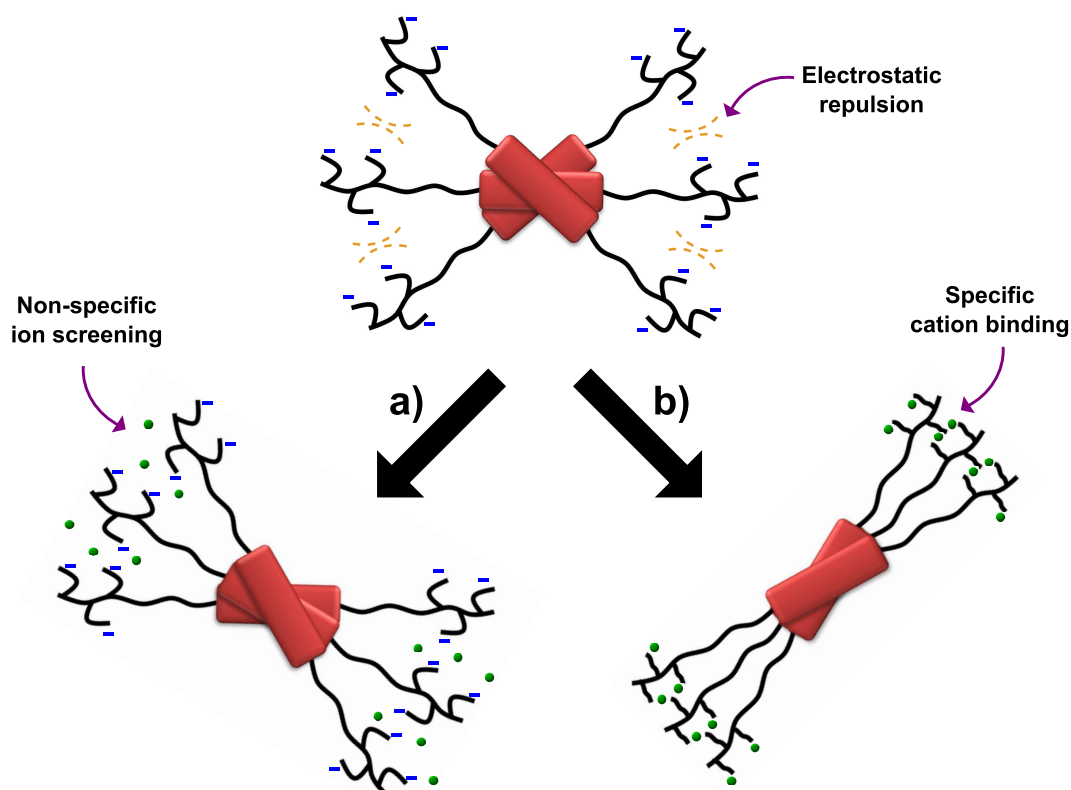


Figure 5.6 Changes in vibronic peak ratio of peptide-PBI **8** (3.0×10^{-6} M) and peptide-PBI **9** (3.0×10^{-6} M) with $\text{Zn}(\text{OAc})_2$ and NaCl as a function of ionic strength. Ratios were extracted from the corresponding spectral series to that depicted in Figure 5.2.

The absolute value of the vibronic peak ratios for both peptide-PBI conjugates is related back to the molecular structure of the compounds and the behaviour in water (see Chapter 3), and imparts no difference in data analysis. However, an important observation is that the vibronic ratio as a function of ionic strength increases in the same manner for the two peptide-PBI conjugates. Due to peptide-PBI **9** having only one glutamic acid residue on each peptide segment on, the chelation of two carboxylate groups is therefore extremely likely to be occurring with carboxylate groups on different molecular building blocks. Although this is not confirmed for certain, the conclusion is reached based on improbability that the distance between the terminal carboxylic acid and the glutamic acid side chain is small enough such that a divalent metal ion (*e.g.* Zn^{2+}) is able to coordinate to both carboxylic acid hydroxyl-groups. However, if the metal ion is coordinated to one glutamic acid carboxylic acid group, it is likely that the neighbouring peptide-PBI conjugate glutamic acid residue will be in relative close proximity to the metal ion, thus allowing the coordination of two glutamic acid residues on different H-aggregate units.

From these comparisons a possible mechanism for the enhanced H-aggregate signatures by the addition of ions can be elucidated. Due to the negatively charged glutamic acid residues in water, cations in solution will be attracted to the peptide-PBI aggregates. When these cations have no direct interaction with the negative

charge the reduced twist is caused by charge screening, and is a non-specific ion interaction. However, if the ion is able to coordinate to the carboxylate groups (and form a metal-carboxylate complex) then neighbouring peptide-PBI molecules are cross-linked due to metal complex formation, which imparts intermolecular non-covalent interactions. This interaction is shown to be ion specific due to the interaction being strongly dependent on the metal ions propensity to form metal-carboxylate complexes. Nevertheless, the cross-linking interaction significantly reduces the twisting within an aggregate, yielding more effective π -orbital overlap of PBI cores, thus a large increase in H-aggregate signature is observed. These two types of interactions are depicted in Scheme 5.1.



Scheme 5.1 Summary of the two types of interactions that can occur with peptide-PBI conjugates and different metal cations. a) Non-coordinating metal cations exhibit a non-specific ion interaction in which no direct interaction occurs but assembly is changed due to charge screening, and b) Metal cations with the ability to form metal-carboxylate complexes cross-link peptide-PBI conjugates through intermolecular non-covalent interactions. Cross-linking involves a direct interaction and is shown to be ion specific enhancing H-aggregate signatures to a greater extent than ion screening.

These results indicate the potential for peptide-PBI conjugates to be used as cation sensors, however further investigations need to be carried out to determine the interactions with various other metal ions (*e.g.* other transition metal ions). Such experiments could determine the stability constants of peptide-PBI metal-carboxylate complexes to examine if there is a high degree of coordination of a particular metal ion. Also, variations in the type of amino acid employed would be interesting to

investigate. For example, there are results in peptide amphiphile literature which show the ability to seed nanoparticles on aggregate via the chelation of Fe^{2+} to the amino acid histidine.¹⁴⁴

5.4 Summary

In summary, this chapter illustrates that peptide-PBI aggregates are sensitive to the presence of ions in solution, due to the ionised glutamic acid residues present in the peptide sequence. The twist between molecules in the peptide-PBI H-aggregate is a result of electrostatic repulsion between neighbouring molecules. Investigations into the sensitivity of these aggregates to the addition of Na^+ involved monitoring the spectroscopic changes that occur as a function of ionic strength. These results showed that weakly coupled H-aggregate signatures were enhanced upon the addition of Na^+ ions. The same spectroscopic changes were also observed for the divalent non-coordinating cation $[\text{Cu}(\text{en})_2]^{2+}$, indicating that this is a non-specific ion interaction and the reduction in twisting is caused by cations screening the negative charges on glutamic acid residues.

Additionally, this chapter demonstrated that although non-coordinating cations have no direct interaction, divalent metal cations with a propensity to form metal-carboxylate complexes can impart a large reduction in H-aggregate twisting. This was achieved by monitoring spectroscopic changes as a function of ionic strength using Zn^{2+} and Mg^{2+} salts, and comparing the relative change to the non-coordinating metal ions. The analysis illustrated that Zn^{2+} and Mg^{2+} ions are able to form peptide-PBI intermolecular metal-carboxylate complexes which cross-link neighbouring molecules in solution. Further to this being a direct interaction, it is also illustrated to be ion selective due to different amounts of twist reduction between metal ion complexation. A schematic of the two types of metal ion interactions that are demonstrated in this chapter is presented in Scheme 5.1. The concept presented may find application in cation sensor and recognition devices by monitoring the spectroscopic changes that occur in the presence of cations in solution.

Chapter 6

Conclusions

In conclusion, through the combination of two well established synthetic protocols, a series of peptides were symmetrically tethered to a PBI core. The presence, and type, of aggregates in solution was elucidated through interpreting the perturbations of monomer optical spectroscopic signatures. By applying the exciton model it was determined that weakly coupled H-aggregates were formed by the peptide-PBI conjugates in water. Employing various peptide designs allowed the influence of the peptide on assembly to be deduced, and no evidence of H-bonding knitting together PBI chromophores was observed. However, reducing the number of ionisable groups, or increasing steric bulk significantly alters the electronic coupling between chromophores.

The tuneability of PBI aggregates was demonstrated through the use of solvent compositions, which allowed semicrystalline PBI aggregates to undergo controlled reorganisation into weakly coupled H-aggregates, with the introduction of electrostatic repulsions between peptide segments the driving force. The PBI aggregates in water were also shown to be sensitive to metal cation additions in solution, through interactions with the glutamic acid residues. A key result is that cations are capable of forming metal-carboxylate complexes which are able to cross-link adjacent chromophores, thereby reducing twisting within the H-aggregate.

While there are a few recent reports of peptide-conjugated organic dyes, studies have been limited to the observation of aggregation (i.e., converting between an aggregated and non-aggregated state). This work successfully demonstrates the ability of peptide segments to drive the assembly of PBI chromophores; moreover, the peptide design imparts the ability to switch between different types of aggregate states and to finely tune the configuration within a given state.

Chapter 7

Future Work

The controlled assembly of PBI chromophores is a significant step toward device application, although future work directed towards transferring the aggregates into thin films is certainly necessary. Solid state devices are the most common in the field of organic electronics, therefore transferring the knowledge of controlled aggregation in solution into thin films is far more applicable to device fabrication.

An interesting path for future work would be a detailed investigation of fibre formation in solution, particularly through the use of cryo-TEM, which was not available at this institution at the time of this work. However, international collaborators have emerged that have now made this a possibility. Such investigations would enable insight into the geometry of PBI chromophores in the fibre, potentially allowing a mechanism of fibre formation to be elucidated. Information of this nature could allow various design aspects to be incorporated to obtain different supramolecular architectures.

Another avenue of future work would be a thorough investigation into the ability of the peptide sequence to induce the formation of chiral aggregates. The initial CD results obtained in this work demonstrated the potential that chiral amino acid residues close to the PBI core are able to cause exciton signatures of helical cofacial PBI aggregates. Future experiments would almost certainly require the use of comparing the D- and L-amino acids in order to determine that the absolute configuration of the amino acid drive the chiral aggregate formation. These could lead to chiro-optical sensing devices for the detection of biomolecules which possess an absolute configuration of interest.

One other interesting future investigation would be to alter the molecular design

so as to obtain asymmetric peptide-PBI derivatives. In particular, the use of an alkyl tail at one imide nitrogen and a peptide sequence at the other. This could allow different supramolecular architectures to be obtained, which could be elucidated through comparison with the optical spectroscopic signatures presented in this work. To this end, an additional asymmetric derivative could be to change a peptide sequence to an aptamer for the explorations into biosensors to be investigated further. Upon inclusion of an aptamer with a binding affinity towards a particular target analyte could allow for colorimetric biosensor devices. The principle of these would be based on the nature of aggregates would change in the presence of the particular analyte. Such sensing devices could find application in detecting the presence of harmful biomolecules which could pose environmental or health hazards.

In a similar vain, future investigations could focus on the sensitivity of aggregates to various metal ions, other than those explored in this work. Through the inclusion of amino acids that have a propensity to form metal complexes (for example, histidine and Fe^{2+} ions) could impart significant alterations between neighbouring chromophores. Exploiting such a tuning of electronic coupling in solution could extend to the formation of colorimetric (and/or fluorometric) metal ion sensors. Devices of this nature could be useful for the detection of heavy metal ions in waterways, of particular importance would be metal ions that are toxic to ecosystems (*e.g.* manganese, mercury, or lead).

Chapter 8

Experimental

General Methods

All chemicals were purchased from Sigma-Aldrich (St. Louis, MO) and used as received, unless otherwise stated. Amino acid derivatives were purchased from Merck KGaA (Darmstadt, Germany). Derivatised resin was purchased from AAPPTec (Louisville, KY, USA) and 2-(1H-benzotriazole-1-yl)-1,1,3,3-tetramethylaminium hexafluorophosphate (HBTU) was purchased from Nova Biochem. Full 1D and 2D NMR data were obtained on a Varian Direct-Drive spectrometer operating at 600 MHz for ^1H and equipped with a HCN coldprobe. All NMR spectra were referenced internally to residual solvent peaks. Fourier-transform infrared (FT-IR) spectroscopy was performed with a Perkin Elmer Spectrum One spectrometer using freshly prepared potassium bromide pellets and recorded in the range of 450-4000 cm^{-1} and averaged over eight scans. Mass spectra were collected on a Waters Q-TOF Premier Tandem Mass Spectrometer for all peptide precursors (**1**, **2**, **3**, **4** and **5**), an Agilent 6530 Series Q-TOF mass spectrometer for alkyl-PBI **11**, and MALDI-MS was collected on an AB SCIEX TOF/TOF 5800 for all peptide-PBI conjugates (**6**, **7**, **8**, **9** and **10**) using 2,5-dihydroxybenzoic acid (DHB) as matrix.

Optical absorption spectroscopy measurements

Absorption spectroscopy (UV-Vis) was performed with an Agilent 8453 UV-Visible spectrophotometer over the range 220-1100 nm using a quartz cuvette with 1 cm path length. All sample solutions analysed had a total volume of 5 mL. Aqueous

samples of each peptide-PBI conjugate was prepared by having the desired solution (*e.g.* altered pH or aqueous salt solution) then 20 μL of a stock solution (1.3 mg/mL in H_2O) of the relevant peptide-PBI conjugate was added. Solvent composition samples of peptide-PBI conjugates were prepared by mixing water and the organic solvent to the desired percentage (by volume) and then adding 20 μL of a stock solution (1.3 mg/mL in H_2O) of the relevant peptide-PBI conjugate to give a series of individual solution from 0-100% solvent percentage. Samples of alkyl-PBI **11** were prepared by adding 100 μL of a stock solution (0.07 mg/mL in CHCl_3) into 5 mL of solvent.

Absorption data analysis

All spectra were baseline corrected ($\text{Abs}_{700\text{ nm}} = 0$) before subtracting an aggregate signal that may be convoluting the spectrum. The absorption spectrum in acetonitrile (MeCN) was used as the aggregate reference spectrum in all cases. This aggregated spectrum was scaled to match the ‘raw’ absorption at 575 nm and subsequently subtracted from the absorption spectrum of interest with the resulting spectrum being considered the ‘vibronically structured’ component of the absorption spectrum. From this ‘vibronically structured’ component the vibronic ratio ($\frac{A_{0-1}}{A_{0-0}}$) and the value of the ‘vibronically structured’ fraction was calculated by dividing its integrated area (on an x-axis of energy) by that area of the raw absorption spectrum.

Fluorescence spectroscopy measurements

Fluorescence spectroscopy was performed with a Shimadzu RF-5301PC spectrofluorophotometer using a quartz cuvette with 1 cm path length and four polished sides, the slit widths on the spectrofluorophotometer were set to 1.5 nm resolution (for both excitation and emission). All excitation wavelengths were at the 0-0 vibronic peak position, unless otherwise stated. Samples were prepared as described above.

Emission data analysis

All emission spectra were corrected for absorption by dividing by the optical density at the fluorescence excitation wavelength.

Circular dichroism (CD) spectroscopy measurements

CD spectra were recorded on a Chirascan CD Spectrometer. Experiments were performed in a quartz cell with a 1 cm path length over the range of 205-500 nm at 25°C. Samples were prepared as described above.

Preparation of an organogel

The gelation of peptide precursor **3** was prepared by dissolving 3.8 mg of peptide **3** in 1 mL of acetonitrile (MeCN) and sonicating until all the solid was dissolved (approximately 1.5 hours), the self supporting organogel was formed overnight with the solution stored at room temperature. The gelation ability was tested through the ‘inversion of the vial’ test, as shown in Figure 8.1.



Figure 8.1 Inversion of vial showing organogelation of peptide **3** in MeCN.

Cryogenic scanning electron microscopy

Cryogenic scanning electron microscopy studies were conducted using a Jeol JSM-6500F fitted with a Gatan Alto 2500 cryo attachment, operated at an accelerating voltage of 4 kV. To achieve quick freezing (under 1 second) samples were dropped onto a copper rivet and plunged into a ‘slushy’ nitrogen mixture, consisting of a mixture of solid and liquid nitrogen at a temperature of -210 °C. They were then mounted to a sample holder and transferred under vacuum to a cryo-preparation chamber operating at a low temperature of -130 °C. A fracture to expose the internal structure of the samples was achieved using a scalpel to break off the top of the frozen droplet. Samples were then sublimated at -95 °C for 5 minutes, to enhance the topological contrast and coated with up to three 120 second sputter coatings of Pt to allow higher imaging in the SEM. Upon cooling to -130 °C samples were

transferred to the microscope chamber via an interlocked airlock and the microscope temperature was maintained at -130 °C.

Preparation of bis(ethylenediamine) copper(II) sulfate

Copper bisethylenediamine sulfate ($\text{Cu(en)}_2\text{SO}_4$) was prepared through refluxing copper sulfate (10 mL, 0.5 M) and ethylenediamine (1.34 mL, 0.02 mol) for approximately 90 minutes. The water is then removed via reduced pressure, and 5 mL of hot water is added to yield a dark purple solution and allowed to cool. The resulting dark purple crystals were collected via vacuum filtration and washed with ethanol and petroleum ether, and dried in an oven at 60 °C overnight. IR (KBr): ν_{max} 3299, 3217, 31138, 2964, 2923, 2880, 1582, 1451, 1391, 1336, 1277, 1125, 1044, 985, 975, 616 cm^{-1} .

Peptide synthesis procedures

General procedure

The peptide sequences were synthesised via standard Fmoc-based solid phase peptide synthesis (SPPS) protocols.⁴⁹ Briefly, approximately 0.5 g of Fmoc-Glu(OtBu) Wang resin (loading of 0.57 mmolg^{-1}) was swelled in dichloromethane (DCM) for 30 minutes and then washed with dimethylformamide (DMF). Fmoc-deprotection steps were carried out using 30% piperidine (in DMF) with gentle shaking for 30 minutes and then washed five times with fresh DMF. Each amino acid coupling step used 4 mole equivalents (to the loading of resin) of the desired amino acid, 3.95 mole equivalents of HBTU, and 6 mole equivalents of DIPEA (Hünigs base) and shaken for 20 minutes. The Kaiser test was used to confirm the coupling had gone to completion. Amino acid derivatives used: Fmoc-Glu(OtBU)-OH, Fmoc-Ala-OH, Fmoc-Leu-OH and Fmoc-Gly-OH.

Cleavage of the complete peptide sequence involved removing the Fmoc protection on the terminal amino acid residue, rinsing the resin in DMF (5x) and then DCM (5x) and allowing the resin to dry by passing a stream of nitrogen gas through the reaction column. The cleavage solution was a freshly prepared cocktail of CF_3COOH /DCM (3:4 v/v). This was shaken with the resin for 3 hours and then collected. Fresh cleavage solution was passed through the column and the resin was

rinsed with DCM. The collected solution was reduced in volume by half and then added dropwise to 20 mL of cold diethyl ether and allowed to crystallise overnight to afford the fully deprotected peptide sequence which was collected via vacuum filtration.

Preparation of H₂N–Gly–(Glu)₃–OH (1)

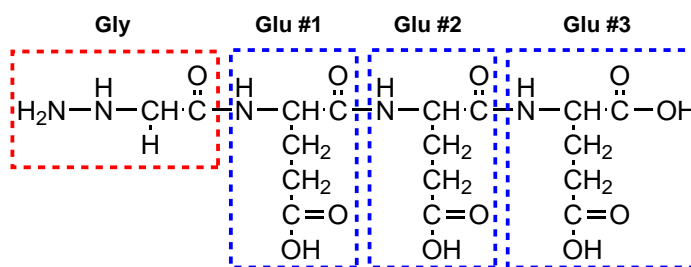


Figure 8.2 Chemical structure of peptide 1

Peptide **1** was obtained using the general procedure described above (Yield: 0.11 g, 72%). ¹H-NMR: (600 MHz, DMSO–d₆) δ_H 8.55 (d, *J*_{HH} = 7.8 Hz, Glu #1), 8.24 (m, 2H, N-H Glu #2, #3), 8.00 (m, 2H, NH₂ Gly), 4.41 (m, 1H, C-H Glu #1), 4.25 (m, 1H, C-H Glu #2), 4.18 (m, 1H, C-H Glu #3), 3.56 (m, 2H, CH₂ Gly), 2.27 (m, 6H, γ-CH₂ Glu #1, #2, #3), 1.84 (m, 6H, β-CH₂ Glu #1, #2, #3); ¹³C-NMR: (150 MHz, DMSO–d₆) δ_C 174.4, 174.3, 174.2, 173.6, 171.5, 171.0, 166.2, 52.2, 52.1, 51.7, 40.6, 30.5, 30.5, 30.4, 28.4, 27.8, 26.6; HR-ESI-MS: *m/z* C₁₇H₂₇N₄O₁₁ [M+H]⁺ calcd 463.1676, found 463.1682.

Preparation of H₂N–Gly–(Gly)₃–(Glu)₃–OH (2)

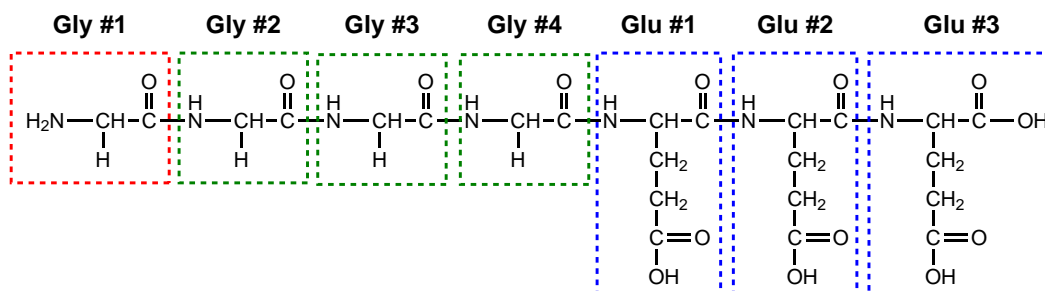


Figure 8.3 Chemical structure of peptide 2

Peptide **2** was obtained using the general procedure described above (Yield: 0.15 g, 67%). ¹H-NMR: (500 MHz, DMSO–d₆) δ_H 8.62 (t, *J*_{HH} = 7.2 Hz, N-H Gly #2), 8.30 (t, *J*_{HH} = 6.6 Hz, N-H Gly #3), 8.17 (d, *J*_{HH} = 9.0 Hz, N-H Glu #3), 8.13 (t, *J*_{HH} = 6.6 Hz, N-H Gly #4), 8.02 (m, 4H, NH₂ Gly #1; N-H Glu #1, #2), 4.26 (m, 2H, C-H Glu #1, #2), 4.17 (m, 1H, C-H Glu #3), 3.85 (d, *J*_{HH} = 6.6 Hz,

CH₂ Gly #2), 3.75 (m, 4H, CH₂ Gly #3, #4), 3.60 (q, $J_{\text{HH}} = 7.2$ Hz, CH₂ Gly #1), 2.26 (m, 6H, γ -CH₂ Glu #1, #2, #3), 1.84 (m, 6H, β -CH₂ Glu #1, #2, #3). HR-ESI-MS: m/z C₂₃H₃₆N₇O₁₄ [M+H]⁺ calcd 634.2320, found 634.2321.

Preparation of H₂N-Gly-(Ala)₃-(Glu)₃-OH (3)

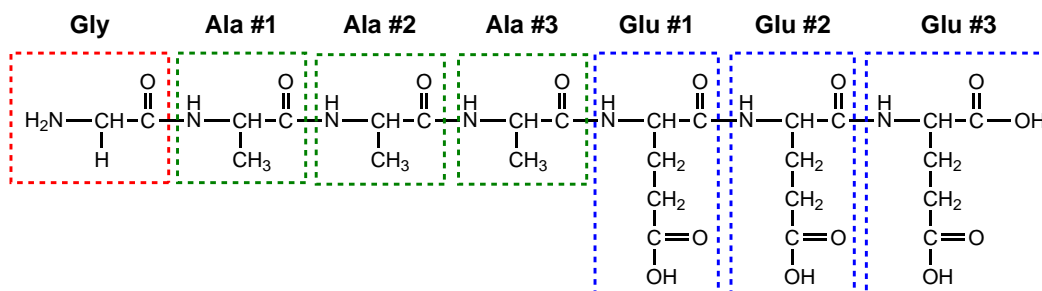


Figure 8.4 Chemical structure of peptide **3**

Peptide **3** was obtained using the general procedure described above (Yield: 0.21 g, 55%). ¹H-NMR: (600 MHz, DMSO-d₆) δ_{H} 8.54 (d, $J_{\text{HH}} = 7.5$ Hz, N-H Ala #1), 8.24 (d, $J_{\text{HH}} = 7.5$ Hz, NH Ala #2), 8.21 (d, $J_{\text{HH}} = 7.5$ Hz, NH Glu #3), 7.95 (m, 5H, NH₂ Gly; NH Glu #1, #2; NH Ala #3), 4.40 (quin, $J_{\text{HH}} = 7.2$ Hz, CH Ala #1), 4.24 (m, 4H, CH Ala #2, #3; CH Glu #1, #2), 4.16 (m, 1H, CH Glu #3), 3.56 (q, $J_{\text{HH}} = 5.3$ Hz, CH₂ Gly), 2.24 (m, 6H, γ -CH₂ Glu #1, #2, #3), 1.81 (m, 6H, β -CH₂ Glu #1, #2, #3), 1.19 (m, 9H, CH₃ Ala #1, #2, #3); ¹³C-NMR: (150 MHz, DMSO-d₆) δ_{C} 174.0, 173.8, 173.1, 171.8, 171.5, 171.1, 170.5, 170.0, 165.5, 51.7, 51.6, 51.3, 48.1, 48.1, 48.0, 40.1, 30.1, 30.1, 29.9, 27.5, 27.4, 26.2, 18.9, 18.1, 18.1; HR-ESI-MS: m/z C₂₆H₄₂N₇O₁₄ [M+H]⁺ calcd 676.2784, found 676.2794; IR (KBr): ν_{max} 3290, 3085, 2983, 2940, 2637, 1716, 1634, 1533, 1443, 1412, 1338, 1201, 1142, 965, 929, 827, 799 cm⁻¹.

Preparation of H₂N-Gly-(Ala)₃-Glu-OH (4)

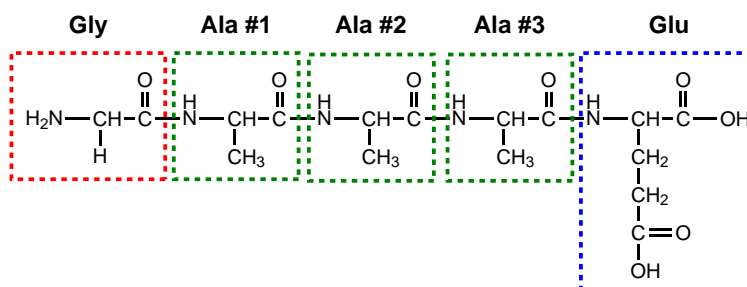


Figure 8.5 Chemical structure of peptide **4**

Peptide **4** was obtained using the general procedure described above (Yield: 0.12 g, 93%). ¹H-NMR: (600 MHz, DMSO-d₆) δ_{H} 8.56 (d, $J_{\text{HH}} = 7.5$ Hz, N-H Ala

#1), 8.24 (d, $J_{\text{HH}} = 7.6$ Hz, N-H Ala #2), 8.11 (d, $J_{\text{HH}} = 7.9$ Hz, N-H Glu), 7.99 (m, 2H, NH_2 Gly), 7.91 (d, $J_{\text{HH}} = 7.3$ Hz, N-H Ala #3), 4.40 (quin, $J_{\text{HH}} = 7.2$ Hz, C-H Ala #1), 4.26 (m, 2H, C-H Ala #2, #3), 4.19 (m, 1H, C-H Glu), 3.56 (q, $J_{\text{HH}} = 4.9$ Hz, CH_2 Gly), 2.27 (m, 2H, $\gamma\text{-CH}_2$ Glu), 1.86 (m, 2H, $\beta\text{-CH}_2$ Glu), 1.21 (m, 9H, CH_3 Ala #1, #2, #3); ^{13}C -NMR: (150 MHz, DMSO-d_6) δ_{C} 174.1, 173.5, 172.6, 171.9, 165.9, 51.5, 48.5, 48.3, 48.2, 40.4, 30.4, 26.8, 19.0, 18.6, 18.5; HR-ESI-MS: m/z $\text{C}_{16}\text{H}_{27}\text{N}_5\text{O}_8$ $[\text{M}+\text{H}]^+$ calcd 418.1932, found 418.1936.

Preparation of $\text{H}_2\text{N-Gly-(Leu)}_3\text{-(Glu)}_3\text{-OH}$ (5)

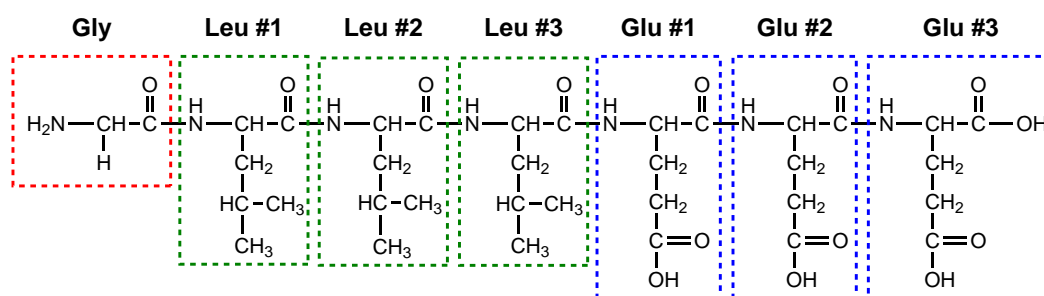


Figure 8.6 Chemical structure of peptide **5**

Peptide **10** was obtained using the general procedure described above (Yield: 0.15 g, 52%). ^1H -NMR: (600 MHz, DMSO-d_6) δ_{H} 8.47 (d, $J_{\text{HH}} = 8.5$ Hz, N-H Leu #1), 8.24 (d, $J_{\text{HH}} = 8.2$ Hz, N-H Leu #2), 8.22 (d, $J_{\text{HH}} = 7.6$ Hz, Glu #3), 7.95 (m, 5H, NH_2 Gly; N-H Glu #1, #2; N-H Ala #3), 4.44 (m, 1H, $\alpha\text{-CH}$ Leu #1), 4.28 (m, 3H, $\alpha\text{-CH}$ Leu #2; Leu #3; Glu #2), 4.17 (m, 2H, C-H Glu #1; Glu #3), 3.56 (q, $J_{\text{HH}} = 5.6$ Hz, $\alpha\text{-CH}_2$ Gly), 2.24 (m, 6H, $\gamma\text{-CH}_2$ Glu #1, #2, #3), 1.81 (m, 6H, $\beta\text{-CH}_2$ Glu #1, #2, #3), 1.57 (m, 3H, $\gamma\text{-CH}$ Leu #1, #2, #3), 1.42 (m, 6H $\beta\text{-CH}_2$ Leu #1, #2, #3), 0.85 (m, 18H, CH_3 Leu #1, #2, #3); ^{13}C -NMR: (150 MHz, DMSO-d_6) δ_{C} 174.5, 174.4, 174.1, 173.5, 172.0, 171.8, 171.5, 171.1, 165.9, 52.0, 51.7, 51.2, 51.2, 41.9, 40.8, 40.5, 30.5, 30.4, 28.0, 27.8, 26.6, 24.6, 24.5, 24.5, 23.6, 23.4, 22.2, 22.1, 21.9; HR-ESI-MS: m/z $\text{C}_{35}\text{H}_{60}\text{N}_7\text{O}_{14}$ $[\text{M}+\text{H}]^+$ calcd 802.4193, found 802.4177.

PBI synthesis procedures

General procedure for peptide-PBI conjugates

Peptide-PBI conjugates were synthesised using the standard method of amine condensation reported in the literature for the synthesis of symmetric perylene bisimide derivatives, developed by Langhals and co-workers.¹⁵ A mixture of the relevant peptide sequence, perylene tetracarboxylic dianhydride (PTCDA) and imidazole were added in a round bottom flask and stirred at 120 °C for 24 hours under a nitrogen atmosphere, after which the mixture was allowed to cool to 90 °C and 3 mL of water was added under nitrogen and allowed to cool to room temperature. The dark red solution was acidified with acetic acid to afford a very fine red precipitate. This solution was then passed through an HP20ss column with addition of increasing amounts of water. Once the crude mixture was loaded onto the column, 3% (400 mL total) and 5% (300 mL) acetic acid washings were passed through the column. The column was then washed with acetone and the desired product was extracted from the column by rinsing the column with pyridine, subsequently removing the solvent via reduced pressure.

Preparation of (H₂N-Gly-(Glu)₃)₂-PBI (6)

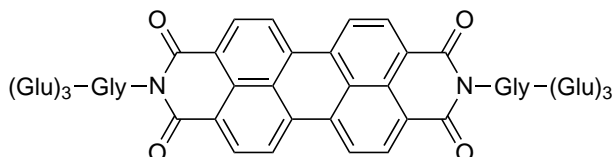


Figure 8.7 Chemical structure of peptide-PBI **6**

Peptide-PBI **6** was synthesised using the general procedure outlined above, using 0.0925 g (0.20 mmol) peptide **1**, 0.0392 g (0.10 mmol) PTCDA, and 2.0198 g imidazole (Yield: 0.09 g, 88%). MALDI-TOF-MS: m/z C₅₈H₅₆N₈O₂₆Na [M+Na]⁺ calcd 1303, found 1303; IR (KBr): ν_{\max} 3430, 3064, 2956, 2925, 2853, 1693, 1658, 1593, 1438, 1401, 1365, 1340, 1302, 1275, 1248, 1174, 1132, 1003, 810 cm⁻¹.

Preparation of (H₂N-Gly-(Gly)₃-(Glu)₃)₂-PBI (7)

Peptide-PBI **7** was synthesised using the general procedure outlined above, using 0.1482 g (0.23 mmol) peptide **2**, 0.0518 g (0.13 mmol) PTCDA, and 2.3496 g imidazole (Yield: 0.15 g, 70%). ¹H-NMR: (600 MHz, CDCl₃/CF₃COOH, 2:1) δ_{H} 8.84

$C_{56}H_{58}N_{10}O_{20}Na$ $[M+Na]^+$ calcd 1213, found 1214; IR (KBr): ν_{\max} 3445, 3280, 3060, 2965, 2928, 1698, 1658, 1630, 1594, 1543, 1439, 1401, 1364, 1340, 1302, 1245, 1172, 1054, 853, 810 cm^{-1} .

Preparation of $(H_2N-Gly-(Leu)_3-(Glu)_3)_2-PBI$ (**10**)

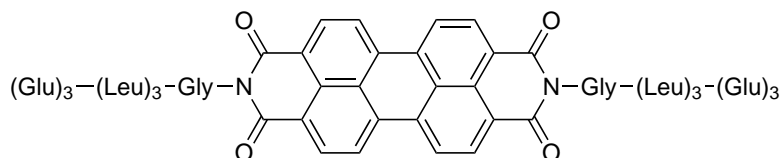


Figure 8.11 Chemical structure of peptide-PBI **10**

Peptide-PBI **10** was synthesised using the general procedure outlined above, using 0.1441 g (0.18 mmol) peptide **5**, 0.0353 g (0.09 mmol) PTCDA, and 2.2023 g imidazole (Yield: 0.12 g, 71%). 1H -NMR: (600 MHz, $CDCl_3/CF_3COOH$, 2:1) δ_H 8.86 (m, Ar-H), 5.15 (m, α -CH₂ Gly), 4.67 (m, α -CH Leu, Glu) 2.63 (m, γ -CH₂ Glu), 2.16 (m, β -CH₂ Glu), 1.63 (m, β -CH₂ Leu; γ -CH Leu), 0.90 (m, CH₃ Leu); MALDI-TOF-MS: m/z $C_{94}H_{122}N_{14}O_{32}Na$ $[M+Na]^+$ calcd 1982, found 1982; IR (KBr): ν_{\max} 3426, 3291, 3074, 2959, 2931, 2872, 1703, 1663, 1642, 1595, 1542, 1438, 1402, 1369, 1341, 1248, 1174, 1130, 1038, 1002, 811 cm^{-1} .

Preparation of $(C_{12}H_{25})_2-PBI$ (**11**)

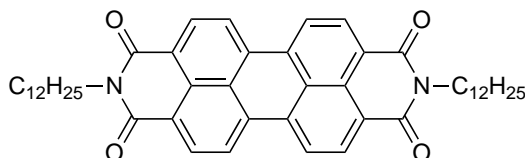


Figure 8.12 Chemical structure of alkyl-PBI **11**

Alkyl-PBI **11** was synthesised following a similar condensation method reported by Balakrishnan *et al.*.²³ A mixture of PTCDA (3.92 g, 10 mmol), dodecylamine (5.53g, 30 mmol), $Zn(OAc)_2$ (0.988 g) and imidazole (40.6 g) were stirred at 130 °C for 24 hours under argon atmosphere. The mixture was cooled to room temperature and dispersed in 500 mL ethanol, and acidified using 2 M HCl until pH 3–4 was reached. A red/brown waxy solid was collected via vacuum filtration and dried in an oven overnight at 120 °C. (Yield: 6.8 g, 93.6%). 1H -NMR: (600 MHz, $CDCl_3$) δ_H 8.77 (d, $J_{HH} = 7.9$ Hz, Ar-H), 8.66 (d, $J_{HH} = 8.1$ Hz, Ar-H), 4.21 (t, $J_{HH} = 7.7$ Hz, α -CH₂), 1.47 (m, 40H, CH₂), 0.83 (m, 6H, CH₃); ^{13}C -NMR: (150 MHz, $CDCl_3$) δ_C 163.4, 134.7, 131.5, 123.3, 123.1, 40.7, 31.9, 29.7, 29.7, 29.6, 29.6, 29.4, 27.2, 22.7, 14.1; HR-ESI-MS: m/z $C_{48}H_{58}N_2O_4Na$ $[M+Na]^+$ calcd 749.4294, found 749.4315;

IR (KBr): ν_{max} 3426, 3070, 2957, 2923, 2850, 1697, 1657, 1594, 1439, 1405, 1345, 1255, 1090, 853, 809, 747 cm^{-1} .

Appendix - NMR Spectra

This appendix contains NMR spectra of peptide-PBI **8**, which was used for structural identity confirmation. Additionally, the NMR spectra of peptide **3** are included for illustration of the data used for structural elucidation of each peptide precursor used in this study. The data for these two compounds are representative of all data obtained for the peptide-PBI conjugates and peptide precursors respectively. All data that are reported, but not presented in this appendix, are available upon request.

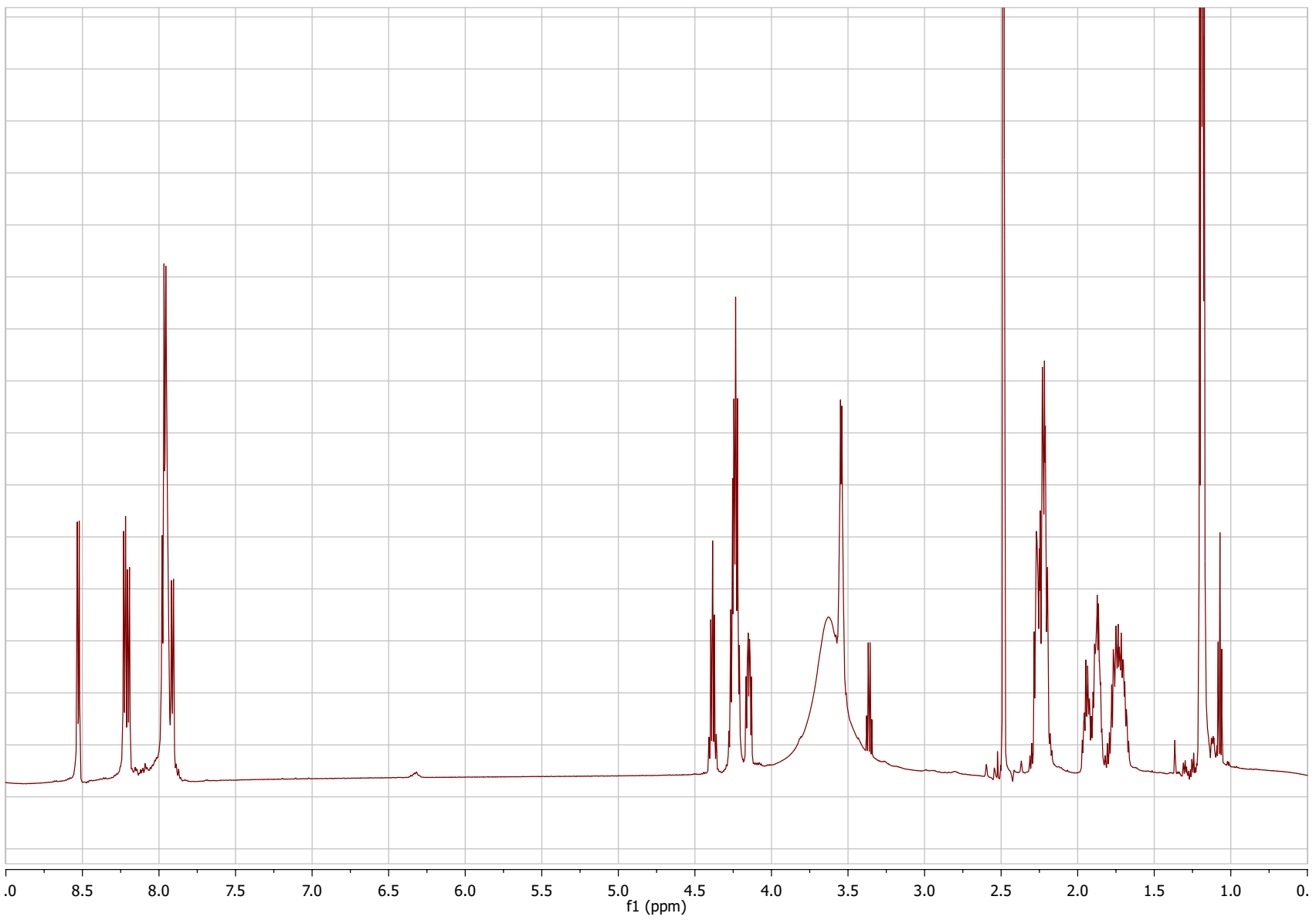
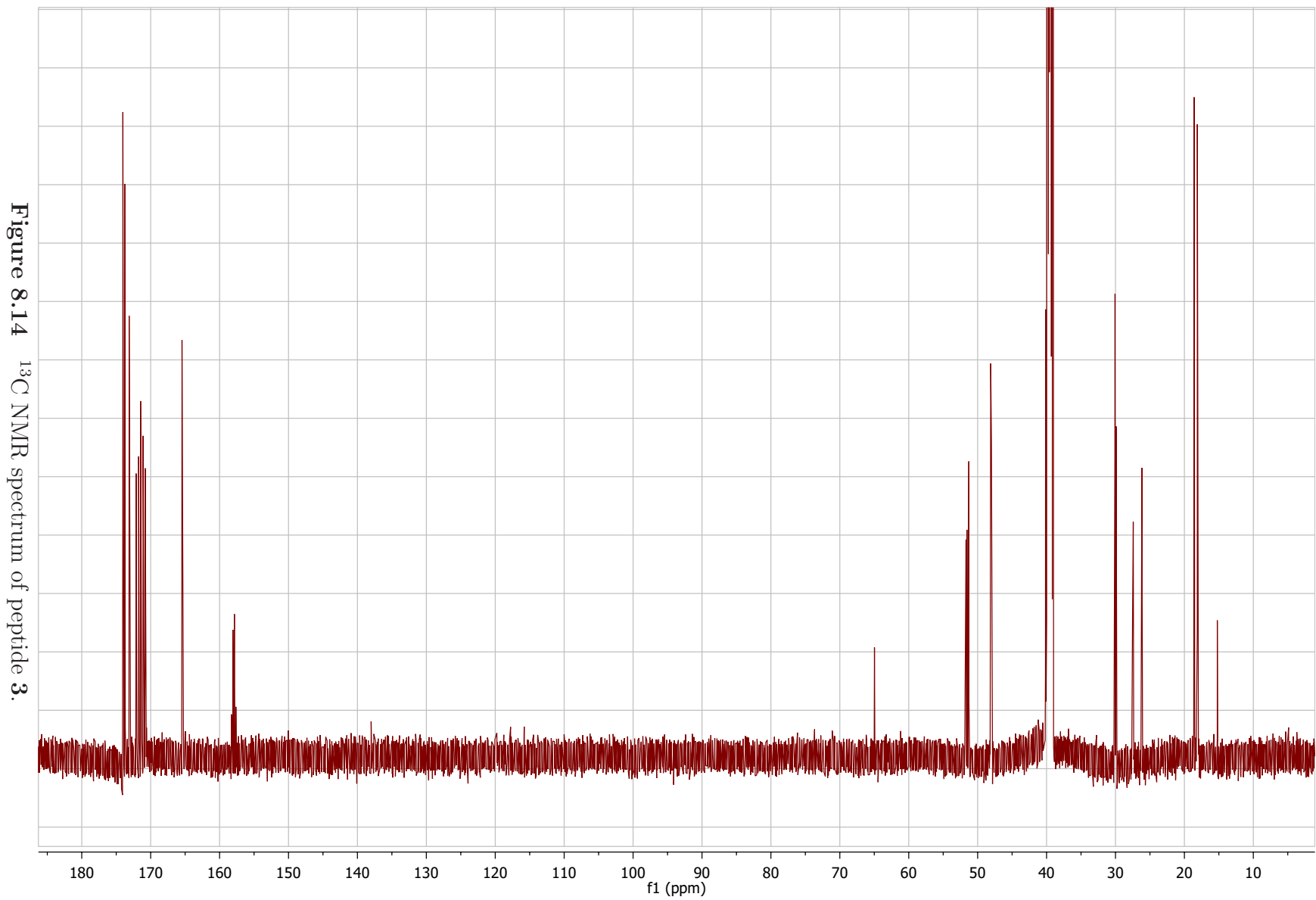


Figure 8.13 ^1H NMR spectrum of peptide 3.



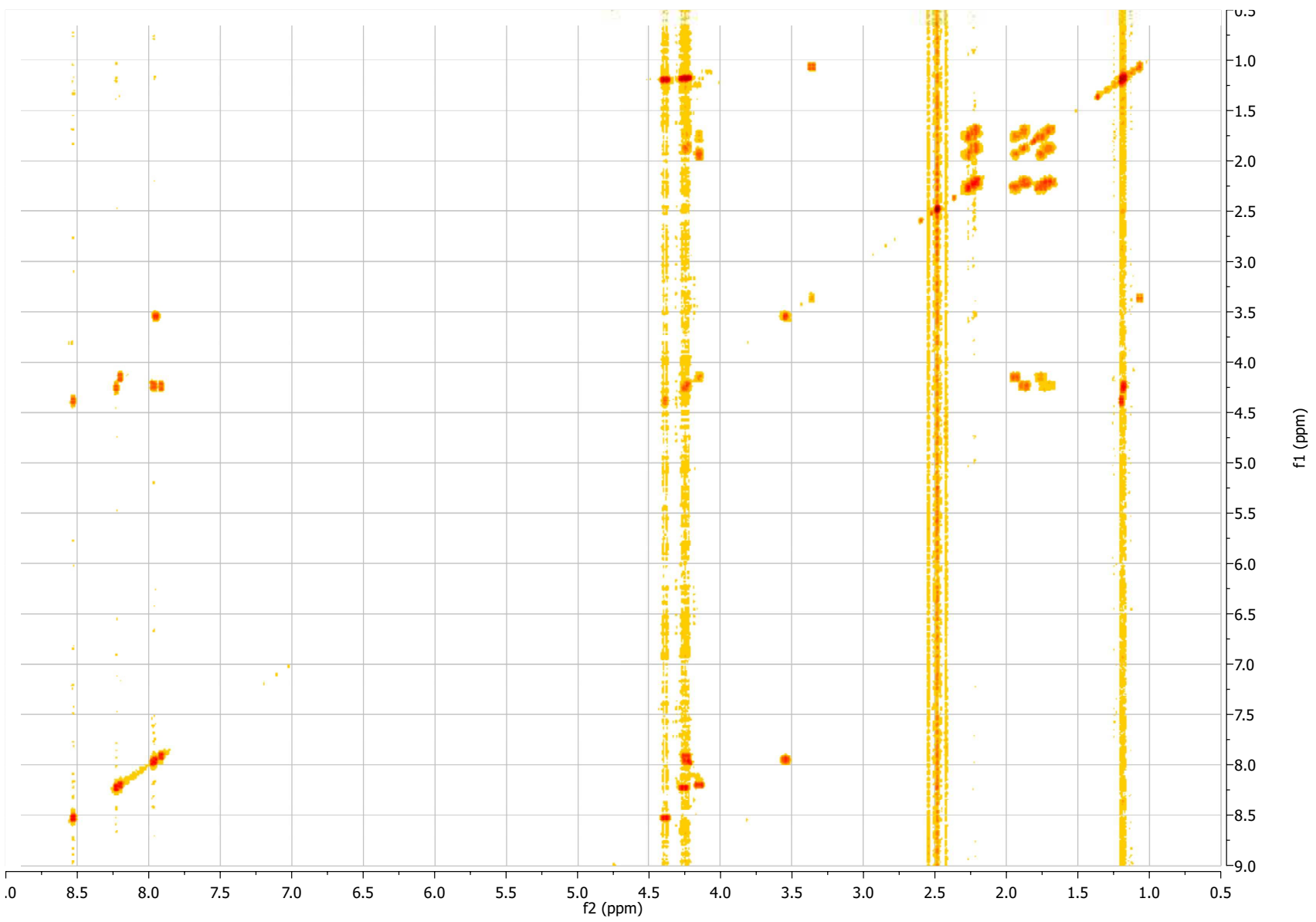


Figure 8.15 COSY NMR spectrum of peptide 3.

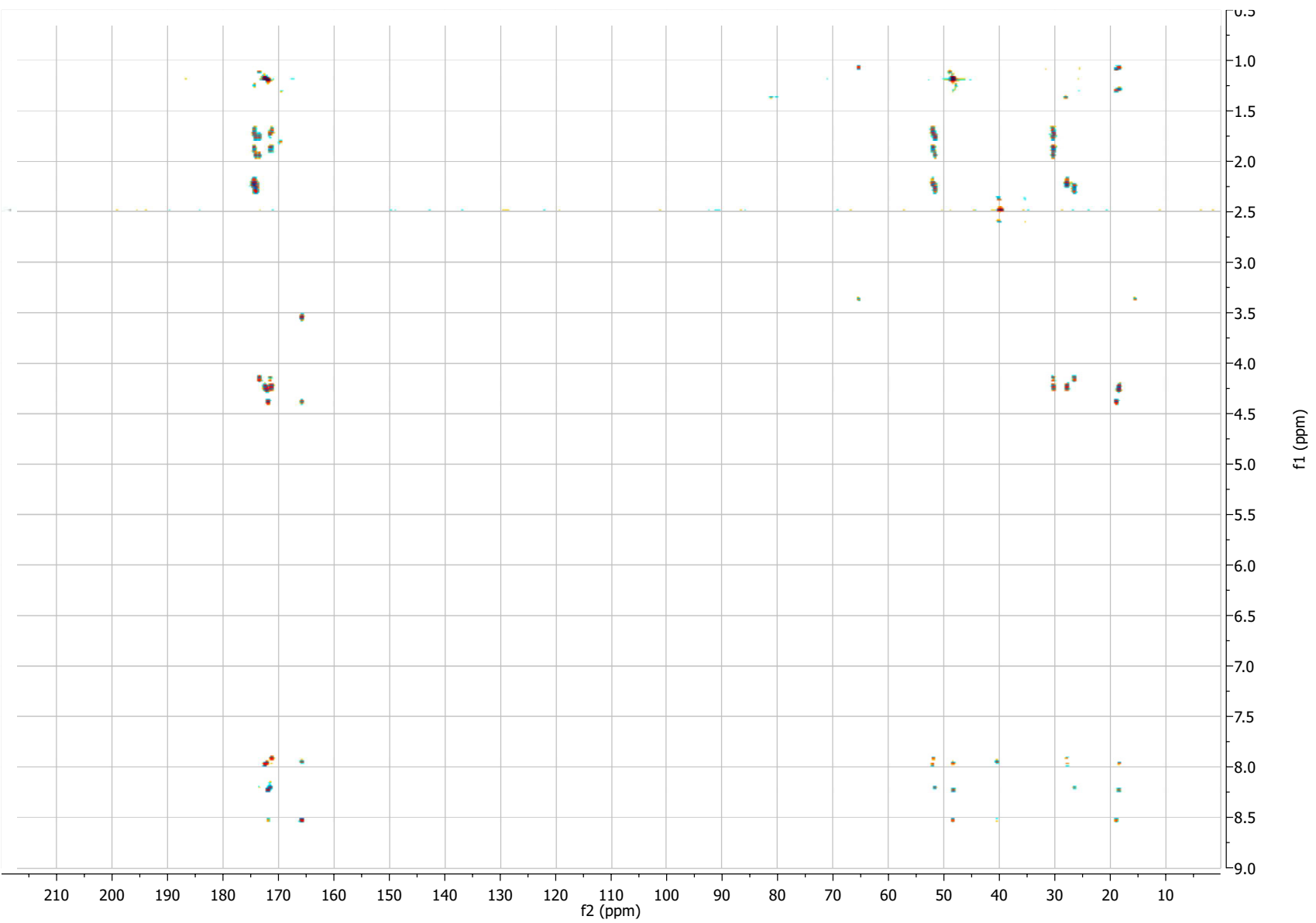
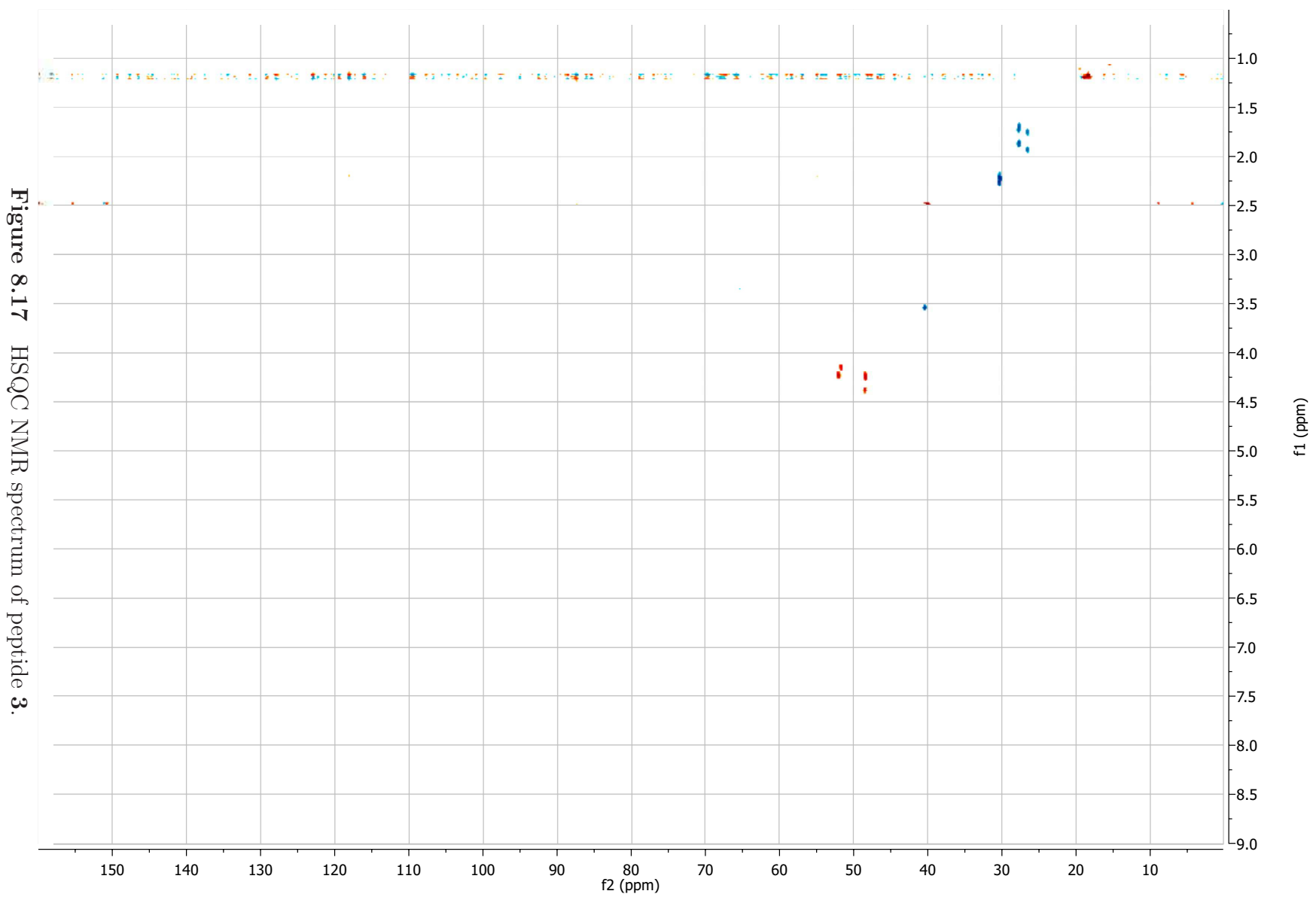


Figure 8.16 HMBC NMR spectrum of peptide 3.



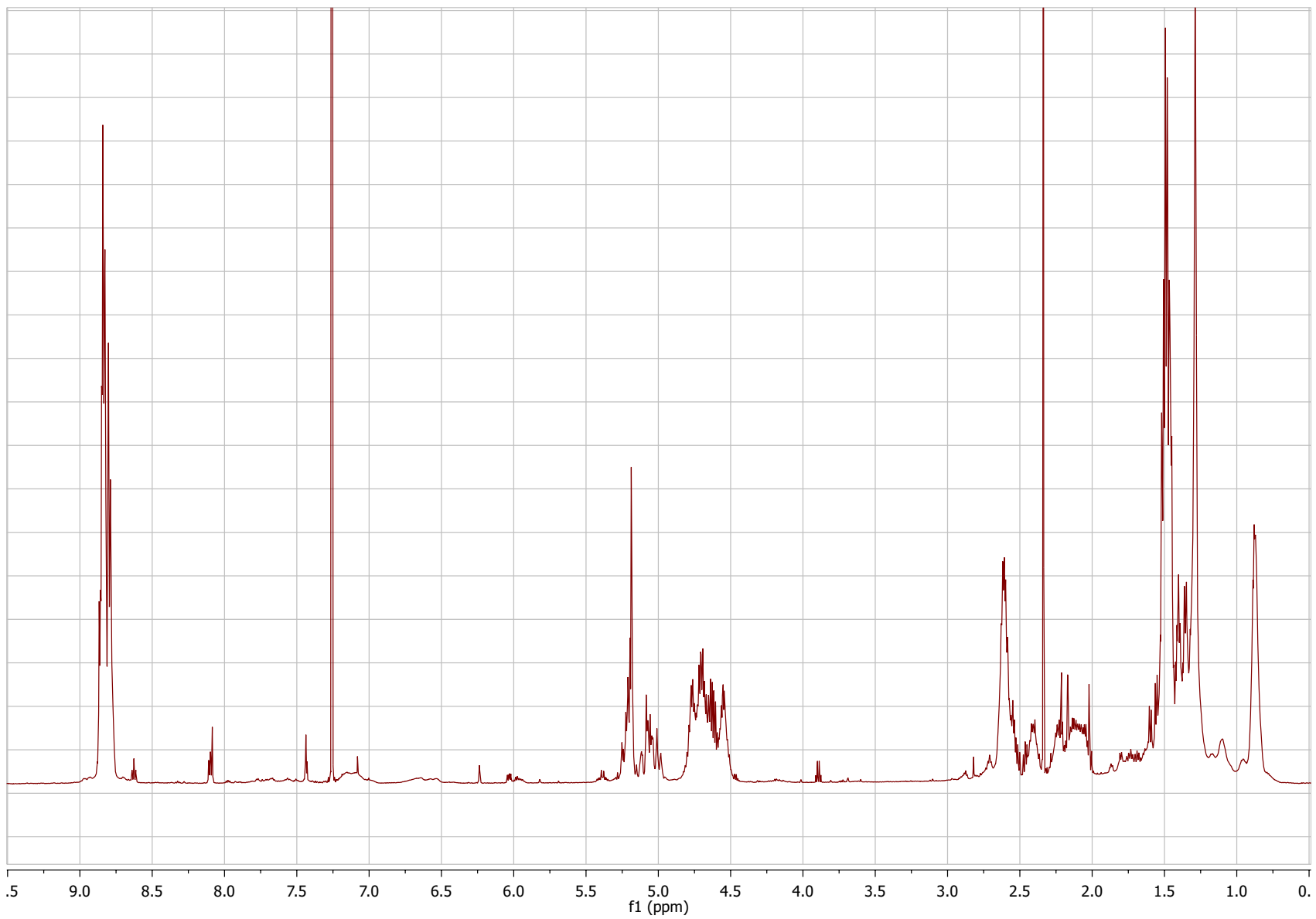
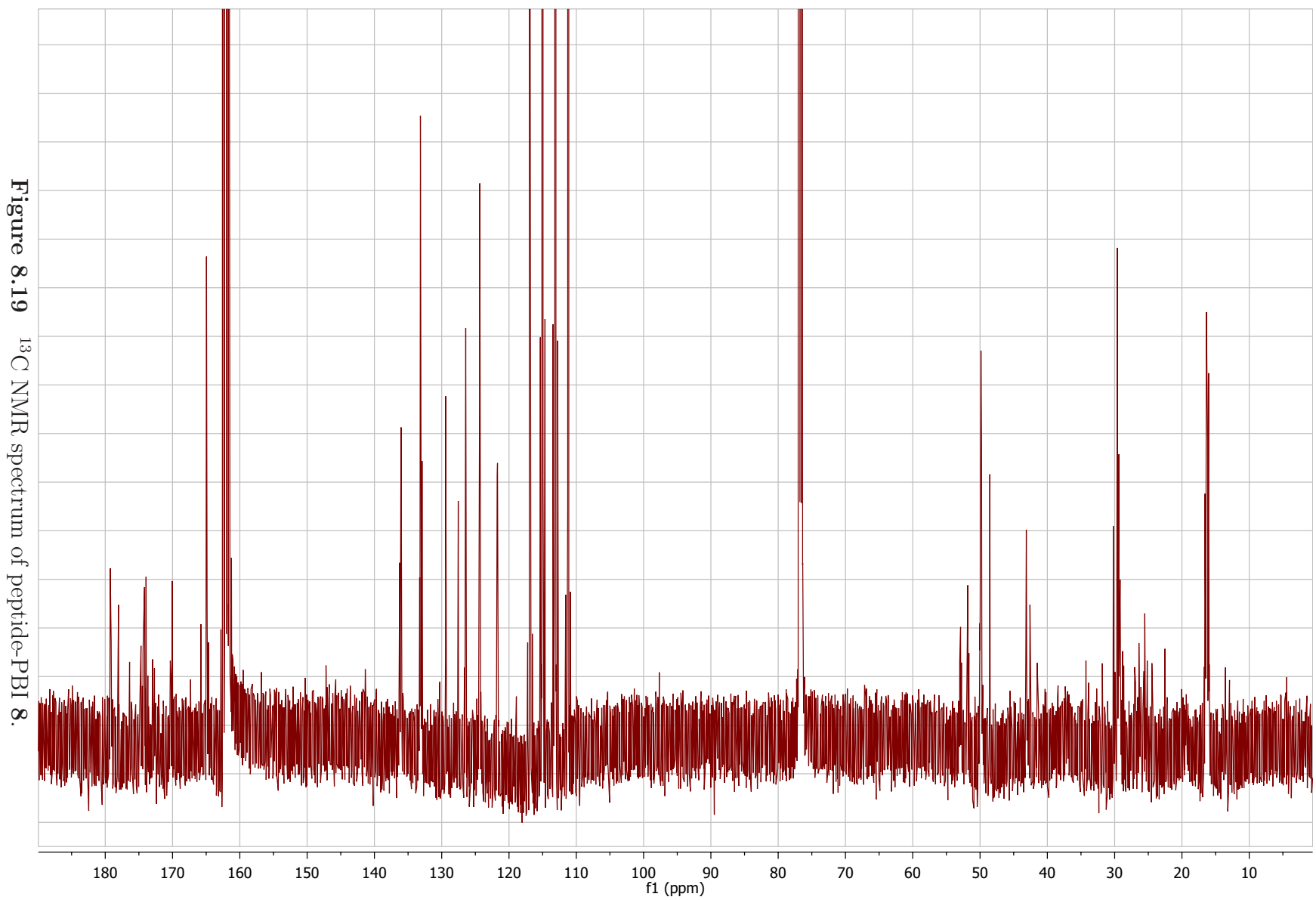


Figure 8.18 ^1H NMR spectrum of peptide-PBI 8.



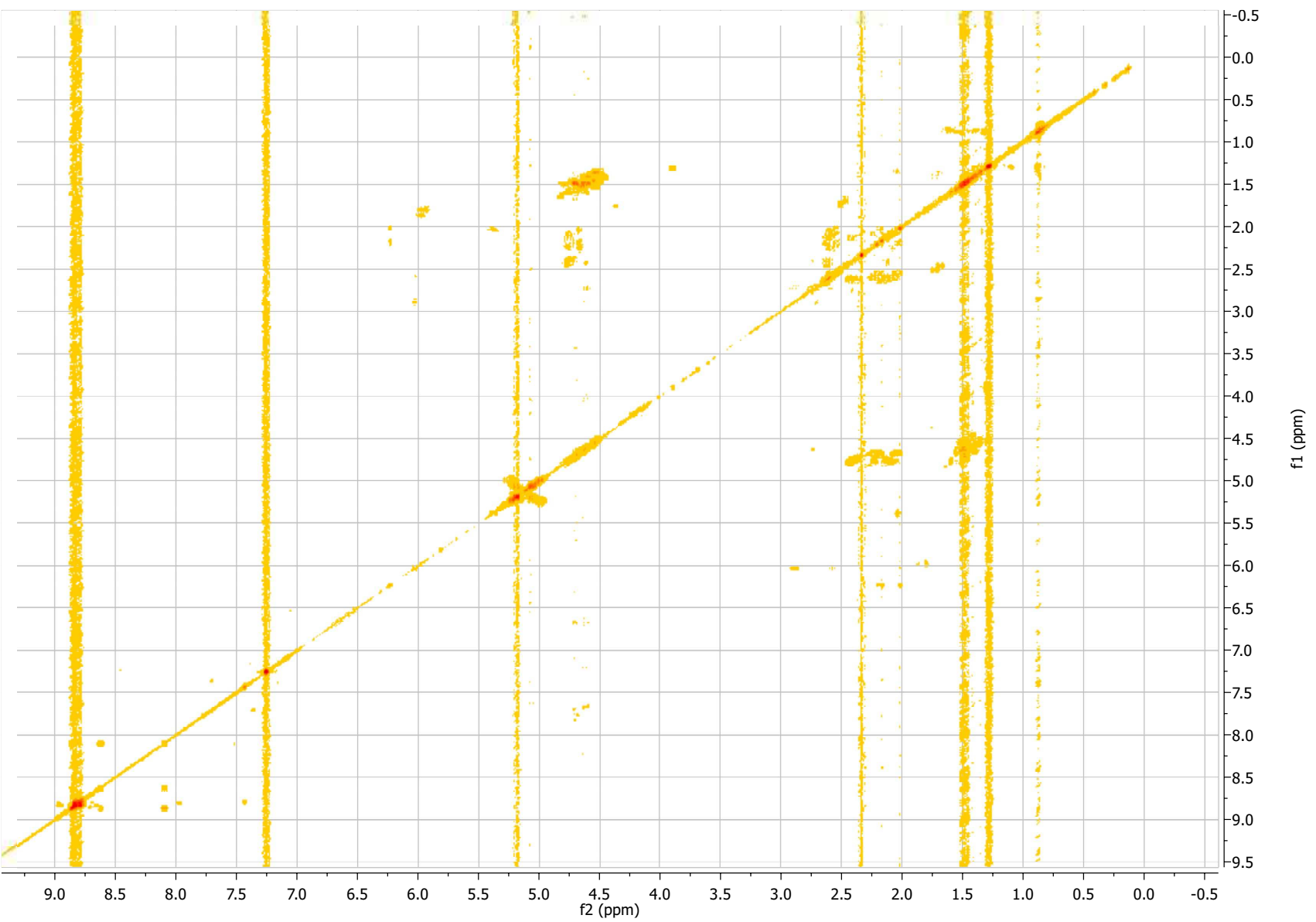


Figure 8.20 COSY NMR spectrum of peptide-PBI 8.

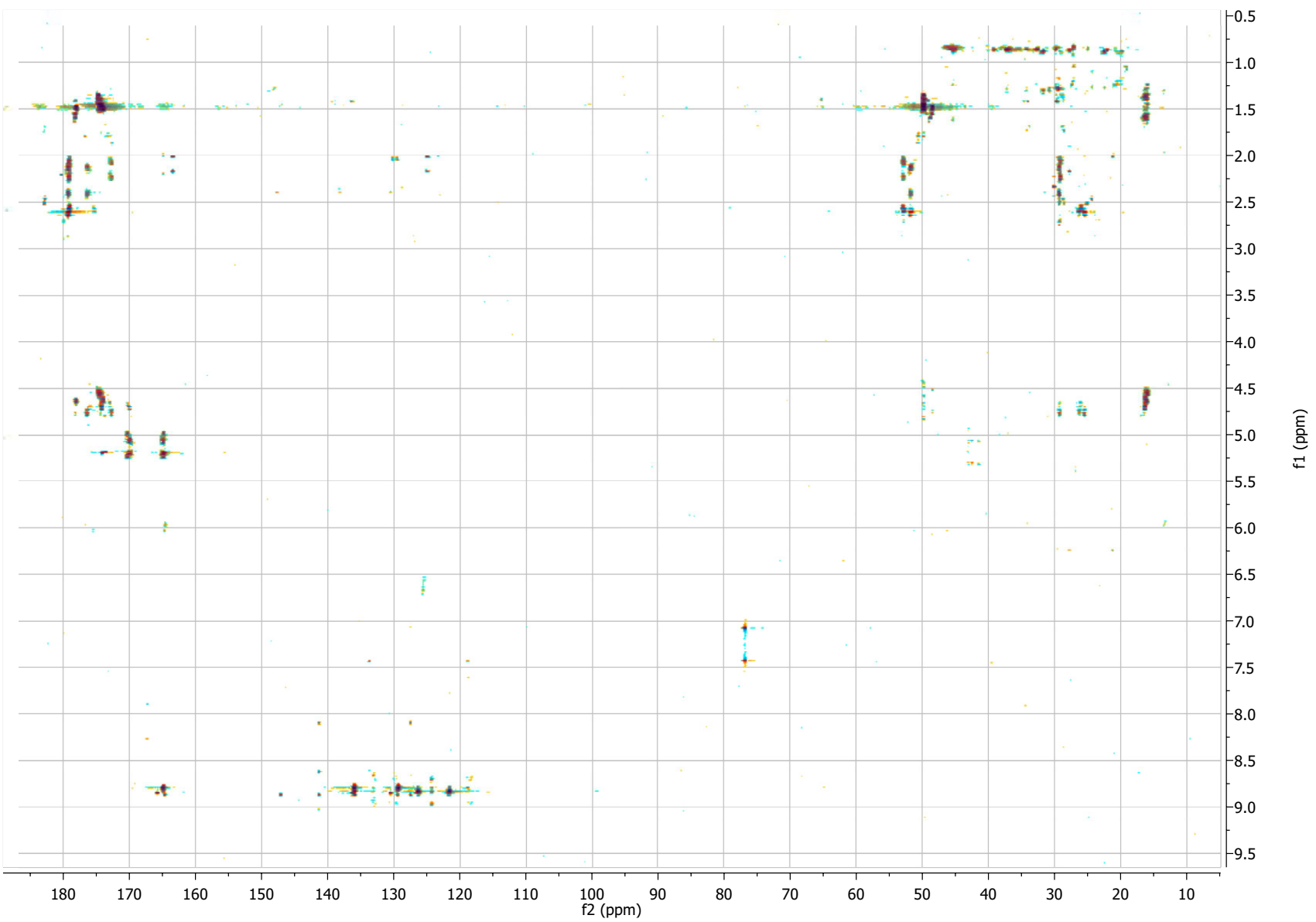
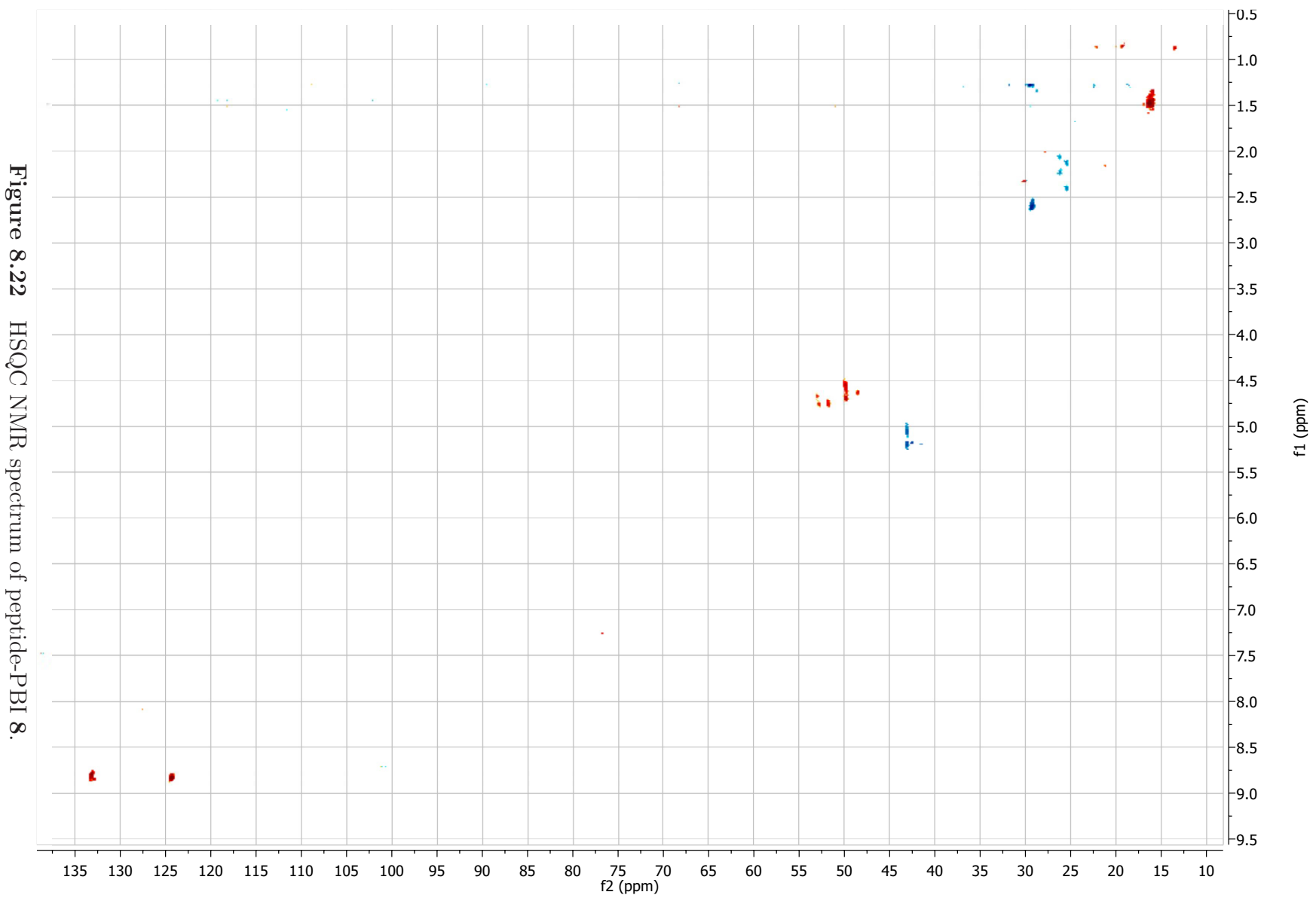


Figure 8.21 HMBC NMR spectrum of peptide-PBI 8.



References

1. Hoeben, F. J. M.; Jonkheijm, P.; Meijer, E. W.; Schenning, A. P. H. J. *Chem. Rev.* **2005**, *105*, 1491–1546.
2. Chen, Z.; Lohr, A.; Saha-Moller, C. R.; Würthner, F. *Chem. Soc. Rev.* **2009**, *38*, 564–584.
3. Kim, H. J.; Kim, T.; Lee, M. *Acc. Chem. Res.* **2011**, *44*, 72–82.
4. Shimizu, T.; Masuda, M.; Minamikawa, H. *Chem. Rev.* **2005**, *105*, 1401–1444.
5. Sundström, V.; Pullerits, T.; van Grondelle, R. *J. Phys. Chem. B* **1999**, *103*, 2327–2346.
6. Cui, H.; Webber, M. J.; Stupp, S. I. *Biopolymers* **2010**, *94*, 1–18.
7. Facchetti, A. *Mater. Today* **2007**, *10*, 28 – 37.
8. Dittmer, J.; Lazzaroni, R.; Leclère, P.; Moretti, P.; Granström, M. et al. *Sol. Energ. Mat. Sol. Cells* **2000**, *61*, 53 – 61.
9. Herbst, K., W.; Hunger *Industrial Organic Pigments*, 2nd ed.; Wiley-VCH: Weinheim, 1997.
10. Pan, J.; Zhu, W.; Li, S.; Zeng, W.; Cao, Y. et al. *Polymer* **2005**, *46*, 7658 – 7669.
11. Breeze, A. J.; Salomon, A.; Ginley, D. S.; Gregg, B. A.; Tillmann, H. et al. *Appl. Phys. Lett.* **2002**, *81*, 3085–3087.
12. Jones, B. A.; Facchetti, A.; Wasielewski, M. R.; Marks, T. J. *J. Am. Chem. Soc.* **2007**, *129*, 15259–15278.
13. Würthner, F. *Chem. Commun.* **2004**, 1564–1579.
14. Hädicke, E.; Graser, F. *Acta Crystallogr., Sec. C* **1986**, *42*, 189–195.
15. Langhals, H. *Heterocycles* **1995**, *40*, 477–500.
16. Klebe, G.; Graser, F.; Hädicke, E.; Berndt, J. *Acta Crystallogr., Sec. B* **1989**, *45*, 69–77.
17. Chen, Z.; Debije, M. G.; Debaerdemaeker, T.; Osswald, P.; Würthner, F. *ChemPhysChem* **2004**, *5*, 137–140.
18. Huang, C.; Barlow, S.; Marder, S. R. *J. Org. Chem.* **2011**, *76*, 2386–2407.

19. Spano, F. C. *Acc. Chem. Res.* **2010**, *43*, 429–439.
20. Dehm, V. C. Synthesis and Characterization of an Oligo(Phenylene Ethynylene)-Based Perylene Bisimide Foldamer. Ph.D. thesis, University of Wuerzburg, Germany, 2010.
21. Nagao, Y. *Prog. Org. Coat.* **1997**, *31*, 43 – 49.
22. Görl, D.; Zhang, X.; Würthner, F. *Angew. Chem., Int. Ed.* **2012**, [Online early access], DOI:10.1002/anie.201108690.
23. Balakrishnan, K.; Datar, A.; Naddo, T.; Huang, J.; Oitker, R. et al. *J. Am. Chem. Soc.* **2006**, *128*, 7390–7398.
24. Ghosh, S.; Li, X.-Q.; Stepanenko, V.; Würthner, F. *Chem.–Eur. J.* **2008**, *14*, 11343–11357.
25. Briseno, A. L.; Mannsfeld, S. C. B.; Reese, C.; Hancock, J. M.; Xiong, Y. et al. *Nano Lett.* **2007**, *7*, 2847–2853.
26. Yang, X.; Xu, X.; Ji, H.-F. *J. Phys. Chem. B* **2008**, *112*, 7196–7202.
27. Balakrishnan, K.; Datar, A.; Oitker, R.; Chen, H.; Zuo, J. et al. *J. Am. Chem. Soc.* **2005**, *127*, 10496–10497.
28. Sinks, L. E.; Rybtchinski, B.; Iimura, M.; Jones, B. A.; Goshe, A. J. et al. *Chem. Mater.* **2005**, *17*, 6295–6303.
29. Zhang, X.; Chen, Z.; Würthner, F. *J. Am. Chem. Soc.* **2007**, *129*, 4886–4887.
30. You, C.-C.; Würthner, F. *J. Am. Chem. Soc.* **2003**, *125*, 9716–9725.
31. Seki, T.; Yagai, S.; Karatsu, T.; Kitamura, A. *J. Org. Chem.* **2008**, *73*, 3328–3335.
32. Sun, Y.; He, C.; Sun, K.; Li, Y.; Dong, H. et al. *Langmuir* **2011**, *27*, 11364–11371.
33. Franke, D.; Vos, M.; Antonietti, M.; Sommerdijk, N. A. J. M.; Faul, C. F. J. *Chem. Mater.* **2006**, *18*, 1839–1847.
34. Thalacker, C.; Würthner, F. *Adv. Funct. Mater.* **2002**, *12*, 209–218.
35. Würthner, F.; Thalacker, C.; Sautter, A.; Schärftl, W.; Ibach, W. et al. *Chem.–Eur. J.* **2000**, *6*, 3871–3886.
36. Whitesides, G. M.; Simanek, E. E.; Mathias, J. P.; Seto, C. T.; Chin, D. et al. *Acc. Chem. Res.* **1995**, *28*, 37–44.
37. Seki, T.; Maruya, Y.; Nakayama, K.; Karatsu, T.; Kitamura, A. et al. *Chem. Commun.* **2011**, *47*, 12447–12449.
38. Rybtchinski, B. *ACS Nano* **2011**, *5*, 6791–6818.
39. Sivakova, S.; Rowan, S. J. *Chem. Commun.* **2003**, 2428–2429.

40. van der Boom, T.; Hayes, R. T.; Zhao, Y.; Bushard, P. J.; Weiss, E. A. et al. *J. Am. Chem. Soc.* **2002**, *124*, 9582–9590.
41. Miao, Q.; Lefenfeld, M.; Nguyen, T. Q.; Siegrist, T.; Kloc, C. et al. *Adv. Mater.* **2005**, *17*, 407–412.
42. Jiang, L.; Hughes, R. C.; Sasaki, D. Y. *Chem. Commun.* **2004**, 1028–1029.
43. Varghese, R.; Wagenknecht, H. A. *Chem.–Eur. J.* **2010**, *16*, 9040–9046.
44. Neelakandan, P. P.; Pan, Z.; Hariharan, M.; Zheng, Y.; Weissman, H. et al. *J. Am. Chem. Soc.* **2010**, *132*, 15808–15813.
45. Weil, T.; Vosch, T.; Hofkens, J.; Peneva, K.; Mllen, K. *Angew. Chem., Int. Ed.* **2010**, *49*, 9068–9093.
46. Malinovskii, V. L.; Wenger, D.; Häner, R. *Chem. Soc. Rev.* **2010**, *39*, 410–422.
47. Channon, K. J.; Devlin, G. L.; Magennis, S. W.; Finlayson, C. E.; Tickler, A. K. et al. *J. Am. Chem. Soc.* **2008**, *130*, 5487–5491.
48. Hartgerink, J. D.; Beniash, E.; Stupp, S. I. *Science* **2001**, *294*, 1684–1688.
49. Coin, I.; Beyermann, M.; Bienert, M. *Nat. Protoc.* **2007**, *2*, 3247–3256.
50. Santoso, S.; Hwang, W.; Hartman, H.; Zhang, S. *Nano Lett.* **2002**, *2*, 687–691.
51. Aggeli, A.; Bell, M.; Carrick, L. M.; Fishwick, C. W. G.; Harding, R. et al. *J. Am. Chem. Soc.* **2003**, *125*, 9619–9628.
52. Kokkoli, E.; Mardilovich, A.; Wedekind, A.; Rexeisen, E. L.; Garg, A. et al. *Soft Matter* **2006**, *2*, 1015–1024.
53. Toksoz, S.; Mammadov, R.; Tekinay, A. B.; Guler, M. O. *J. Colloid Interface Sci.* **2011**, *356*, 131 – 137.
54. Silva, G. A.; Czeisler, C.; Niece, K. L.; Beniash, E.; Harrington, D. A. et al. *Science* **2004**, *303*, 1352–1355.
55. Xu, X.-D.; Jin, Y.; Liu, Y.; Zhang, X.-Z.; Zhuo, R.-X. *Colloids Surf., B* **2010**, *81*, 329 – 335.
56. Vauthey, S.; Santoso, S.; Gong, H.; Watson, N.; Zhang, S. *Proc. Natl. Acad. Sci. U.S.A.* **2002**, *99*, 5355–5360.
57. Niece, K. L.; Hartgerink, J. D.; Donners, J. J. J. M.; Stupp, S. I. *J. Am. Chem. Soc.* **2003**, *125*, 7146–7147.
58. Behanna, H. A.; Donners, J. J. J. M.; Gordon, A. C.; Stupp, S. I. *J. Am. Chem. Soc.* **2005**, *127*, 1193–1200.
59. Paramonov, S. E.; Jun, H.-W.; Hartgerink, J. D. *J. Am. Chem. Soc.* **2006**, *128*, 7291–7298.
60. Anderson, J. M.; Andukuri, A.; Lim, D. J.; Jun, H.-W. *ACS Nano* **2009**, *3*, 3447–3454.

61. Adams, D. J.; Topham, P. D. *Soft Matter* **2010**, *6*, 3707–3721.
62. Hsu, L.; Cvetanovich, G. L.; Stupp, S. I. *J. Am. Chem. Soc.* **2008**, *130*, 3892–3899.
63. Klok, H.-A.; Rosler, A.; Gotz, G.; Mena-Osteritz, E.; Bauerle, P. *Org. Biomol. Chem.* **2004**, *2*, 3541–3544.
64. van Hest, J. C. M.; Tirrell, D. A. *Chem. Commun.* **2001**, 1897–1904.
65. Afzali, A.; Breen, T. L.; Kagan, C. R. *Chem. Mater.* **2002**, *14*, 1742–1746.
66. Ma, M.; Kuang, Y.; Gao, Y.; Zhang, Y.; Gao, P. et al. *J. Am. Chem. Soc.* **2010**, *132*, 2719–2728.
67. Wu, W.; Liu, Y.; Zhu, D. *Chem. Soc. Rev.* **2010**, *39*, 1489–1502.
68. Newman, C. R.; Frisbie, C. D.; da Silva Filho, D. A.; Brédas, J. L.; Ewbank, P. C. et al. *Chem. Mater.* **2004**, *16*, 4436–4451.
69. Shao, H.; Parquette, J. R. *Chem. Commun.* **2010**, *46*, 4285–4287.
70. Langhals, H.; Ismael, R.; Yürük, O. *Tetrahedron* **2000**, *56*, 5435 – 5441.
71. Merrifield, R. B. *J. Am. Chem. Soc.* **1963**, *85*, 2149–2154.
72. Albericio, F. *Curr. Opin. Chem. Biol.* **2004**, *8*, 211 – 221.
73. Brédas, J.-L.; Beljonne, D.; Coropceanu, V.; Cornil, J. *Chem. Rev.* **2004**, *104*, 4971–5004.
74. Idé, J.; Mereau, R.; Ducasse, L.; Castet, F.; Olivier, Y. et al. *J. Phys. Chem. B* **2011**, *115*, 5593–5603.
75. Clark, J.; Silva, C.; Friend, R. H.; Spano, F. C. *Phys. Rev. Lett.* **2007**, *98*, 206406.
76. Clark, A. E.; Qin, C.; Li, A. D. Q. *J. Am. Chem. Soc.* **2007**, *129*, 7586–7595.
77. Olmsted, J. *J. Phys. Chem.* **1979**, *83*, 2581–2584.
78. Chen, Z.; Stepanenko, V.; Dehm, V.; Prins, P.; Siebbeles, L. A. et al. *Chem.–Eur. J.* **2007**, *13*, 436–449.
79. Cormier, R. A.; Gregg, B. A. *Chem. Mater.* **1998**, *10*, 1309–1319.
80. Struijk, C. W.; Sieval, A. B.; Dakhorst, J. E. J.; van Dijk, M.; Kimkes, P. et al. *J. Am. Chem. Soc.* **2000**, *122*, 11057–11066.
81. Langhals, H.; Ismael, R. *Eur. J. Org. Chem.* **1998**, *1998*, 1915–1917.
82. Hansen, C. M. *Ind. Eng. Chem. Prod. Res. Dev.* **1969**, *8*, 2–11.
83. Wang, Y.; Xu, H.; Zhang, X. *Adv. Mater.* **2009**, *21*, 2849–2864.
84. Kasha, M.; Rawls, H. R.; El-Bayoumi, M. A. *Pure Appl. Chem.* **1965**, *11*, 371–392.

85. McRae, E. G.; Kasha, M. *J. Chem. Phys.* **1958**, *28*, 721–722.
86. Eisfeld, A.; Briggs, J. *Chem. Phys.* **2006**, *324*, 376 – 384.
87. Jukes, T. H.; Schmidt, C. L. A. *J. Biol. Chem.* **1934**, *105*, 359–371.
88. Giaimo, J. M.; Lockard, J. V.; Sinks, L. E.; Scott, A. M.; Wilson, T. M. et al. *J. Phys. Chem. A* **2008**, *112*, 2322–2330.
89. Kistler, K. A.; Pochas, C. M.; Yamagata, H.; Matsika, S.; Spano, F. C. *J. Phys. Chem. B* **2012**, *116*, 77–86.
90. Tidhar, Y.; Weissman, H.; Wolf, S. G.; Gulino, A.; Rybtchinski, B. *Chem.–Eur. J.* **2011**, *17*, 6068–6075.
91. Krieg, E.; Shirman, E.; Weissman, H.; Shimoni, E.; Wolf, S. G. et al. *J. Am. Chem. Soc.* **2009**, *131*, 14365–14373.
92. Cui, H.; Hodgdon, T. K.; Kaler, E. W.; Abezgauz, L.; Danino, D. et al. *Soft Matter* **2007**, *3*, 945–955.
93. Beniash, E.; Hartgerink, J. D.; Storrie, H.; Stendahl, J. C.; Stupp, S. I. *Acta Biomater.* **2005**, *1*, 387 – 397.
94. Telfer, S. G.; McLean, T. M.; Waterland, M. R. *Dalton Trans.* **2011**, *40*, 3097–3108.
95. Schmidt, C. D.; Büttcher, C.; Hirsch, A. *Eur. J. Org. Chem.* **2009**, *2009*, 5337–5349.
96. Zahn, S.; Canary, J. W. *Science* **2000**, *288*, 1404–1407.
97. Goto, H.; Yashima, E. *J. Am. Chem. Soc.* **2002**, *124*, 7943–7949.
98. Minor, D.; Kim, P. *Nature* **1994**, *367*, 660–663.
99. Wu, H.; Xue, L.; Shi, Y.; Chen, Y.; Li, X. *Langmuir* **2011**, *27*, 3074–3082.
100. Würthner, F.; Bauer, C.; Stepanenko, V.; Yagai, S. *Adv. Mater.* **2008**, *20*, 1695–1698.
101. Li, X. Q.; Zhang, X.; Ghosh, S.; Würthner, F. *Chem.–Eur. J.* **2008**, *14*, 8074–8078.
102. Lehn, J. M. *Proc. Natl. Acad. Sci. U.S.A.* **2002**, *99*, 4763–4768.
103. Zang, L.; Che, Y.; Moore, J. S. *Acc. Chem. Res.* **2008**, *41*, 1596–1608.
104. Ryu, J. H.; Hong, D. J.; Lee, M. *Chem. Commun.* **2008**, 1043–1054.
105. Palmer, L. C.; Stupp, S. I. *Acc. Chem. Res.* **2008**, *41*, 1674–1684.
106. Zhang, X.; Wang, C. *Chem. Soc. Rev.* **2011**, *40*, 94–101.
107. Zhan, C.; Gao, P.; Liu, M. *Chem. Commun.* **2005**, 462–464.
108. Cui, J.; Zheng, J.; Qiao, W.; Wan, X. *J. Colloid Interface Sci.* **2008**, *326*, 267 – 274.

109. Xu, S.; Sun, J.; Ke, D.; Song, G.; Zhang, W. et al. *J. Colloid Interface Sci.* **2010**, *349*, 142 – 147.
110. Golubkov, G.; Weissman, H.; Shirman, E.; Wolf, S. G.; Pinkas, I. et al. *Angew. Chem., Int. Ed.* **2009**, *48*, 926–930.
111. Chen, Y.; Feng, Y.; Gao, J.; Bouvet, M. *J. Colloid Interface Sci.* **2012**, *368*, 387 – 394.
112. Würthner, F.; Thalacker, C.; Diele, S.; Tschierske, C. *Chem.–Eur. J.* **2001**, *7*, 2245–2253.
113. Sauer, M. *Angew. Chem., Int. Ed.* **2003**, *42*, 1790–1793.
114. McQuade, D. T.; Pullen, A. E.; Swager, T. M. *Chem. Rev.* **2000**, *100*, 2537–2574.
115. Heeger, P. S.; Heeger, A. J. *Proc. Natl. Acad. Sci. U.S.A.* **1999**, *96*, 12219–12221.
116. Wang, B.; Yu, C. *Angew. Chem.* **2010**, *122*, 1527–1530.
117. Wang, K. R.; An, H. W.; Wu, L.; Zhang, J. C.; Li, X. L. *Chem. Commun.* **2012**, *48*, 5644–5646.
118. Eckert, F.; Leito, I.; Kaljurand, I.; Kütt, A.; Klamt, A. et al. *J. Comput. Chem.* **2009**, *30*, 799–810.
119. de Miguel, G.; Ziólek, M.; Zitnan, M.; Organero, J. A.; Pandey, S. S. et al. *J. Phys. Chem. C* **2012**, *116*, 9379–9389.
120. Marsh, R. A.; Hodgkiss, J. M.; Friend, R. H. *Adv. Mater.* **2010**, *22*, 3672–3676.
121. Lawrence, D. S.; Jiang, T.; Levett, M. *Chem. Rev.* **1995**, *95*, 2229–2260.
122. Philp, D.; Stoddart, J. F. *Angew. Chem., Int. Ed.* **1996**, *35*, 1154–1196.
123. Mateos-Timoneda, M. A.; Crego-Calama, M.; Reinhoudt, D. N. *Chem. Soc. Rev.* **2004**, *33*, 363–372.
124. Hoeben, F. J. M.; Pouderoijen, M. J.; Schenning, A. P. H. J.; Meijer, E. W. *Org. Biomol. Chem.* **2006**, *4*, 4460–4462.
125. Yagai, S.; Monma, Y.; Kawauchi, N.; Karatsu, T.; Kitamura, A. *Org. Lett.* **2007**, *9*, 1137–1140.
126. Yagai, S.; Seki, T.; Karatsu, T.; Kitamura, A.; Würthner, F. *Angew. Chem., Int. Ed.* **2008**, *47*, 3367–3371.
127. Yagai, S.; Seki, T.; Murayama, H.; Wakikawa, Y.; Ikoma, T. et al. *Small* **2010**, *6*, 2731–2740.
128. Faul, C.; Antonietti, M. *Adv. Mater.* **2003**, *15*, 673–683.
129. Faul, C. F. J.; Antonietti, M. *Chem.–Eur. J.* **2002**, *8*, 2764–2768.

130. Wei, Z.; Laitinen, T.; Smarsly, B.; Ikkala, O.; Faul, C. F. J. *Angew. Chem., Int. Ed.* **2005**, *44*, 751–756.
131. Guo, D. S.; Jiang, B. P.; Wang, X.; Liu, Y. *Org. Biomol. Chem.* **2012**, *10*, 720–723.
132. Ma, T.; Li, C.; Shi, G. *Langmuir* **2008**, *24*, 43–48.
133. Winkler, J. D.; Bowen, C. M.; Michelet, V. *J. Am. Chem. Soc.* **1998**, *120*, 3237–3242.
134. Czarnik, A. W. *Acc. Chem. Res.* **1994**, *27*, 302–308.
135. Cho, E. J.; Ryu, B. J.; Lee, Y. J.; Nam, K. C. *Org. Lett.* **2005**, *7*, 2607–2609.
136. Liu, B.; Bao, Y.; Wang, H.; Du, F.; Tian, J. et al. *J. Mater. Chem.* **2012**, *22*, 3555–3561.
137. He, X.; Liu, H.; Li, Y.; Wang, S.; Li, Y. et al. *Adv. Mater.* **2005**, *17*, 2811–2815.
138. Chen, Z. J.; Wang, L. M.; Zou, G.; Zhang, L.; Zhang, G. J. et al. *Dyes Pigm.* **2012**, *94*, 410 – 415.
139. Backes, C.; Schunk, T.; Hauke, F.; Hirsch, A. *J. Mater. Chem.* **2011**, *21*, 3554–3557.
140. Davies, R. P.; Less, R. J.; Lickiss, P. D.; White, A. J. P. *Dalton Trans.* **2007**, 2528–2535.
141. Dudev, T.; Lim, C. *J. Phys. Chem. B* **2004**, *108*, 4546–4557.
142. Eddaoudi, M.; Moler, D. B.; Li, H.; Chen, B.; Reineke, T. M. et al. *Acc. Chem. Res.* **2001**, *34*, 319–330.
143. Bunting, J.; Thong, K. *Can. J. Chem.* **1970**, *48*, 1654–1656.
144. Sone, E. D.; Stupp, S. I. *Chem. Mater.* **2011**, *23*, 2005–2007.